

AN ABSTRACT OF THE THESIS OF

Ian W. Whidden for the degree of Master of Science in Water Resources Science presented on August 23, 2023.

Title: Forest Canopy Effects on Snow Depth and Density of Seasonal and Transient Mountain Snowpack in a Maritime Snow Climate

Abstract approved: _____

Julia A. Jones

Relatively little is known about how various factors influence snow water storage in forested mountain landscapes in maritime (warm winter) climates. This study took advantage of multiple snow data sources including long-term data, synoptic sampling, remote sensing, and modeling to examine factors influencing snow dynamics in the H.J. Andrews Experimental Forest, western Cascade Range, Oregon. The study combined two field campaigns, long-term snow survey data, long-term data from meteorological stations, lidar-derived snow depth maps, and snow modeling to quantify effects of forest canopy structure, landscape position, and season on snowpack depth and density in a ~52 km² portion of forested watershed ranging from 800 to 1600 m in elevation. Methods included (1) collecting field measurements of snow in March of 2022 and 2023, (2) comparing long-term (1978-2022) snow measurements at the paired forested vs. open sites, (3) examining SWE and snow depth data at four meteorological stations (1997-2022), (4) using a lidar-derived snow height model of the upper elevations of the Andrews Forest acquired March 2022 to assess spatial patterns of snow depth, and (5) simulating snow water equivalent at forest and open sites using a snow model forced with meteorological data for the period 2014 to 2018.

Field sampling indicated that snow depth in March 2022 was as much as 130 cm greater in the clearing at the Upper Lookout meteorological station (1298 m) than in the adjacent forest plantation. Field sampling was used to validate lidar-derived snow depth.

Long-term snow survey data from paired sites in forest gaps created by roads and beneath adjacent forests (1978-2022) indicated that average annual snow depth was two to three times greater in openings than in adjacent forest sites. Snow density was similar (about 365-366 kg/m³) in forest and open snow survey sites. Snow disappeared earlier at snow survey sites under forest than in openings, but snow melt was more rapid in openings than under forest at snow survey sites.

Analysis of daily snow depth and SWE records from three meteorological stations (1997-2014) revealed a concave upward curve of average daily snow density over the snow season. Snow density ranged from 200 to 350 kg/m³ in November to January, 380 to 400 kg/m³ in February to early April, to higher values in May. Analysis of the 1995-2022 precipitation and SWE data from the Upper Lookout meteorological station also revealed that maximum snow water equivalent on April 1 was on average 38% of cumulative precipitation in the water year (Oct 1 to April 1).

Analysis of the lidar image of 52 km² of the upper elevation portion of the Andrews Forest (600 to 1600 m) indicated that lidar-derived snow depth in March 2022 varied with landscape position and forest canopy structure: deeper snow occurred on north- and east-facing slopes, in valley bottoms, and openings such as avalanche tracks, montane meadows, access roads, and forest clearings created for meteorological stations. Lidar-derived snow depth was greater in plantations than in adjacent mature-old forest in valley bottoms affected by cold air drainage but was not related to forest canopy height in other landscape positions, based on a small sample of paired 60x60m polygons. Lidar-derived snow depth tended to overestimate field measurements, indicating that the post-survey elevation correction (+295 mm) may not be appropriate. The total volume of water stored in the snowpack in March 2022 based on the lidar-derived snow depth model (average depth 54 cm, average density 380 to 400 kg/m³) was approximately equivalent to 30 days of mean daily flow at Lookout Creek, which drains the H.J. Andrews Experimental Forest.

Modeling of snow using the SUMMA model reproduced the measured snowpack in an opening at the Upper Lookout meteorological station when the model was forced with data from that station. However, modeling of snowpack under forest using parameterizations of

forest interception developed at a nearby site in the Umpqua National Forest did not reproduce snow measured under forest in the field or at the long-term snow stakes. Snow modeling results demonstrated the importance of early winter air temperature effects on snowpack formation and persistence.

These results demonstrate that conifer forests substantially reduce snow accumulation in a maritime climate, but these effects vary among years, with elevation, and with canopy structure. Further study is needed to better understand how landforms, climate, and conifer forest canopy influence snow accumulation and melt in the transient to seasonal snow zones of maritime climates.

©Copyright by Ian W. Whidden

August 23, 2023

All Rights Reserved

Forest Canopy Effects on Snow Depth and Density of Seasonal and Transient Mountain
Snowpack in a Maritime Snow Climate

by
Ian W. Whidden

A THESIS
submitted to
Oregon State University

in partial fulfillment of
the requirements for the
degree of

Master of Science

Presented August 23, 2023

Commencement June 2024

Master of Science thesis of Ian W. Whidden presented on August 23, 2023.

APPROVED:

Major Professor, representing Water Resources Science

Director of Water Resources Graduate Program

Dean of the Graduate School

I understand that my thesis will become part of the permanent collection of Oregon State University libraries. My signature below authorizes release of my thesis to any reader upon request.

Ian W. Whidden, Author

ACKNOWLEDGEMENTS

Thank you to the National Science Foundation (NSF) and the LTER Network. I implore the NSF to continue its funding of the H.J. Andrews Experimental Forest after the Lookout Fire in 2023. Without your help the Andrews cannot go on. Thank you to my committee, my family, and my girlfriend Valerie. I would not have gotten here without Valerie's never-ending love and support. Finally, thank you to the United States Forest Service (USFS). Without the interest on the USFS, the field of hydrology would not be where it is today.

CONTRIBUTION OF AUTHORS

Dr. Jones for assisted with long term data analysis. Dr. Bennett assisted with pySUMMA set up and functions. Dr. Raleigh instructed in snow hydrology, snow modeling, and remote sensing. Dr. Raleigh also assisted with March 2022 fieldwork. Dr. Bladon instructed on forest hydrology.

TABLE OF CONTENTS

	<u>Page</u>
1. Introduction	1
1.1 Motivation.....	1
1.2 Gaps in knowledge	2
1.3 Objectives and research questions	4
2. Study site description	5
3. Methods.....	9
3.1 Field methods.....	17
3.1.1 Field sampling of snow and forest characteristics	17
3.1.2 Lidar image acquisition.....	36
3.1.3 Meteorological station data about snow and other climate variables	40
3.1.4 Snow survey stake methods.....	41
3.2 Data analysis	41
3.2.1 Validation of lidar image vs. field, meteorological station, and snow stakes	41
3.2.2 Comparison of lidar snow depth by forest cover type	42
3.3 Snow modeling.....	51
3.3.1 Model forcing	53
3.3.2 Sensitivity analysis, presence of conifer forest	55
3.3.3 Sensitivity analysis, snow interception parameterization	58
4. Results.....	60
4.1 Field comparisons	60
4.2 Validation of lidar derived snow depth with data from field sampling, meteorological stations, and snow stakes	63
4.2 Data analysis	76
4.2.1 Lidar comparisons between different forest cover types	76
4.2.2 Meteorological station snow analysis	82
4.2.3 Snow survey stake analysis	87
4.3 Snow modeling.....	95
5. Discussion	102
5.1 Effects of forest structure and topographic factors on snow	102
5.1.1 Maritime climate effects	104
5.1.2 Effects of elevation.....	104
5.1.3 Effects of slope orientation	105
5.1.4 Effects of landform position and air drainage.....	106
5.1.5 Effect of vegetation cover type	106
5.1.6 Effects of forest structure	107
5.3 Limitations and recommendations	113
5.3.1 Snow surveying.....	113

TABLE OF CONTENTS (Continued)

	<u>Page</u>
5.3.2. Lidar snow survey.....	113
5.3.3 Snow modeling.....	114
6. Conclusion.....	116
References.....	118
Appendix A – Long-term snow stake data.....	127
Appendix B – Equations.....	140
Appendix C – SUMMA code.....	141

LIST OF FIGURES

<u>Figure</u>	<u>Page</u>
1. Locations of field samples, lidar survey, meteorological stations, and snow stakes in the study site in the H.J. Andrews Experimental Forest.....	7
2. Study site with canopy height model overlay.....	8
3. Canopy height model of planted stands relative to March 16, 2022, snow sample locations.....	19
4. Lidar image of snow depth (flight on March 17, 2022) relative to March 16, 2022 snow sample locations.....	20
5. Mean snow depth sampled in the field at 23 sites on March 16, 2022.....	23
6. Canopy height model of planted stands relative to March 1 and 2, 2023 snow sample locations.....	27
7. Lidar image of snow depth (taken on March 17, 2022) relative to March 1 and 2, 2023 snow sample locations.....	28
8. Snow water equivalent during WY 2022 measured at the Upper Lookout meteorological station (UPLMET) (1298 m).....	38
9. Snow height model on March 17, 2022 over all of the upper elevations of Andrews Forest.....	39
10. Locations of 60x60 polygons used for sampling of canopy height and snow depth in planted forest stands and adjacent mature/old growth forest stands.....	44
11. Ten pairs of 60x60 m polygons sampled for lidar-derived snow depth superimposed on the canopy height model.....	47
12. Ten pairs of 60x60 m polygons sampled for lidar-derived snow depth superimposed on the snow height model (lidar-derived snow depth).....	50
13. Canopy interception of snow model equations, where L is the amount of snow intercepted by the canopy depending on HP98 (left hand side equation) or Andreadis 2009 (right hand side equation) (Lundquist et al., 2021).....	59

LIST OF FIGURES (Continued)

<u>Figure</u>	<u>Page</u>
14. Effect of lidar spatial resolution and forest cover type on difference between field-measured and lidar-derived snow depth.....	67
15. Effect of lidar spatial resolution on difference between snow depth from a snow depth sensor and lidar-derived snow depth.....	70
16. Lidar validation using a 1-meter resolution snow height model with snow depth collected in the UPLMET clearing and beneath the surrounding planted forest on March 16, 2022.....	72
17. Effect of lidar spatial resolution and forest cover type on difference between snow depth measured at snow stakes and lidar-derived snow depth. Raster.....	75
18. Mean and standard error (SE) of lidar-derived snow depth (1-meter raster) by elevation in ten pairs of polygons of 60x60 m in planted and mature/old-growth forest.....	79
19. Mean and standard error (SE) of snow depth in lidar image by forest cover type, ten paired sites.....	80
20. Difference of canopy height, mature/old-growth minus planted forest, vs. difference in snow depth in lidar image, 1-meter raster.....	81
21. Average snow density from 1997 to 2014 at Upper Lookout, Vanilla Leaf, and Central meteorological stations.....	82
22. SWE and cumulative precipitation, 1997-2014, Upper Lookout.....	83
23. Ratio of SWE to cumulative precipitation, 1994-2014, Upper Lookout.....	83
24. SWE (m) vs. snow density (g/cc), 1997-2014, Upper Lookout.....	84
25. Relationship of daily change in SWE to daily change in minimum T, Upper Lookout, for 1996-2019.....	86
26. Difference in snow disappearance date, open – forest, 2014-2022.....	88
27. Mean snow depth loss rate using peak snow depth date, amount, and snow disappearance date, 2014-2022.....	89

LIST OF FIGURES (Continued)

<u>Figure</u>	<u>Page</u>
28. Difference in snow depth loss rate, open – forest, 2014–2022.....	89
29. Snow density (%) at 10 paired forest and open sites sampled from 1994 to 2016.....	91
30. Cumulative snow depth, forest as % of open.....	94
31. Simulated snow depth (top) and SWE (bottom) output over a five-year period, covering water years 2014-2018, based on SUMMA model forced with data from the Upper Lookout benchmark meteorological station.....	96
32. Measured precipitation (top), simulated snow depth and snowpack temperature (middle), and measured minimum and maximum daily temperature for water years 2014-2018.....	97
33. SUMMA snow depth and SWE output over a five-year period, covering water years 2014-2018.....	99
34. Snow depth and SWE output from a sensitivity analysis with the canopy interception of snow option.....	101

LIST OF TABLES

<u>Table</u>	<u>Page</u>
1. Mean air temperature, December - February (°C), Upper Lookout meteorological station (1300 m), water year 2011-2015.....	6
2. Description of data sources and models used in this study.....	11
3. Characteristics of the planted forest stands in the H.J. Andrews Experimental Forest that were sampled for SWE and snow depth during March 2022 and March 2023.....	24
4. Summary of mean snow depth, SWE, and snow density at 23 sites sampled on March 16, 2022.....	25
5. Model decisions used in SUMMA.....	52
6. Nash-Sutcliffe efficiency (NSE) values for SUMMA simulation output of snow depth and SWE for water years 2014 to 2018.....	57
7. Variation of snow depth by elevation, measurement type, and distance from road at four planted forest stands, March 1 and 2, 2023.....	62
8. Lidar snow depth at 3m, 5m, and 10m resolution on March 17, 2022, compared to snow depth data collected in the field using snow pits, a Federal sampler, and an avalanche probe on March 16, 2022.....	65
9. Lidar snow depth at 1,3, and 5m resolution compared to snow depth data measured by an acoustic snow depth sensor at sites of the MS001 meteorological stations.....	69
10. Lidar snow depth at 1m resolution on March 17, 2022, compared to snow depth data collected in the field using an avalanche probe, two snow pits, and a Federal sampler at Upper Lookout meteorological station clearing and adjacent forest, March 16, 2022.....	71
11. Lidar snow depth at 3, 5, and 10m resolution compared to snow depth data measured at snow stakes (MS00701), March 17, 2022.....	73
12. Characteristics of 60x60 m plots sampled for lidar-derived snow depth and canopy height in planted and mature/old forest stands.....	77
13. Results of differencing the canopy height model and snow height model between planted and mature/old-growth forests using 60x60 m polygons, 1-meter raster.....	78

LIST OF TABLES (Continued)

<u>Table</u>	<u>Page</u>
14. Average snow disappearance date, 2014-2022, open minus forest, and mean snow depth loss rate at ten MS00701 sites with paired snow stakes beneath the forest and in the open (on the road).....	87
15. Snow density (%) at ten pairs of snow survey stakes in forested sites over the period 1994-2016.....	90
16. Cumulative snow depth on April 1, forest as percent of open, at nine snow stakes with continuous (daily) records from 2015 to 2022.....	92
17. Relationships of snow depth under forest and in openings at snow survey stakes, 1994-2022, by elevation.....	93
18. Lidar-derived snow depth on March 17, 2022 as a volume of water based on average daily SWE measured 1997-2014 at the three meteorological stations and expressed in terms of equivalent streamflow at the mouth of Lookout Creek.....	111

LIST OF APPENDICES

<u>Appendix</u>	<u>Page</u>
Appendix A. Long-term snow stake data.....	127
Appendix B. Equations.....	140
Appendix C. SUMMA code.....	141

LIST OF APPENDIX FIGURES

<u>Figure</u>	<u>Page</u>
A-1. Snow depth in openings increases relative to under forest based on long-term paired snow stakes in the Andrews Forest.....	130
A-2. Historical snow depth at snow stakes.....	132
A-3. Complete measurement series of SWE (mm) in openings and under forest at paired snow stakes, Andrews Forest (RS04, RS12, RS26) and Wildcat Mountain (RS13, RS14), dataset MS00702, 1978 to 2003.....	137

LIST OF APPENDIX TABLES

<u>Table</u>	<u>Page</u>
A-1. Summary of snow depths measured at snow stakes in forest and openings in dataset MS00701 (1994 to 2022).....	127
A-2. Summary of SWE (mm) measured at snow stakes in forest and openings in dataset MS00702 (1978 to 2003).....	129

1. Introduction

1.1 Motivation

This study was motivated by a need to improve understanding of processes that influence the snowpack in a maritime climate, especially processes involving conifer forests. Snow accumulation responds to climate and forest management and influences water supply. Effects of climate and forest management on snow are a major issue in the Pacific Northwest of the United States, which is dominated by conifer forest and is one of the most productive timber producing regions in the world (Alig et al., 2000). More than half of commercial land used for timber harvest in western Oregon falls into the transient snow zone (~350–1100 m), and forest management has many effects on snowpack dynamics (Berris & Harr, 1987).

In maritime climates of the western U.S., with wet winters and dry summers, water stored in the snowpack beneath conifer forests supplements streamflow in spring and summer. A maritime snowpack can accumulate to depths exceeding 3 m, has a snow-ground interface temperature near 0 °C throughout the winter, and has coarse grained snow due to ubiquitous wetting of the snowpack throughout the winter (Sturm et al., 1995; Sturm & Liston, 2021). Sixty to eighty percent of the source water for summer streamflow in the Willamette River, Oregon originates in the snow zone (>1200 m) (Brooks et al., 2012). The upper elevation areas of the Willamette River in the western Cascade Range of Oregon are “at risk” of shifting from a snow- to a rain-dominated winter precipitation regime, which would significantly decrease snow water storage (Mote, 2003; Nolin & Daly, 2006). Increases in air temperature associated with climate change exacerbate these risks to the snowpack in the western Cascade Range of Oregon (Sproles et al., 2013). Continued warming may push continental and boreal snow climate processes to regimes similar to those observed in maritime sites today (S. Dickerson-Lange et al., 2017).

Pioneering work on snow in the maritime climate of the Pacific Northwest occurred in the late 1940s and early 1950s at the Willamette Basin Snow laboratory in the upper Blue River basin, just north of the H.J. Andrews Experimental Forest (44.2332 °N. 122.1762 °W) (USACE, North Pacific Division, Portland, OR, 1956; USACE, South Pacific Division, San Francisco, CA,

1956). Storck et al (2002) examined effects of forest canopy on snow interception in the Umpqua National Forest, about 300 km south of the Andrews Forest. Within the Andrews Forest, other seminal work focused of clearcutting and rain-on-snow influences on a maritime snowpack (Berris & Harr, 1987; Dennis Harr, 1981; Harr, 1986).

Losses in snow water storage can increase wildfire risk, forest susceptibility to pests, and water shortages, with implications for the socio-economic well-being of the Pacific Northwest (Li et al., 2017). A greater understanding of processes affecting snow within forests, particularly canopy interception, is essential for assessing the combined effects of global warming and continued timber harvest in the region. Improved understanding of how forests affect accumulation and ablation in a maritime climate could be transferrable to other locations as they experience climate warming.

Forest conditions influence the amount of snow that is contributed to the underlying snowpack, the phase and density of the new snow contribution, and the snowpack energy balance (Andreadis et al., 2009). In a maritime snow climate, canopy interception may decrease snow accumulation by up to 60% (Storck et al., 2002). Parameterizations for snow models of canopy interception of snow have been developed for a maritime climate based on empirical measurements by Storck et al. (2002) and for a continental climate based on Hedstrom and Pomeroy (1998). The small number of empirical studies used for modeling of snow interception may limit model capacity to represent interception (Lundquist et al., 2021).

1.2 Gaps in knowledge

The effects of forests on snowpack in maritime climates are imperfectly understood. Canopy interception of snow plays a significant role in subcanopy snow accumulation in a maritime snow climate because air temperature and wind strongly influence interception processes (Andreadis et al., 2009; Roth & Nolin, 2019). In the western Cascade Range of Oregon winter air temperature is warm and wind speeds are low. Snow modeling using the DHSVM model in wet/warm climates indicated that snow water equivalent and snow duration under forest increase as canopy density decreases (Sun et al., 2022). Musselman et al. (2008) and Veatch et al. (2009) hypothesize that selective thinning can increase snow water storage in a

continental climate, while Lundquist et al. (2013) found that lower total canopy cover in warm/wet winter climates is likely to enhance snowpack retention. The dominant processes accounting for snow accumulation and ablation beneath forests differ in a maritime (warm/wet) and continental climate (cold/dry). Snow interception is the dominant control on accumulation in warmer climates due to higher snow cohesion at warmer temperatures. The fraction of total precipitation intercepted by a tree branch more than doubles when storm air temperature increases from -3°C to -1°C (S. E. Dickerson-Lange et al., 2021). During the melt season, sublimation accounts for 100mm of snow loss per season in a maritime climate (Storck et al 2002), but nine times more than this in a continental climate (Lundquist et al., 2021). The collective effects of climate on the deposition and removal of snow from the canopy in warm/wet climates is not well understood.

The effects of past forest management on snow are unclear. Planted forests may have a higher density of tree wells and higher canopy closure compared to mature/old-growth forest. These factors may increase longwave radiation input to the snowpack and reduce snow accumulation in planted forests, but this effect may vary among planted stands with different ages and forest structure. Timber harvest influences rain-on-snow floods in the Pacific Northwest (Harr, 1986; Jennings & Jones, 2015), but process understanding is insufficient to connect fine-scale snowpack dynamics to regional timber harvest and extreme rain-on-snow flood events (J. A. Jones & Perkins, 2010). Apart from limited measurements at the H.J. Andrews Experimental Forest in Oregon and other locations in the Pacific Northwest, information concerning the snowpack energy balance during rain-on-snow events is lacking (Mazurkiewicz et al., 2008).

The accurate estimation of snow water storage over the landscape is a key parameter for water resource managers, but full spatial coverage of snow water is difficult to obtain. Methods are lacking to accurately estimate the spatial variability of snow water storage and how it responds to changes in forest cover (Clark et al., 2011; Lundquist et al., 2021). For example, snow water equivalent typically is measured at only a few points in the landscape, but point based measurements of snow water equivalent are inadequate to capture the spatial distribution of snow water storage due to the high spatial and temporal variability of mountain

snowpack (Molotch & Meromy, 2014). Furthermore, remotely sensed spaceborne retrievals of snow water equivalent and model-based snow estimates in mountains are often inaccurate (Largeron et al., 2020). Airborne lidar offers the potential to estimate synoptic coverage of snow depth. Prior lidar retrievals of snow depth have been focused in alpine and sub-alpine areas of the Sierra Nevada in California and the Rocky Mountains in Colorado and Wyoming (Painter et al., 2016). However, few or no studies have used lidar to detect snow in lower elevations (<1500 m) of a forested maritime climate setting.

Snow simulation models can permit testing how various processes affect interception of snow in forest canopies. However, models of snow processes at the rain-snow transition near 0°C have high rates of error (Wayand et al., 2016). Snow simulations (using PRMS) indicated that snow water equivalent was an order of magnitude lower under forest than measurements in openings (Perkins & Jones 2008). Measurements of accumulation, ablation, and interception using automated snow stations and paired snow stake sites have the potential to help improve model representations of canopy interception of snow in a maritime snow climate.

1.3 Objectives and research questions

The objectives of this study were to characterize snowpack dynamics in forests in a maritime climate using diverse data sources and contemporary methods. We drew on various long-term and short-term datasets on snow available from the H.J. Andrews Experimental Forest in western Oregon. Datasets include long-term paired snow stake data in openings and under forest canopy; long-term meteorological station data on snow depth and density, precipitation, air temperature, atmospheric pressure, and radiation; in situ snow field sampling; and an airborne lidar image of snowpack acquired in March 2022.

We asked the following questions:

- 1) What processes govern snowpack dynamics in the transient to seasonal snow zone in a maritime snow climate?
- 2) What factors affect the spatial distribution of snow depth?

- 3) How well do snow model representations of forest canopy interception agree with field-measured estimates of snow in openings vs. under forest?

2. Study site description

The 64 km² Lookout Creek drainage basin (Figure 1) comprises the H.J. Andrews Experimental Forest (hereafter, “Andrews Forest”) in the western Cascade Range, Oregon. Lookout Creek drains into Blue River, which drains to the McKenzie River, a tributary to the Willamette River. The Andrews Forest has been part of the National Science Foundation’s Long Term Ecological Research program since 1980.

The Andrews Forest ranges in elevation from 420 to 1,630 meters. The landscape in the Andrews is steep, with slopes as great as sixty percent.

The climate in the Andrews Forest is cool and wet in the winter and warm and dry in the summer. Four benchmark climate stations established in 1987 (Vanmet) and 1994 (Cenmet, Uplmet, Varmet) are located in the seasonal snow zone and coincide with the study area (Figure 1). These stations measure air temperature, precipitation, snow, wind, atmospheric pressure, radiation, and other variables used in analyses. Warm snowpack conditions cause frequent melt events during the winter months of December, January, and February. The mean winter (December to February) air temperature at the Upper Lookout meteorological station at 1,298 m elevation (Figure 1) fluctuates around 0°C and varies among years (Table 1). A transient snowpack may accumulate and melt several times throughout a season at 350 to 1,100 meters in elevation (Harr, 1986). Above 1,100 m a seasonal snowpack forms in November, accumulates to 2 to >7 m, and melts from March to June (Jefferson et al., 2008; Perkins & Jones, 2008). Snowpack in the Pacific Northwest Cascades is particularly sensitive to air temperature, and lower elevation zones in the western Oregon Cascades are classified as the most ‘at-risk’ snow within the region (Nolin & Daly, 2006).

Vegetation in the Andrews Forest consists of mature and old-growth forest dominated by Douglas-fir (*Pseudotsuga menziesii*), western hemlock (*Tsuga heterophylla*), and western redcedar (*Thuja plicata*), with about 25% of area in young Douglas-fir dominated patches created by timber harvest from 1948 to the mid-1970s (Goodman et al., 2023; J. Jones & Grant,

1996). Mature/old-growth stands range in age from 150–700 years and can have trees as tall as 75 meters (Figure 2).

Table 1. Mean air temperature, December - February (°C), Upper Lookout meteorological station (1300 m), water year 2011-2015.

Water year	2011	2012	2013	2014	2015
	-0.07	0.78	-0.67	1.43	3.51

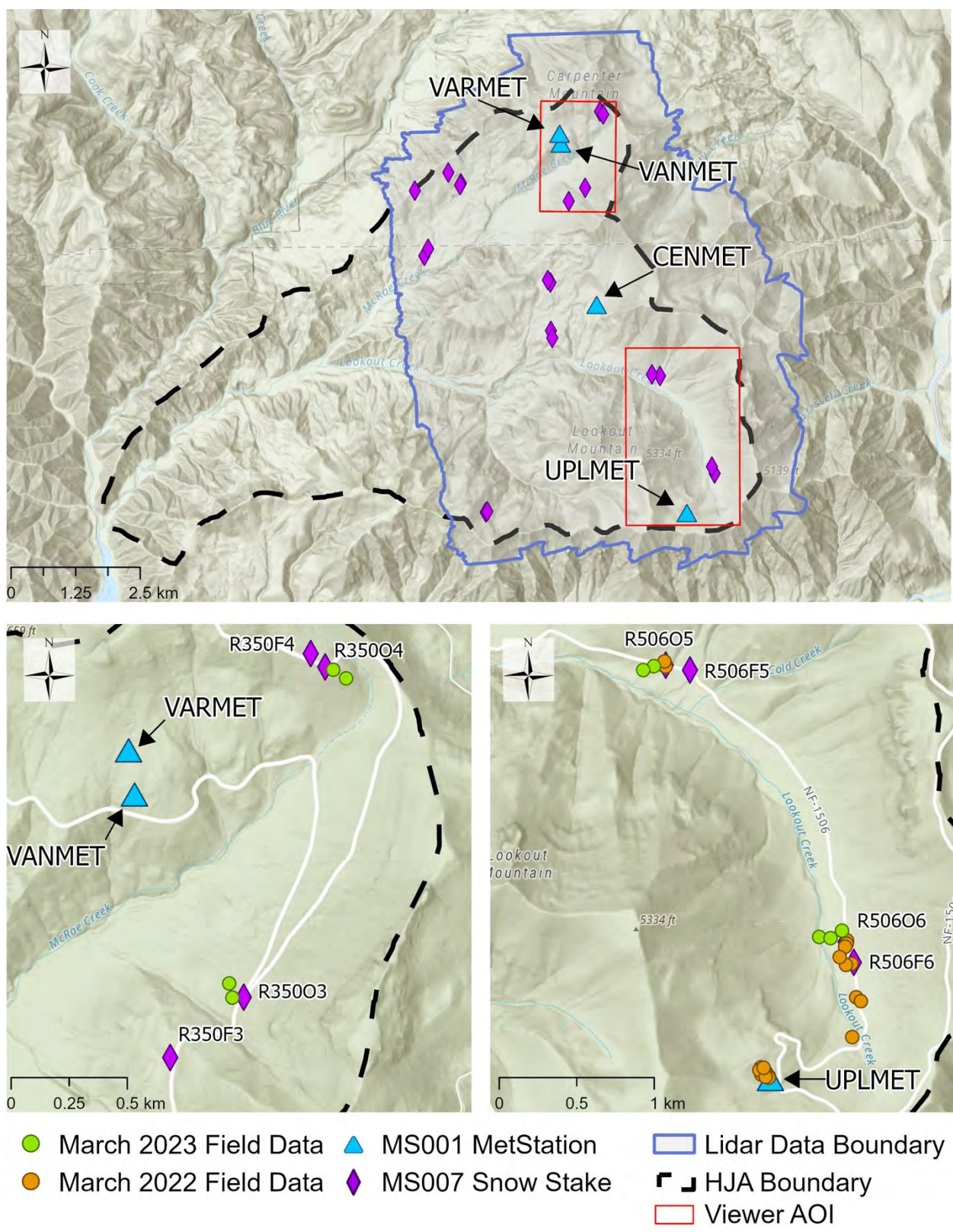


Figure 1. Locations of field samples, lidar survey, meteorological stations, and snow stakes in the study site in the H.J. Andrews Experimental Forest.

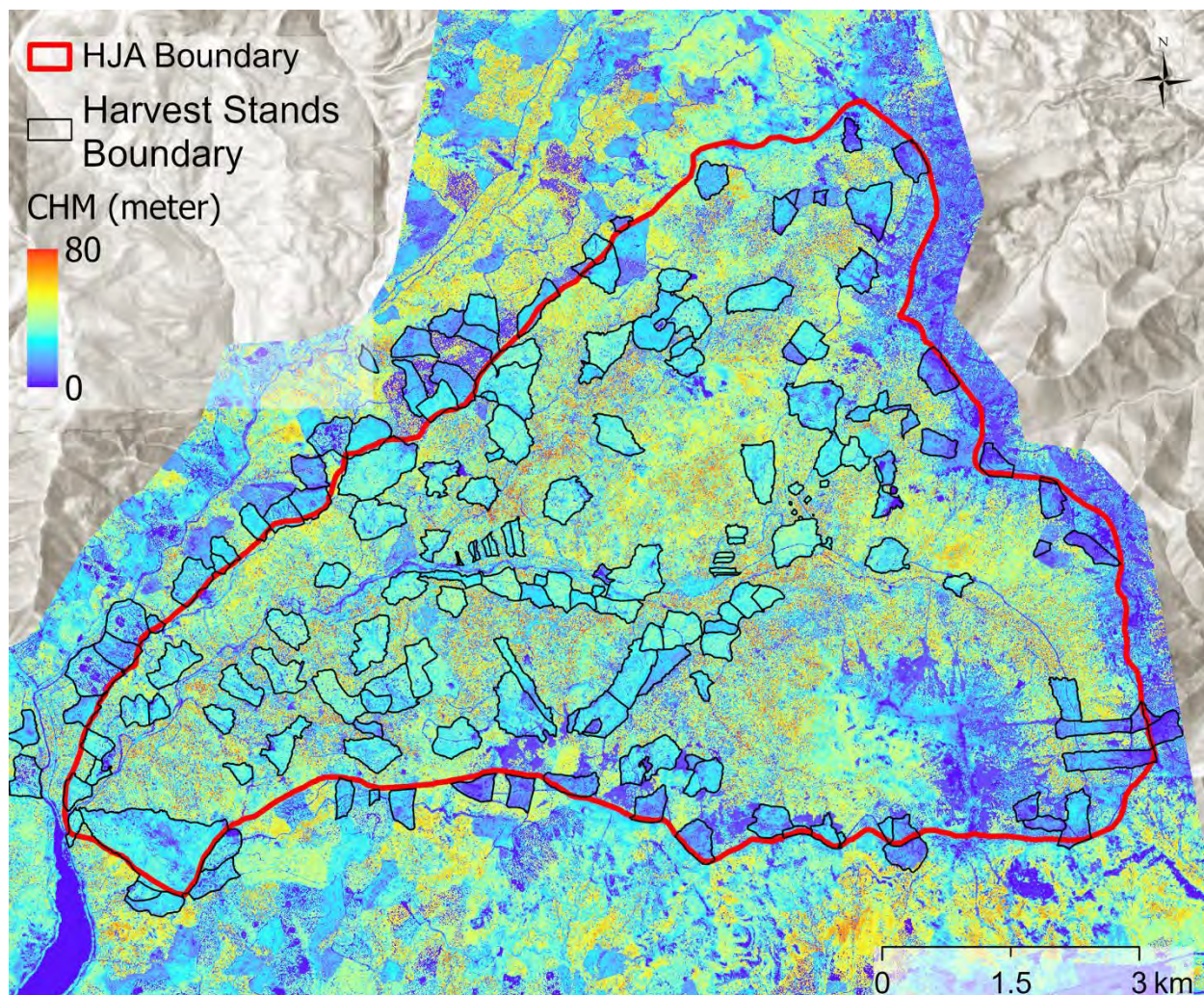


Figure 2. Study site with canopy height model overlay (Dave Bell, 2023; Quantum Spatial, 2020).

3. Methods

This study applied multiple snow measuring, modeling, and estimating methods to investigate the factors and processes affecting snow accumulation and melt in the Andrews Forest, Oregon (Table 2). Long-term snow data from paired forest and open sites since 1978 were combined with meteorological station records, a lidar survey, and snow modeling to investigate various effects on seasonal snowpack accumulation and ablation.

Snow sampling of the transient and seasonal snowpack in the Andrews Forest at elevations ranging from 800 to 1400 m was conducted in March 2022 and March 2023. (Figure 1, Table 2). Snow surveying tools included an avalanche probe, a Federal sampler, and snow pits.

A snow-on lidar survey was flown on March 17, 2022 to obtain the surface elevation of the snowpack. Snow depth was calculated by differencing a digital terrain model (DTM) containing the snowpack surface elevation with the USGS 3DEP (Thatcher et al., 2017) bare earth DTM, and the resulting spatial layer of lidar-derived snow depth was validated by comparison with snow depth measured from field sampling, snow survey stakes, and meteorological stations collected on the same date as the lidar survey (Figure 1, Table 2).

Snowpack evolution was modeled over the period of water year 2014 to water year 2018 using the Structure for Unifying Multiple Modelling Alternatives (SUMMA) as a snow model (Clark et al., 2015a, 2015b). The model was forced using meteorological data from the Upper Lookout meteorological station (Figure 1, Table 2) and the phase two of the North America Land Data Assimilation System (NLDAS-2) (Table 2). The Python wrapper used to manipulate the SUMMA model is pySUMMA (Choi et al., 2018).

Long term meteorological and snow data (described below) were obtained from the Andrews LTER database and used to force the SUMMA model, to validate the lidar-derived snow depths, and to estimate snow density over time. Data from meteorological stations (MS001) included snow depth and SWE, air temperature, precipitation, relative humidity, wind, radiation, and air pressure (Table 2) (Daly et al., 2019). Vegetation classifications and history from the Willamette National Forest (TV061) were used to characterize vegetation conditions (Lienkaemper & Schulze, 2015).

Long-term snow stake measurements (MS007) included snow depth and SWE since 1978 in paired openings and forest sites (Levno et al., 2023). The long-term snow depth data at paired snow stakes from the MS007 dataset were used to determine the effects of forest canopy on snow disappearance date, peak snow depth, snow water equivalent, and snow density (Table 2). The MS00701 dataset (Appendix A) includes paired measurements of SWE and snow depth in ten paired open and forest sites ranging in elevation from 450 m to 1400 m along major roads (1506, 1507, 320, 350 roads) in the Andrews Forest. Measurements from 1994 to 2014 were obtained using a Federal sampler by technicians traveling to each stake two to ten times throughout the winter. In 2014, cameras were installed in small bunk houses attached to the trees pointing at the snow stakes (Photograph 1). The cameras are programmed to take an image at 9:00 AM, 12:00 PM, and 3:00 PM. These images are stored, uploaded by a technician, and converted to daily snow depth values by reading the height of the snow on the stake on each day that an image was captured. Each snow stake is made of PVC marked with tape at known heights (Photograph 2, Photograph 4). Processing of photos corrects for cones of depression or accumulation around snow stakes (e.g. Photograph 2).

Of the 40 snow stakes in the entire MS00701 dataset, this study utilized the 20 that were included in the snow-on lidar survey extent (Figure 1). Little to no snow was present at the other 10 forest stakes on the date of the lidar survey (March 17, 2022).

The lidar survey covered the range of elevation in which the transient snow zone transitions to the seasonal snow zone (600 to 1400 m), including research watersheds such as Watershed 6, Watershed 7, and Watershed 8 (Figure 1). Of the 20 snow stakes that were selected for this study, only 13 had snow present at the time of the lidar survey.

The MS00702 dataset contains additional measurements of SWE at snow stakes in open and forest sites at long-term old-growth forest Reference Stands from 1978 to 2003 (Appendix Table A-2).

Table 2: Description of data sources and models used in this study.

Data analysis activity	Date source name	Description	Application	Citation
Field snow sampling				
	March 16, 2022, snow survey	Snow survey with Mark Raleigh to validate lidar. Methods: transects (5), 3x3m plots (16), and snow pits (2).	Determine landscape patterns of snow, spatial analysis, validate lidar survey.	
	March 1, 2, 2023, snow survey	Four planted forest stands (L305, L306, L704A, and L703) sampled with 30 m transects.	Field data used to determine snow depth and SWE in planted forests.	
Geospatial data				
	March 17, 2022, lidar survey	Lidar survey with airborne laser scanner on helicopter.	This data is used as a high-resolution snow depth dataset.	
	USGS 3D Elevation Program (3DEP)	1-m bare earth digital terrain model.	Differenced with 'snow-on' lidar derived snow surface.	(Lukas & Baez, 2021)
	Canopy height model	1-m canopy height model derived from a 2020 lidar survey.	Raster used for analysis, provided by Dave Bell, USFS.	(Dave Bell, 2023; Quantum Spatial, 2020)
Snow modeling				
	Structure for Unifying Multiple Modelling Alternatives (SUMMA)	Hydrologic model.	Used as a point-based snow model to simulate snowpack at the Upper Lookout benchmark meteorological station site.	(Clark et al., 2015a; Clark et al., 2015b)
	pySUMMA	Python wrapper.	Wrapper used to work with SUMMA.	(Choi et al., 2018)

	North American Land Data Assimilation System	Land-surface model/climate reanalysis hourly data on a 1/8 degree (13.875 km) resolution.	This gridded product was used as forcing data for SUMMA.	(Xia et al., 2012)
	MeteoIO	Open source C++ library specifically designed for using met data for hydrologic science.	Used in Matlab to downscale the climate data from a single NLDAS grid cell.	(Bavay & Egger, 2014)
	Downscaled WY 2010-2022 NLDAS data	Precipitation, air temperature, wind, specific humidity, and longwave and shortwave radiation. Missing pressure needed for SUMMA.	Longwave radiation used as meteorological forcing for SUMMA.	
Snow stake analysis				
	MS00702 – Reference Stand and Historic Road snow course	Snow dataset that includes Federal sampler measurements at 3- to 5-week resolution, 1978-2003, at 6 paired sites in historic Reference Stands.	Historic snow depth and SWE data used in analysis.	(Levno et al., 2023)
	MS00701 – Paired snow stakes	Snow depth and SWE, 1994-2023, measured at 20 paired sites with snow courses and automated snow stakes.	Snow depth and SWE data used in analysis.	(Levno et al., 2023)
Meteorological data				
	Meteorological Data from Benchmark Stations at	Air temperature, relative humidity, dew point, soil temperature, soil	Provisional precipitation, snow, and air temperature used for analysis with	(Daly et al., 2019)

the H.J. Andrews Experimental Forest, 1957 to Present	moisture, battery supply, precipitation (stand-alone), and wind speed and direction. Provisional data files: uplmet_235_5min_2022, uplmet_236_5min_2022	MS007 snow stakes, as well as validate lidar.	
MS00110	Snow water equivalent and snow depth (daily midnight), 1987-2014.	Snow data used for analysis.	(Daly et al., 2019)
MS00111	Air temperature measured by a thermistor.	Meteorological forcing data for SUMMA.	(Daly et al., 2019)
MS00112	Relative humidity measured by a	Meteorological forcing data for SUMMA.	(Daly et al., 2019)
MS00113	Precipitation measured by a heated shelter gauge.	Meteorological forcing data for SUMMA.	(Daly et al., 2019)
MS00114	Wind measured by a propellor anemometer.	Meteorological forcing data for SUMMA.	(Daly et al., 2019)
MS00115	Shortwave radiation measured by pyranometer.	Meteorological forcing data for SUMMA.	(Daly et al., 2019)
MS00120	Snow water equivalent and snow depth (median depth for each hour), 1987-2014.	Snow data used for analysis.	(Daly et al., 2019)
MS00136	Air pressure measured by barometric pressure sensor.	Meteorological forcing data for SUMMA.	(Daly et al., 2019)
Vegetation data			
TV061	Vegetation classification, Andrews	Characterize vegetation in sampled forest stands.	(Lienkaemper et al., 2015)

Experimental Forest
and vicinity
(1988,1993,1996,19
97,2002, 2008).



Photograph 1. Forest stake, close up of camera house. March 2, 2023.



Photograph 2. Open stake. March 2, 2023.

3.1 Field methods

3.1.1 Field sampling of snow and forest characteristics

Snow surveying in the Andrews Forest was conducted in March of 2022 and 2023. Snow depth and snow water equivalent (SWE) were collected at elevations ranging 800 to 1400 m at sites in the open, in former clearcuts, which are now forest plantations (hereafter, “planted forest”), and in mature/old-growth forests (dataset TV061, Table 2) (Lienkaemper & Schulze, 2015). In total, the field sampling was conducted in six planted forests over both surveys in March of 2022 and March of 2023 (Table 3). The planted forest stands were established after clearcutting from 1961 to 1970. Stands ranged in elevation from 950 meters to 1380 meters and had NE, SE, SW, W, and NW aspects. Forest regenerated at different rates in these stands, and forest establishment dates ranged from 1963 to 1981; in many cases forest establishment (i.e., successful survival and growth of planted trees) required one or two decades (Table 3).

The first snow field sampling was conducted in March 2022. Samples were obtained on March 16, 2022, and the lidar survey was completed on March 17, 2022. The goal of the March 2022 field campaign was to validate snow depth values derived from a lidar survey. This is discussed in further detail in Section 3.2.1. Samples were collected along the 1506 road, in adjacent forests, and in a forest clearing created for the Upper Lookout meteorological station. In total there were 14 sites in the open, 6 sites beneath planted forests, and 3 beneath mature forests. Two planted stands, L708 and L704C were sampled for snow depth and SWE on March 16, 2022 (Table 3, Figure 3). Along the 1506 road, snow samples were collected at the R50606 and the R506F6 snow stakes (Figure 3). Of the 23 sites, 18 were plots of 9 m², 3 were 15-meter transects, and 2 were snow pits (Table 3). Snow sampling methods included an avalanche probe, a Federal sampler, and snow pits (see details of field sampling in Section 3.2.1). In general, the forest canopy in the planted stands is only about 30 m tall, whereas trees in the adjacent mature/old-growth forest may reach 80 m, as shown in the canopy height model of 2020 (Figure 2). The L708 stand was certified as reforested in 1976 and the L704C was certified in 1981. These stands have had ~50 years of growth but have canopy conditions that are very different from adjacent unharvested forests (Figure 2).

Snow depth and SWE samples were collected along the road, in the meteorological station clearing, in planted forests, and in mature/old-growth forests (Figure 3). Sampling in 2022 did not extend downslope to the valley floor of Lookout Creek, where the lidar image shows deeper snowpack (Figure 3). See section 3.1.2 for details on lidar acquisition.

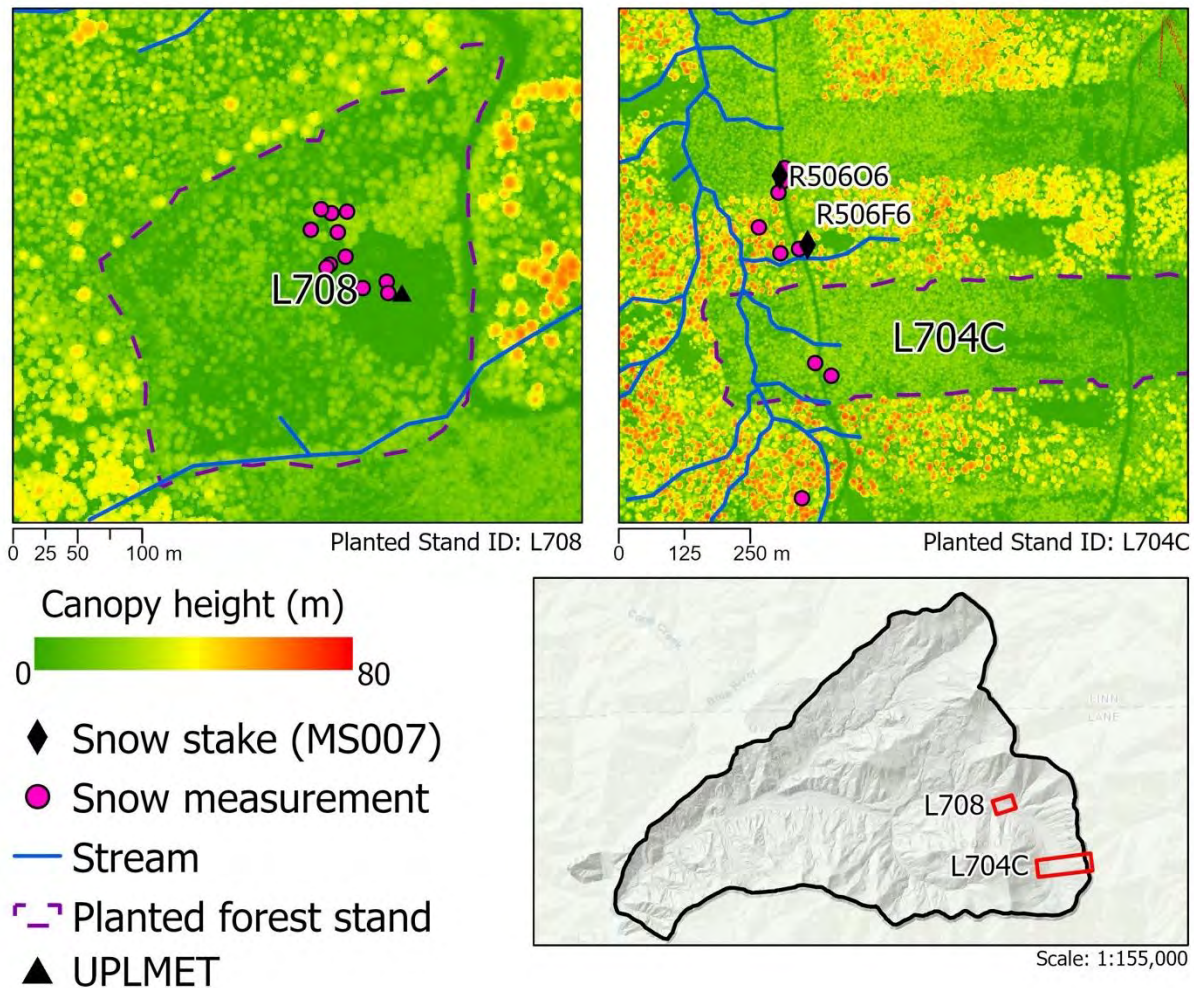


Figure 3. Canopy height model of planted stands relative to March 16, 2022, snow sample locations. The canopy height model was derived from a lidar survey obtained 2020 (Dave Bell, 2023; Quantum Spatial, 2020).

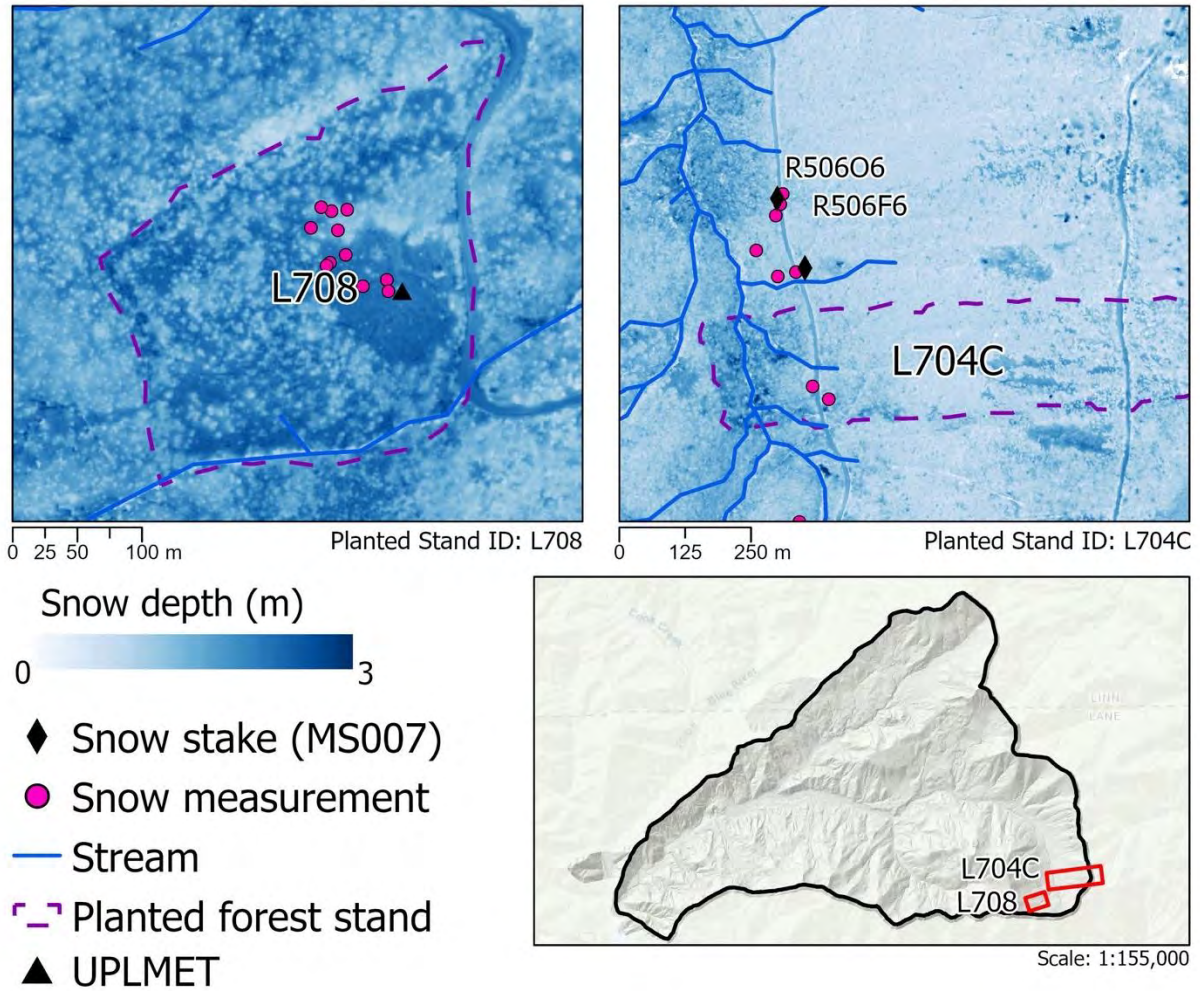


Figure 4. Lidar image of snow depth (flight on March 17, 2022) relative to March 16, 2022 snow sample locations.

The mean canopy height of each of the planted stands that were sampled for snow generally decreased with increased elevation (Table 3). The L708 stand has a particularly low mean canopy height value because the clearing for the Upper Lookout meteorological station is in the center of it. The mean canopy height is an average of all the raster cells that are within the L708 stand. Douglas-fir was the most abundant tree species (Species 1) in the primary canopy layer in the six planted forests that were sampled for snow in stands with elevations below 1,300 meters, and Noble fir was the most abundant tree species in stands with elevations above 1,300 meters. Noble fir was the second most abundant tree species (Species 2) in the planted forest stands below 1,300 m in elevation, and Douglas-fir was the second most abundant species in stands above 1,300 m in elevation, while western hemlock was the second most abundant species in the stand that is less than 1,000 m in elevation. Prior to harvest in the mid-twentieth century these stands consisted of Douglas fir and true fir. These sites were mature/old-growth stands that were harvested in the 1960-1970s and certified as reforested two to more than 20 years later, indicating that these planted forests regenerated slowly. The harvest method in all six of the stands was clearcutting.

On March 1-2, 2023, SWE and snow depth were sampled using a Federal sampler and an avalanche probe at four sites (L704A, L703, L306, and L305) ranging in elevation from 950 to 1380 m (Table 3). Paired snow measurements were taken concurrently at a road site, a plantation stand, and a mature/old-growth stand (Figure 1, Figure 6, Figure 7). Each of the four planted stands was co-located with one of the snow stake pairs from the MS00701 dataset (Figure 6, Figure 7). The MS00701 snow stakes include one stake on the road within the planted forest and one snow stake in the adjacent mature/old-growth forest. Snow measurements were taken at the two stake locations while additional measurements were taken in the planted forest. Canopy height and canopy closure varied, including among the open sites. The roads in which the open stakes are located are generally 5-8 meters across, or five to twenty percent of the height of the adjacent canopy.

After clearcut and planting, the L704A, L703, L306, and L305 stands were certified as reforested in 1981, 1962, 1983 and 1963 respectively. The four stands were replanted with Noble fir and Douglas-fir. Prior to harvest the stands primarily consisted of Douglas-fir and true

fir (Table 3). After 50–70 years of growth the forest canopy in the planted stands is shorter than adjacent older forests (Figure 6), and some of the stands, such as L703, have a higher tree bole density than older forests (Photograph 7).

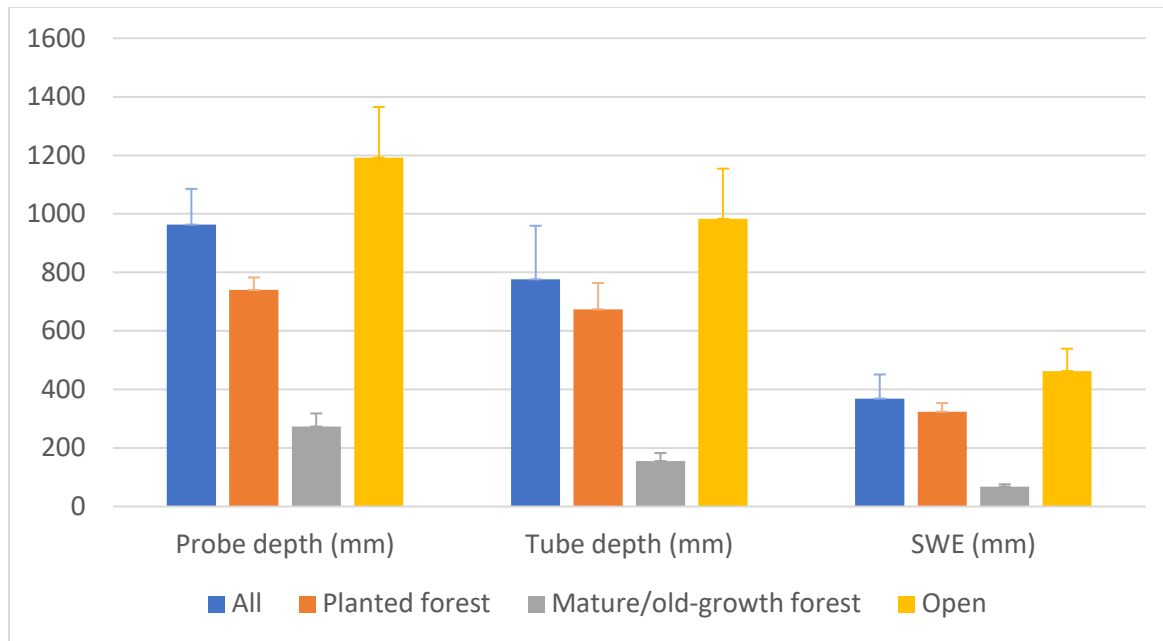


Figure 5. Mean snow depth sampled in the field at 23 sites on March 16, 2022.

Table 3. Characteristics of the planted forest stands in the H.J. Andrews Experimental Forest that were sampled for SWE and snow depth during March 2022 and March 2023. ID = Planted stand identification code and Date = Date of sampling (Lienkaemper & Schulze, 2015). PSME = *Pseudotsuga menziesii*, Douglas-fir, TSHE = *Tsuga heterophylla*, western hemlock, ABPR = *Abies procera*, noble fir.

Stand ID	Elev (m)	Canopy height (m)	Year clearcut	Year certified as reforested	Aspect	Species 1	Species 2	Original stand species	Day sampled
L703	988	25.1	1960	1962	SW	PSME	TSHE	PSME/TSHE	3/2/23
L704A	1145	13.3	1970	1981	W	PSME	ABPR	PSME/true fir	3/2/23
L704C	1163	11.4	1970	1981	W	PSME	ABPR	PSME/true fir	3/16/22
L305	1225	16.7	1961	1963	NW	PSME	ABPR	PSME/true fir	3/1/23
L708	1298	8.7	1965	1976	NE	ABPR	PSME	PSME/true fir	3/16/22
L306	1380	9.9	1961	1982	SE	ABPR	PSME	PSME/true fir	3/1/23

Table 4. Summary of mean snow depth, SWE, and snow density at 23 sites sampled on March 16, 2022. Site: T = 15 m transect, SP = snow pit, UPL = plot in the UPL met station area, 1506 = 1506 road. Cover = P = planted forest, M = mature/old-growth forest, O = opening. Probe depth = field measured snow depth by avalanche probe, tube depth = field measured snow depth by Federal sampler. Note that values for snow pits are only one sample, whereas values for transects are means of 15 samples, and values for plots are means of 16 samples.

Site	Cover	Elevation (m)	Probe depth (mm)	Tube depth (mm)	SWE (mm)	Density (%)
T 3	P	1163	760	--	--	--
SP	P	1298	680	--	300	44
UPL 6	P	1300	670	580	305	52
UPL 8	P	1300	840	655	330	50
UPL 7	P	1301	610	529	254	48
UPL 9	P	1303	880	932	432	46
1506 6	M	1117	250	189	76	40
1506 6	M	1128	360	176	76	43
1506 6	M	1136	210	101	51	50
1506 5	O	965	380	340	178	52
1506 5	O	966	390	290	152	52
1506 5	O	967	220	290	127	43
1506 6	O	1120	750	743	330	44
1506 6	O	1122	830	832	356	42
1506 6	O	1122	910	882	356	40
T 2	O	1157	1210	--	--	--
T 1	O	1187	1100	--	--	--
UPL 4	O	1299	1680	1084	559	51
UPL 5	O	1299	1850	1714	660	38
UPL 1	O	1302	1830	1651	762	46
SP	O	1304	1830	--	777	42
UPL 2	O	1305	1790	1348	610	45
UPL 3	O	1305	1920	1638	686	42
Ave-All		1194	963	776	369	46
SD			586	531	234	4
n			23	18	20	20
SE			122	183	82	10
Ave P		1277	740	674	324	48
SD			105	180	66	3
n			6	4	5	5
SE			43	90	30	1
Ave- M		1127	273	155	68	44
SD			78	48	15	5

n		3	3	3	3
SE		45	28	8	3
Ave- O	1173	1192	983	463	45
SD		648	569	265	5
n		14	11	12	12
SE		173	172	77	1

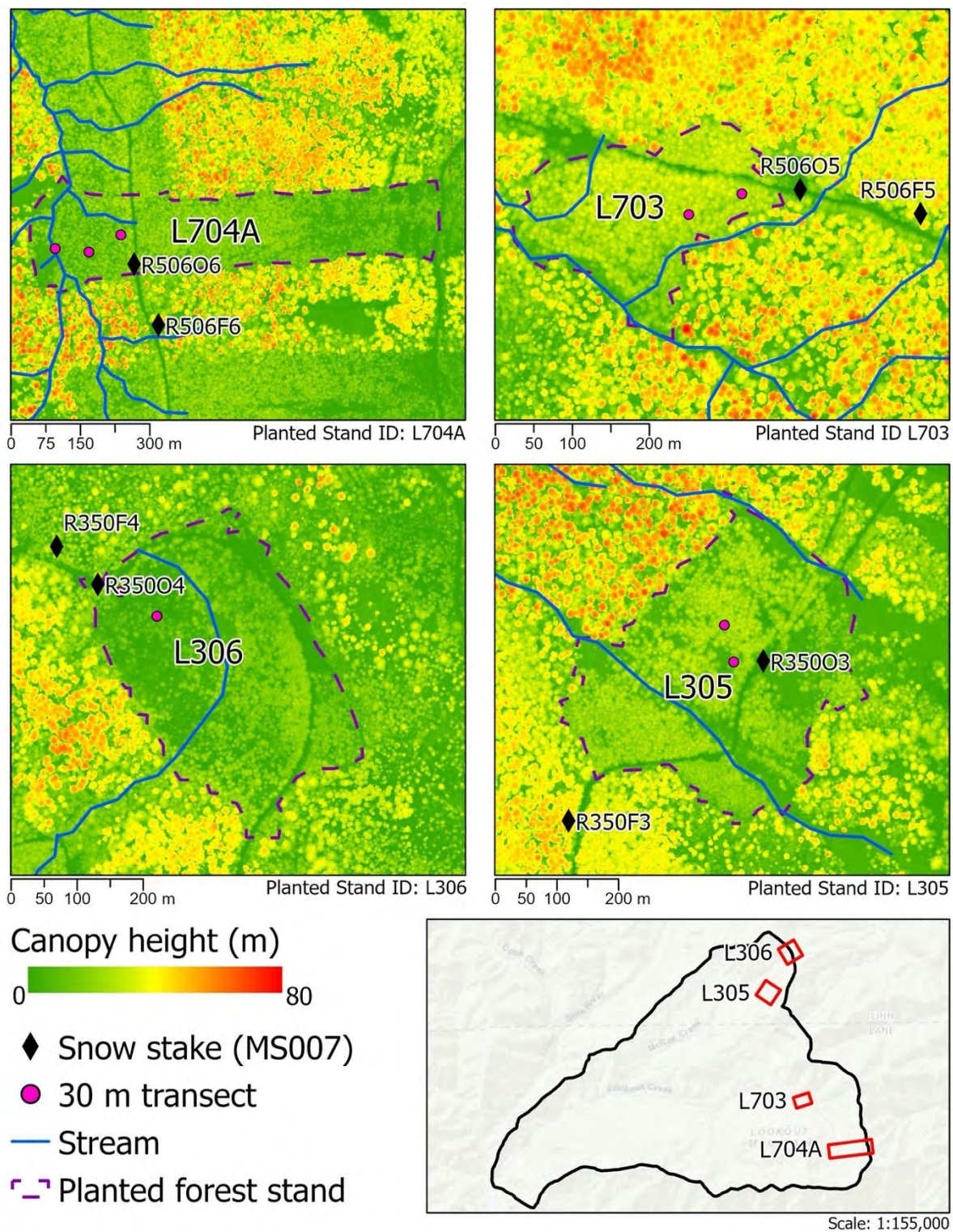


Figure 6. Canopy height model of planted stands relative to March 1 and 2, 2023 snow sample locations. The canopy height model was based on lidar obtained in 2020 (Quantum Spatial, 2020).

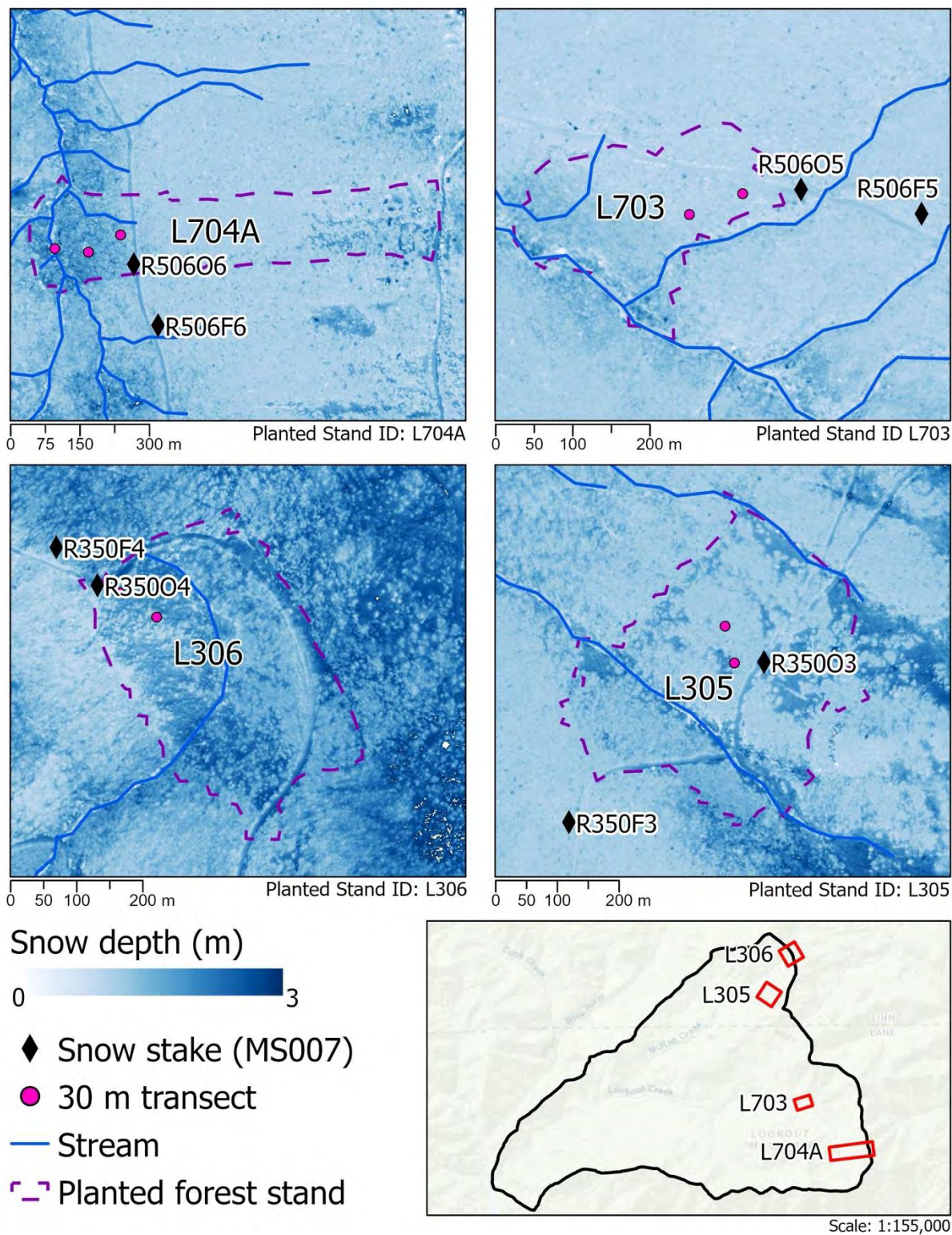


Figure 7. Lidar image of snow depth (taken on March 17, 2022) relative to March 1 and 2, 2023 snow sample locations.

Each site sampled during the March 1-2, 2023 field campaign included a road site, a site beneath a planted forest, and a site under a mature/old-growth forest stand. To collect concurrent snow measurements at these three site types, the snow survey was completed by a team of three people. I collected snow measurements in the planted forest with an avalanche probe and a Federal sampler, while Andrews Forest staff (Ben Nash and Greg Downing) collected snow measurements with a Federal sampler at the snow stake in the open and snow stake in the older forest (Photograph 1). This sampling design allowed snow depth and SWE to be sampled (1) beneath a planted forest canopy (2) beneath a mature/old-growth forest canopy and (3) at the adjacent road site representative of a forest opening. In the planted forests, snow was sampled along two, 30-meter transects parallel to contours approximately 20- and 100-meters downslope from the road. Ten snow depth measurements were taken with an avalanche probe at 3-meter intervals along each transect. SWE was collected with a Federal sampler at 10 m intervals along the transect, but SWE measurements were incomplete due to lack of time. The sampling scheme was slightly different at the snow stakes, where Ben and Greg took three samples with a Federal sampler at 1–2-meter distances from each stake at random points around the stake.

On March 1, 2023, the L305 (NW/1248m) and L306 (SE/1379m) planted stands were sampled along the 350 road. The highest elevation site (L306) was sampled in the morning, while the lower-elevation site (L305) was sampled in the afternoon. The weather was partly cloudy, and temperature fluctuated above and below zero degrees Celsius as clouds passed over and caused periods of shading. The SE-facing L306 stand has sparse tree cover despite 60 years of regeneration since clearcutting in 1963 and a deep snowpack (Table 3, Photograph 3). In contrast, the L305 planted forest stand has a very dense, closed canopy, a NW aspect, and a shallow snowpack (Photograph 4).

On March 2, 2023, the L704A (1145m) and L703 (988m) planted stands were sampled along the 1506 road. The higher elevation site, L704A, was sampled in the morning, while the lower elevation site, L703, was sampled in the afternoon. The L704A stand had deeper snow, particularly at sampling locations closer to the valley floor of Lookout Creek (Photograph 5). Snow at the bottom of the Lookout Creek (Photograph 6) bridges the creek and surrounding

riparian vegetation. Snow depth at this location was measured as $> 2\text{m}$ on March 2, 2023. The L703 stand has a high tree bole density and canopy closure with some near ground vegetation such as vine maple (Photograph 7). Snow beneath the canopy of the L703 stand was dense and had a high water content at the time of sampling. Snow in the L703 stand stuck to the tree boles and the tree branches.



Photograph 3: L306 stand and transect (20 m from road) location.



Photograph 4: L305 stand and transect location. The top images are 20 m from road and the bottom images are 100 m from the road.



Photograph 5. L704A stand and transect location. The top images are 20 m from road and the bottom images are 100 m from the road.



Photograph 6. The valley floor of Lookout Creek in the L704A stand. The top images are 20 m from road and the bottom images are 100 m from the road.



Photograph 7. L703 stand and transect location. The top images are 20 m from road and the bottom image is 100 m from the road.

3.1.2 Lidar image acquisition

A 'snow-on' airborne lidar survey was conducted in the Andrews Forest on March 17, 2022. The lidar survey was conducted by the National Center for Airborne Laser Mapping (NCALM), a collaboration between the University of Houston (the operational center) and the University of California Berkeley (the data processing center) supported by the Division of Earth Sciences at the National Science Foundation (NSF) (<https://ncalm.cive.uh.edu>).

Snow water storage is often quantified by peak SWE amount and peak SWE date (Sproles et al., 2013), so efforts to measure snow are often focused on collecting measurements on that date. Based on historical data, the lidar survey was scheduled for the estimated peak SWE period (mid-March). The lidar image was obtained on March 17, 2022, four to five weeks before the realized date of maximum SWE at the UPLMET snow pillow, which occurred on May 3, 2022 (Figure 8). Peak SWE was expected to occur in early March, but during WY 2022 a significant accumulation period occurred in April, following a significant mid-winter melt period (Figure 8). The lidar survey (orange dashed line) was completed at a time after some mid-winter melt, but still in the accumulation season. Although the survey date did not align with the peak SWE date, it was conducted within the snow season at the end of a 2.5-month period of relatively constant snow, and it was completed before a large melt event (Figure 8). The SWE at the UPLMET snow pillow at the time on the lidar survey was ~ 625 mm and the peak SWE for the water year was ~800 mm, on May 3, 2022.

To collect the 'snow-on' survey NCALM employed an airborne laser scanning (ALS) system (RIEGL VG-580 H2225798) mounted to a Robinson R66 helicopter. The system was configured with pulse repetition frequency of 300 kHz, a scanning rate of 200/s, scan angle of +/- 37.5 degrees, a scan overlap of 50%, and a beam divergence of 0.25 mrad, which yielded a laser footprint diameter of 12.5 cm. The average altitude of the helicopter was 500 m. NCALM lidar products have a typical nominal elevation accuracy of 5 to 10 cm with a horizontal uncertainty of 20 to 40 cm over flat open surfaces. The mean point density for the 'snow-on' survey was 23.3 points per square meter, but this density metric for returns varies considerably given the significant terrain and forest structure variation of the area of interest (AOI) (OpenTopography, 2022).

Data collected from the 'snow on' lidar survey were classified and QA/QC processed by NCALM. Due to the remoteness of the area, ground control points could not be collected, so NCALM collected kinematic GPS in the instrument calibration area during the flight. The calibration area was near Creswell, OR, about 80 km WSW of the Andrews Forest. The NCALM data processing team produced lidar-derived surface models, including a 1 m-resolution snow surface digital terrain model (DTM) and a 1 m digital surface model (DSM) (OpenTopography, 2022).

A map of lidar-derived snow depth was created by differencing the 'snow-on' DTM collected by NCALM with a 'snow-off' DTM collected on July, 2022 by the United States Geological Survey (USGS) as part of the 3D Elevation Program (3DEP) (Thatcher et al., 2017). 3DEP data are free and open source. The data were downloaded as individual tiles that were combined to form one continuous raster using the Mosaic geoprocessing tool in ArcGIS Pro. Differencing was conducted using the Raster Calculator in ArcGIS Pro. The extent of the snow-free lidar exceeded the snow-covered extent in all cases. The result was a raster of 1 m resolution in which each one square meter cell represents a difference in ground surface and snow surface elevations, equivalent to a snow depth measurement. To better account for the high spatial variability of snow in this analysis, the raster was resampled to images with 3, 5, and 10 m spatial resolution using bilinear interpolation. The result of the difference of the two raster datasets will hereafter be referred to as a snow height model (SHM). This is a 1 m raster consisting of snow depth estimates for each raster cell. The resulting raster contained 2.9% negative values, mainly located in areas of high topographic relief. High elevation areas had some cloud cover that may have increased the occurrence of negative values in those areas.

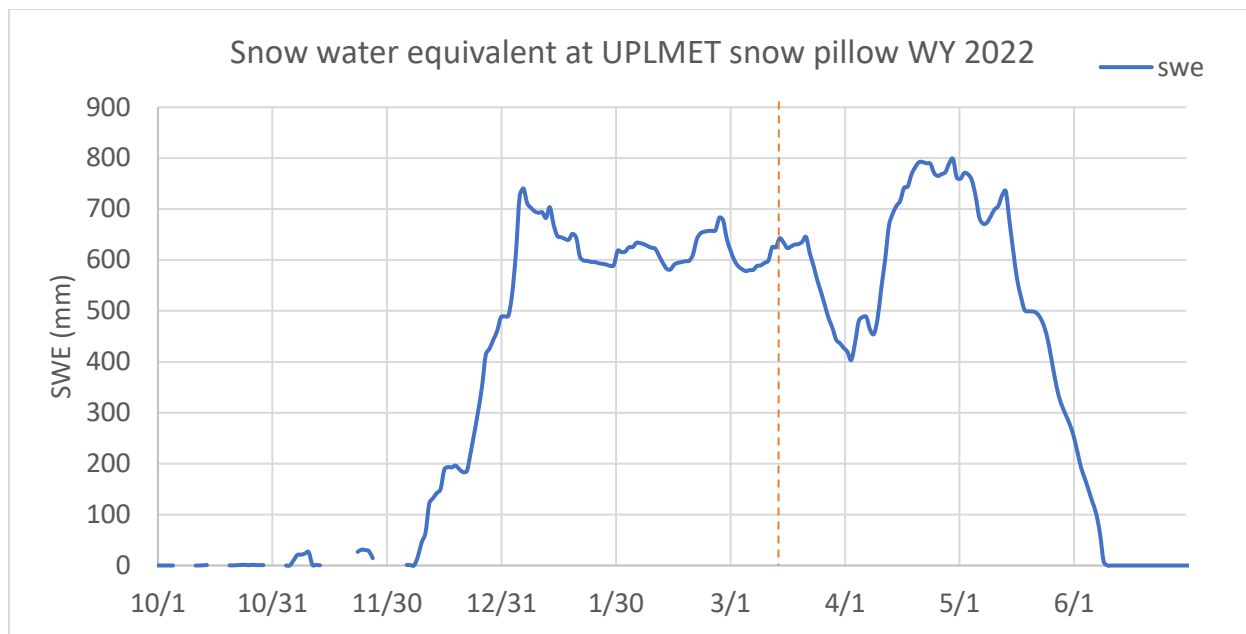


Figure 8. Snow water equivalent during WY 2022 measured at the Upper Lookout meteorological station (UPLMET) (1298 m). The dashed line indicates when the 'snow-on' lidar survey was collected.

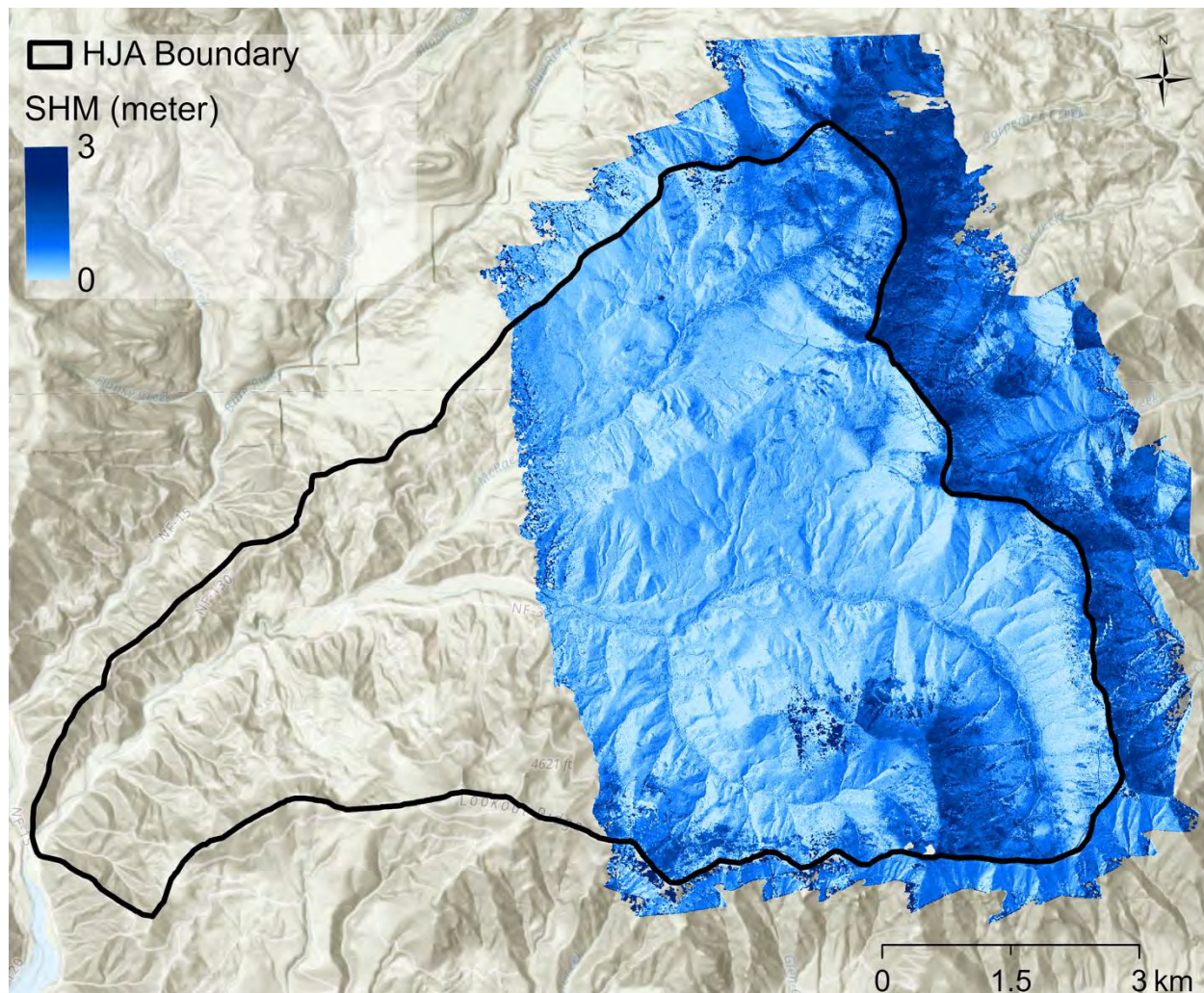


Figure 9. Snow height model on March 17, 2022 in a 52 km² survey area of the upper elevations of Andrews Forest and adjacent watersheds.

3.1.3 Meteorological station data about snow and other climate variables

Snow depth and SWE are measured at the CENMET, UPLMET, VANMET, and VARMET meteorological stations in the Andrews Forest (Figure 1). The snow measuring sites include a sonic snow depth sensor (since 1997) and a pressure sensing snow pillow containing an anti-freeze solution. The snow pillow measures how much liquid water equivalent is in the snowpack by weighing the snow with a pressure transducer. Snow density is calculated from the snow depth measured at the acoustic depth sensor and SWE from the snow pillow. At UPLMET the acoustic sensor is above the pillow but at CENMET, VANMET, and VARMET the acoustic sensor is not above the pillow, introducing uncertainty in the density measurements. Furthermore, the error in the acoustic sensor measurements increases in snow depth <10 cm. SWE has been measured continuously from 1987 (at Vanmet) or 1994 (at Cenmet and Uplmet) to the present, whereas snow depth measurements began in 1997 at these sites (Table 2). QA/Qced data were available until 2014, and provisional data were available starting in 2014 to 2023. Snow data from UPLMET were used for model analysis and calibration.

Besides snow data, this study used air temperature, relative humidity, air pressure, precipitation, shortwave radiation, and wind speed measured at the Upper Lookout meteorological station (UPLMET) (Daly et al., 2019) as forcing data in the SUMMA model. Air temperature (method AIRUPL01) is measured by a thermometer at 450 cm height; mean output is every 5 minutes. Relative humidity (method RELUPLO01/REL012) is sampled using a Campbell Scientific model HMP45C probe housed in a R.M. Young Gill radiation shield at 450 cm height; mean output every 15 minutes. Air pressure (ATMUPLO1) is sampled by a Campbell Scientific barometric pressure sensor, output every 15 minutes. Precipitation (method PPT016) is measured using a shelter-top heated rain gage with 13.3-inch orifice, tank gage, and a wind shield at 625 cm on the tower with a Campbell Scientific data logger. Shortwave radiation (method RAD021) is measured by a Kipp and Zonen solar radiation pyranometer, model CM-6B, with a Campbell Scientific data logger at 615 cm height; mean, total, and maximum solar radiation is output every 5 minutes. Wind (method WND008) speed and direction are sampled every 15 seconds by a propeller anemometer (RM Young Model 05103 Wind Monitor) mounted

to the tower at 1000 cm with a Campbell Scientific datalogger. Mean wind speed and direction are output hourly with a detection level 1 m/sec, for wind speeds >0.4 m/s.

3.1.4 Snow survey stake methods

Long-term snow data were available from 1994 to 2022 (MS00701), as well as 1978 to 2003 (MS00702) (Levno et al., 2023). These data were used to calculate snow disappearance date and snow depth loss rates, and to compare snow depths and SWE values between paired sites in openings and under forests (Appendix A).

Annual, mean snow density by water year was calculated at ten sites of paired snow stakes from 1994 to 2014 using long-term SWE measurements from the MS00701 dataset. Long-term SWE data were used to calculate the annual mean snow density for each forest and open site. This density value was applied to the continuous snow depth at camera-sampled snow stakes following the SWE equation (Dewalle, 2008):

$$SWE = d \frac{\rho_s}{\rho_w}$$

Where SWE is water equivalent (m), d is snowpack depth (m), ρ_s is snowpack bulk density (kg/m^3), and ρ_w is the density of liquid water (kg/m^3).

3.2 Data analysis

3.2.1 Validation of lidar image vs. field, meteorological station, and snow stakes

Lidar-derived snow depth values were compared to data collected in the field, data measured at the paired snow stakes, and data measured at the snow pillows of the meteorological stations in the Andrew Forest.

Field snow depth data were collected by a team of four on March 16, 2022 using procedures described above in Section 3.1.1. The snow survey was conducted on the day that the lidar survey was scheduled to take place, March 16, 2022, but cloudy weather delayed the flight to March 17, 2022. This one-day lag should not cause any significant discrepancies in snow depth. The goal of the snow survey was to collect snow depth ground truth measurements that could be compared to the value of a raster cell, so the sampling scheme

was focused on establishing plots as 3x3 m squares that could be compared to 3-meter raster cells in the snow height model. Site locations were recorded using a recreational-grade GPS, so there was uncertainty of 2-6 meters. Each square plot was measured in the snow using an avalanche probe of 3 meters. The square plots were established along the 1506 road beginning at 950 m in elevation and ending at the Upper Lookout Meteorological station (UPLMET) at 1298 m. The station is located in a forest clearing that is 100 meters in diameter. The forest was cut for the installation of UPLMET and further clearing of trees occurred in 2018. The greatest number of snow samples collected during the survey were in the UPLMET clearing and adjacent forests.

Snow depth and density data on March 16, 2022 were collected at 23 locations along the 1506 road in the Andrews Forest, using procedures described above in Section 3.1.1. Of the 23 measurements, eighteen were plots, three were transects, and two were snow pits (Table 4, Figures 3 and 4). The area of each plot was 9 m². Plots were designed as squares with the intent to mimic a single pixel to facilitate comparison to the snow depth values from one pixel within the snow height model. Snow depth measurements were taken at 16 points along the edges of each plot using a 3-meter long avalanche probe. SWE was also collected at 3 of the 16 points in each plot using a Federal sampler. The 16 snow depth measurements were averaged to obtain a mean depth for each plot. The three SWE measurements were averaged to obtain a mean SWE value for each plot. Snow depth measurements did not differ between avalanche probe and snow pits (Figure 5).

3.2.2 Comparison of lidar snow depth by forest cover type

Zonal statistics of the snow height model and canopy height model were calculated at ten paired sites of mature/old-growth forest and planted forest (Figure 10). Planted forest sites were located within the forest plantations that were closest in proximity to each of ten pairs of the MS00701 snow stakes that were located within the 'snow-on' lidar survey. Ten pairs of 60x60 m polygons were located on the snow depth model and canopy height model (Figures 11 and 12). Each pair consisted of a polygon in a planted forest and a polygon in an adjacent mature/old-growth forest at the same elevation and at a minimum distance of 25 m from the

edge of the stand (Figure 10, Figure 11). The 60x60 m polygons were selected visually to represent average canopy conditions, avoiding valley floors, very steep slopes, and openings. Summary statistics of the canopy height model and the snow height model raster cells within the polygons were produced using geoprocessing tools in ArcGIS Pro. The mean and standard error of lidar-derived snow depth within each polygon were calculated using the Zonal Statistics and Raster to Point geoprocessing tools in ArcGIS Pro.

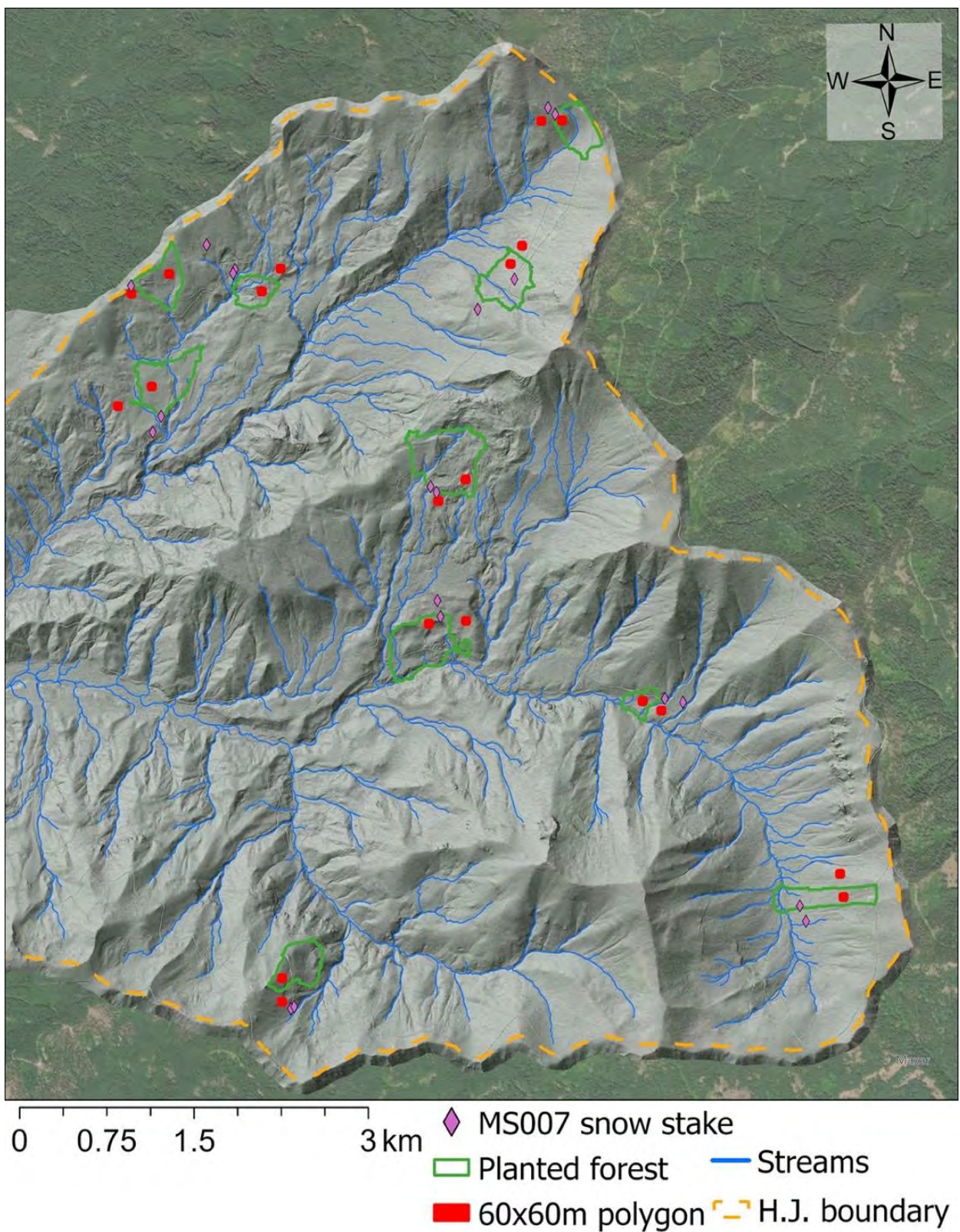
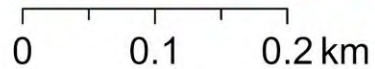
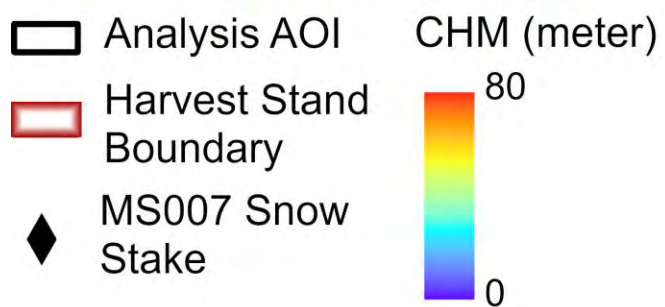
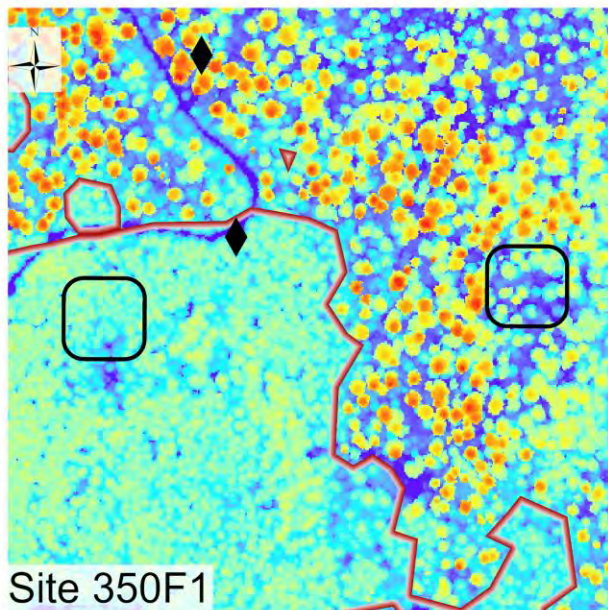
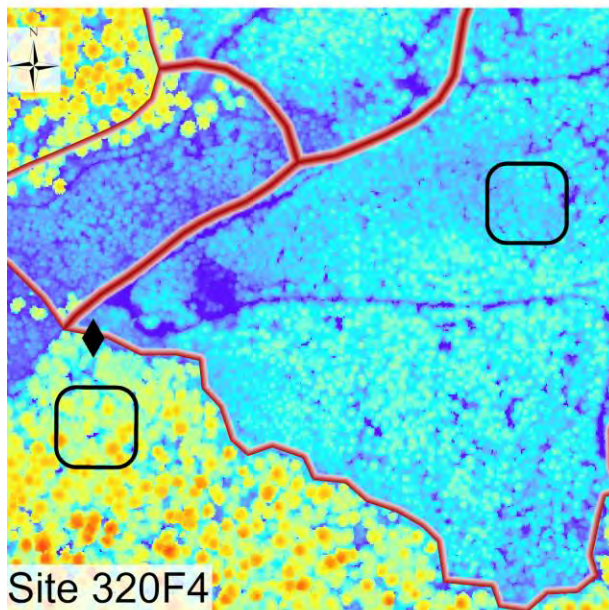
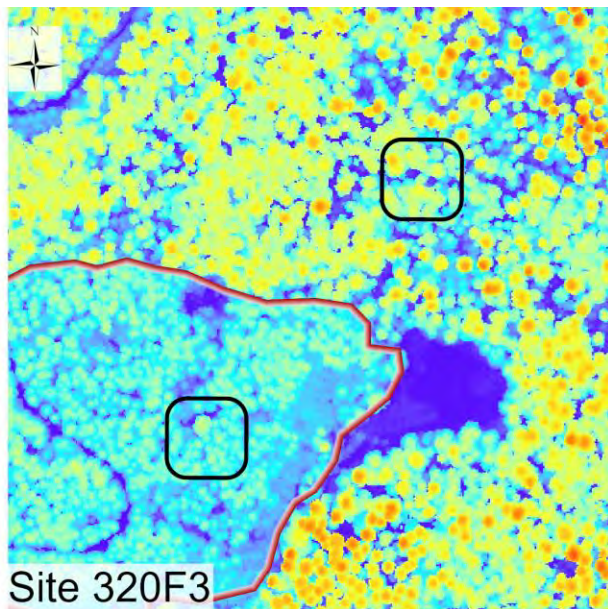
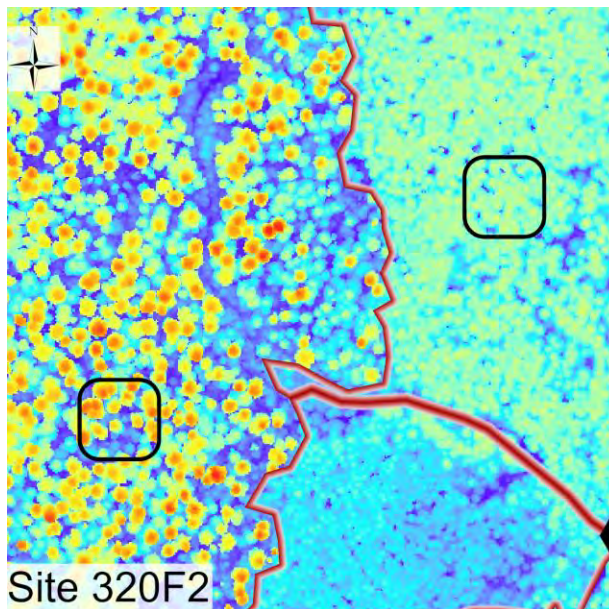
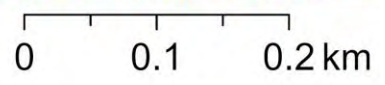
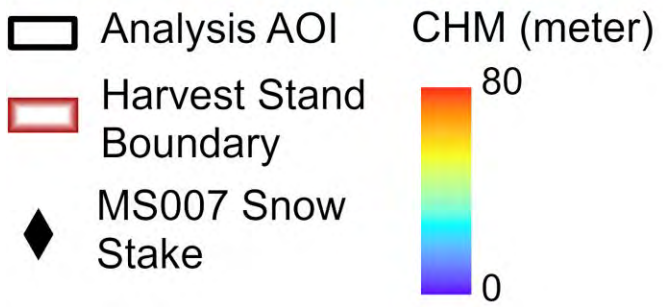
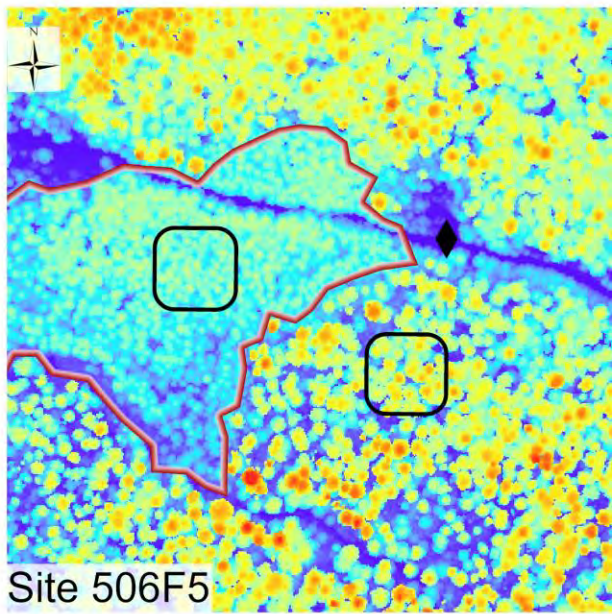
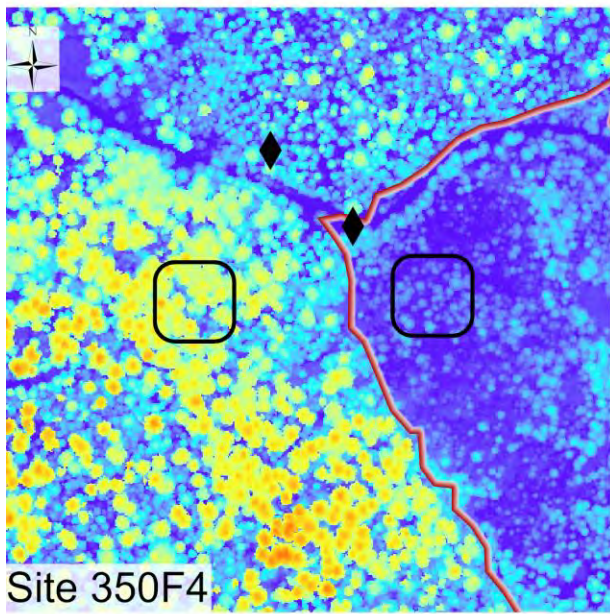
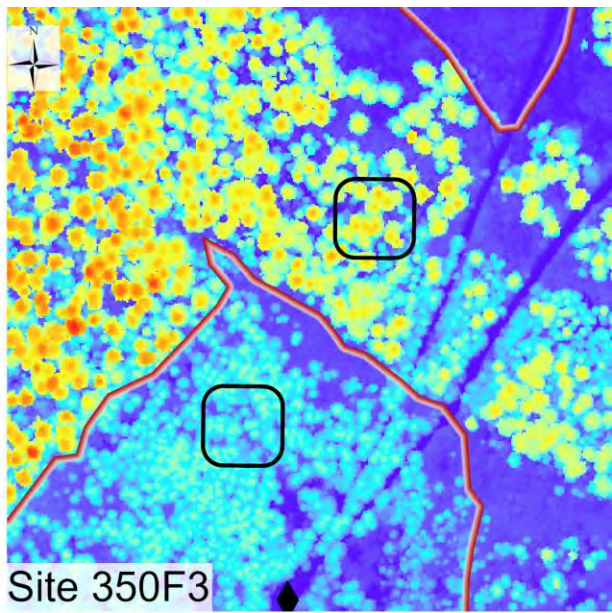
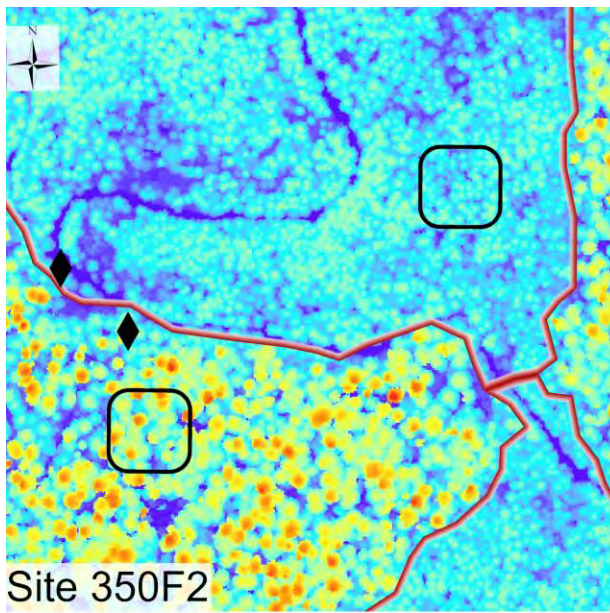


Figure 10. Locations of 60x60 m polygons used for sampling of canopy height and snow depth in planted forest stands and adjacent mature/old growth forest stands.





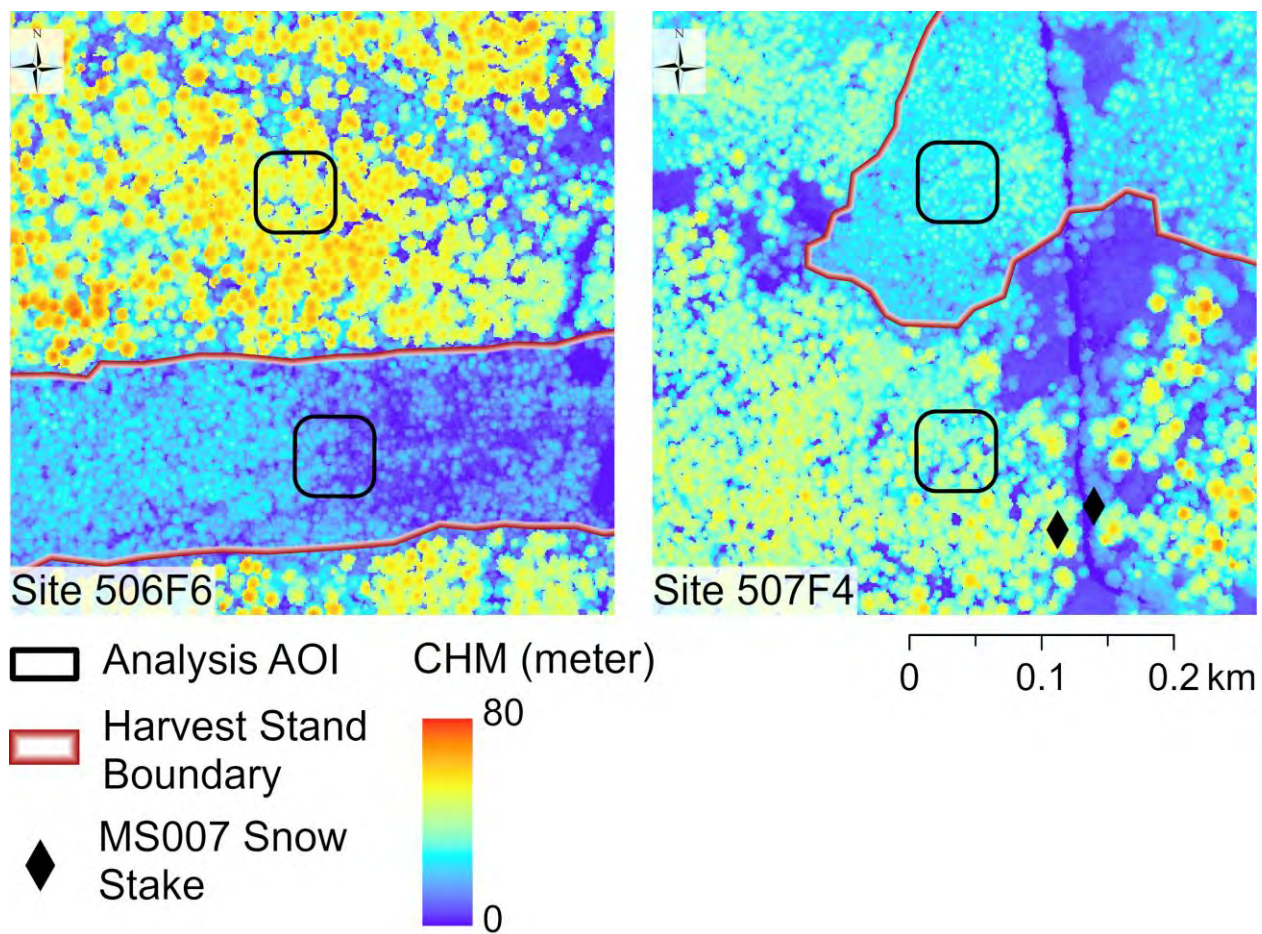
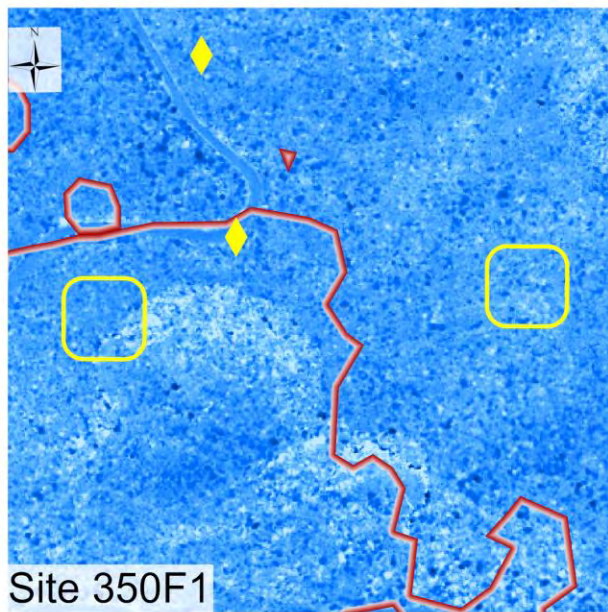
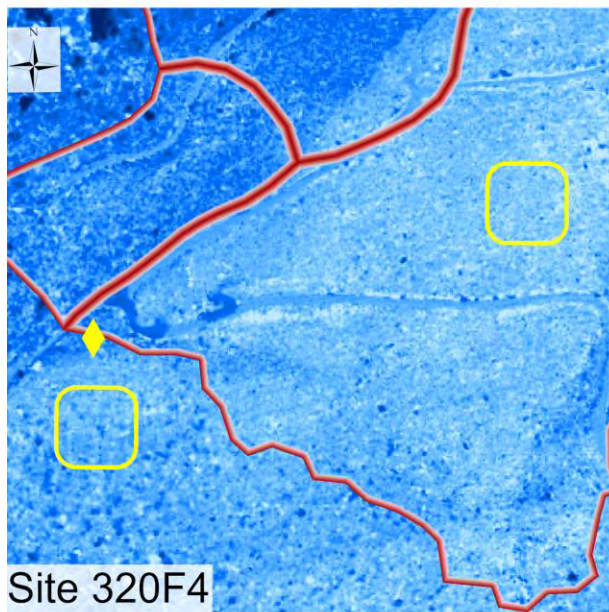
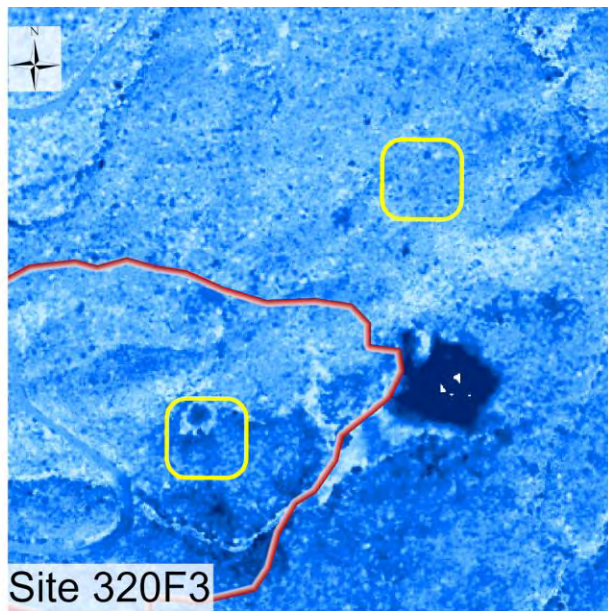
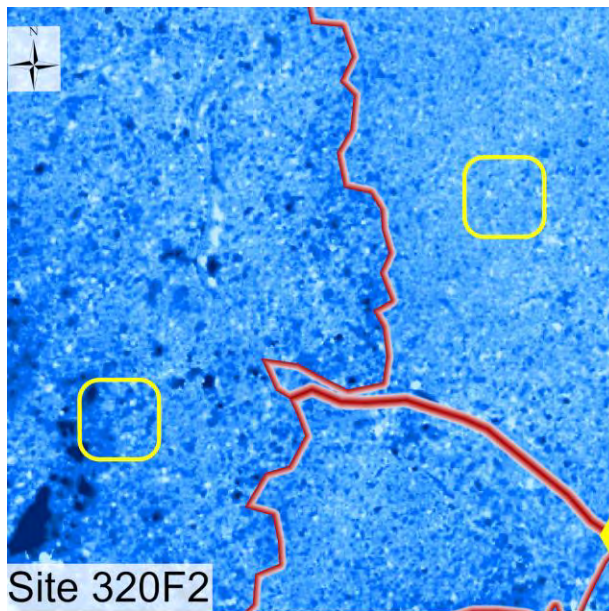
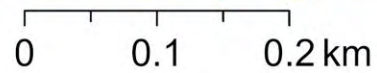


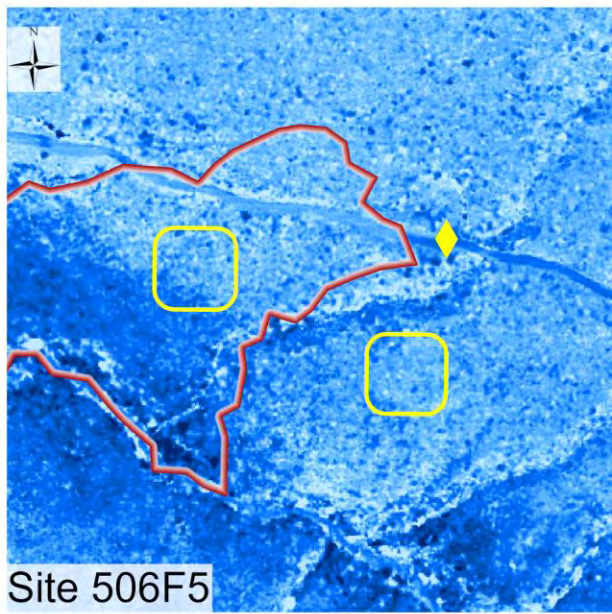
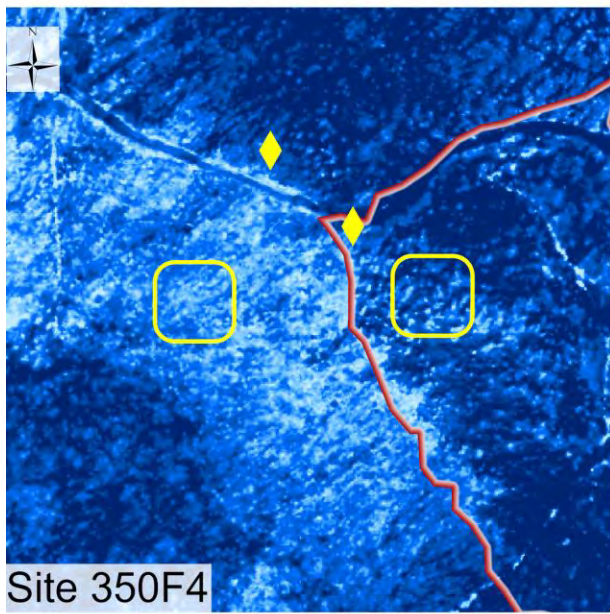
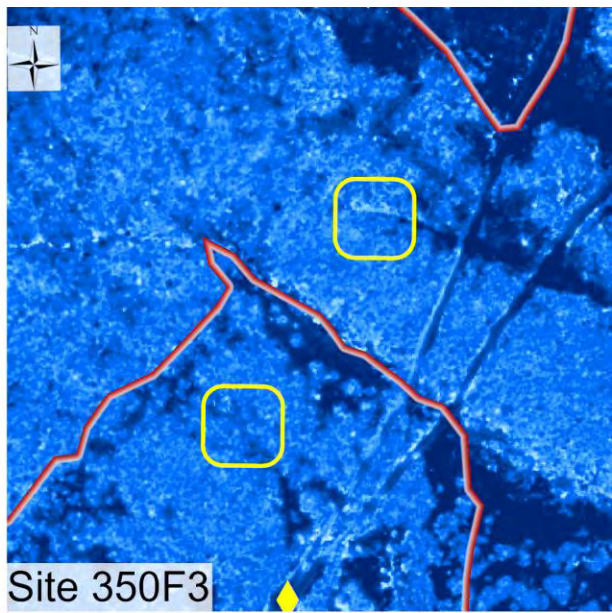
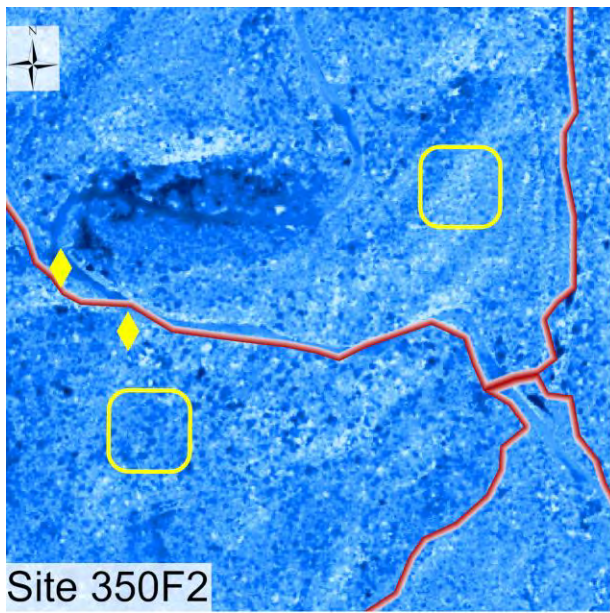
Figure 11. Ten pairs of 60x60 m polygons sampled for lidar-derived snow depth superimposed on the canopy height model.






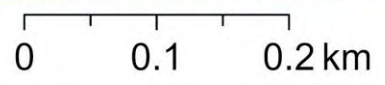
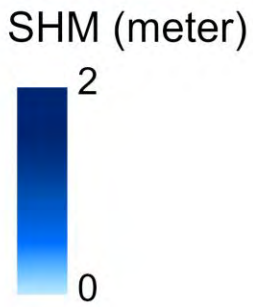
-  Analysis AOI
-  Harvest Stand Boundary
-  MS007 Snow Stake

SHM (meter)





-  Analysis AOI
-  Harvest Stand Boundary
-  MS07 Snow Stake



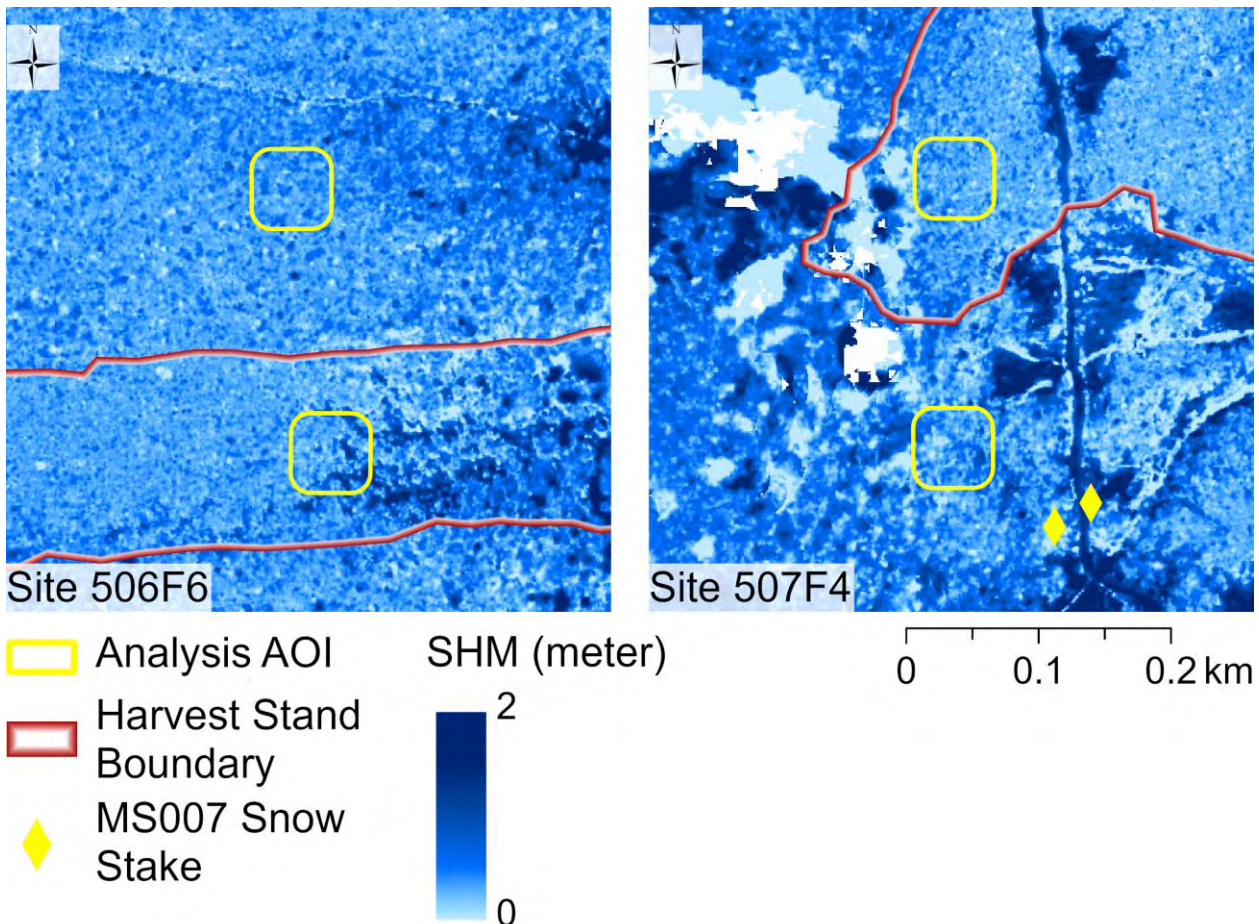


Figure 12. Ten pairs of 60x60 m polygons sampled for lidar-derived snow depth superimposed on the snow height model (lidar-derived snow depth).

3.3 Snow modeling

The structure for unifying multiple modeling alternatives (SUMMA) (Clark et al., 2015a, 2015b) was applied as a point-based snow model to simulate seasonal snowpack in the open and beneath a conifer forest from the water year 2014 to water year 2018. The process-based, hydrologic modeling framework is a multi-physics model that simultaneously simulates multiple process of the hydrologic cycle. The SUMMA modeling framework allows the user to experiment with different model representations of each part of a hydrologic system, enabling a researcher to perform a systematic evaluation of different parametrizations of the same process, parameter values, and flux parameterizations. The design of the SUMMA model integrates multiple modeling approaches with a common set of conservation equations enabling researchers to understand the impact of different modeling assumptions on model behavior. This study applied SUMMA to (1) attempt to reproduce measured snowpack in the opening at the Upper Lookout meteorological station using forcing data from that meteorological station, (2) test how the parameterization for canopy interception of snow affects simulated accumulation, using two of the most common interception models in global snow models, Hedstrom and Pomeroy (1998) and Andreadis (2009), and (3) simulate snowpack response to the presence of canopy cover in conifer stands such as those of the Andrews. Canopy interception decreases snow accumulation significantly beneath forests in warm snow climates, so this study uses SUMMA to investigate that process.

SUMMA is written in Fortran 90, so in order to work with SUMMA in an objected-oriented computer programming language, this study utilized a Python library for wrapping the SUMMA modeling framework called pySUMMA (Choi et al., 2018).

Table 5. Model decisions used in SUMMA.

Decision	Used	Default replaced
soilCatTbl	ROSETTA	
vegeParTbl	MODIFIED_IGBP_MODIS_NOAH	
soilStress	NoahType	
stomResist	BallBerry	
fDerivMeth	analytic	
num_method	iterative	
LAI_method	monTable	
f_Richards	mixdform	
groundwatr	bigBuckt	
hc_profile	pow_prof	
bcUpprTdyn	nrg_flux	
bcLowrTdyn	presTemp	
bcUpprSoiH	liq_flux	
bcLowrSoiH	drainage	
veg_traits	CM_QJRMS1988	
rootProfil	powerLaw	
canopyEmis	difTrans	
snowIncept	stickySnow	lightSnow
windPrfile	logBelowCanopy	
astability	louisinv	
compaction	anderson	
snowLayers	CLM_2010	
thCondSnow	smnv2000	jrjn1991
thCondSoil	funcSoilWet	
canopySrad	noah_mp	BeersLaw
alb_method	varDecay	
spatial_gw	localColumn	
snowDenNew	hedAndPom	
snowUnload	meltDripUnload	

3.3.1 Model forcing

The SUMMA framework simulates thermodynamics (storage and flux of energy) and hydrology (storage and flux/transmission of water). The modeling domain extends from the atmosphere above the canopy to the river channel and includes the dominant biophysical and hydrologic processes such as runoff generation, canopy transpiration, canopy interception, within and below-canopy turbulence, and radiation transfer through the canopy. For each physical process, SUMMA includes equations that represent hypotheses of process representations that are used in global land surface and hydrologic models (Clark et al., 2015a, 2015b). Generally, the meteorological forcing data that are required to drive processes within hydrologic models are: air temperature, air pressure, wind speed, specific humidity, precipitation, incoming short wave, and incoming long wave radiation.

In this study, the SUMMA framework was applied as a snow model to investigate 1) how snowpack varies interannually, 2) how the presence or absence of canopy affects snowpack, and 3) how snowpack ablation and accumulation under a conifer forest varies depending on representation of canopy interception. Using meteorological forcing data from the Upper Lookout station, SUMMA simulated snowpack accumulation and ablation at a 1-hour resolution. The model uses the five-layer snow layering scheme from the Community Land Model to simulate energy and water exchange between layers within the snowpack (Lawrence et al., 2011).

The meteorological forcing data for WY 2014-2018 used in this model were obtained from the Upper Lookout Meteorological Station (UPLMET) and the Phase 2 of the North American Land Data Assimilation System (NLDAS-2) (Mitchell et al., 2004). Data on air temperature, air pressure, wind speed, relative humidity, precipitation, and incoming short wave were obtained from UPLMET and longwave radiation data were obtained from NLDAS (Table 2). Specific humidity was not available at UPLMET, so it was calculated using relative humidity, air temperature, and pressure using Equation 1 (C. Lumbrazo, personal communication):

Equation 1

$$\text{spechum} = RH * \varepsilon^{((17.67 * (Tn - Tfrz))/(Tn - 29.65)) / (0.263 * Pn)}$$

where P is pressure (Pa), T is air temperature (K), and RH is relative humidity (%).

The meteorological station, UPLMET, does not have a pyrgeometer that measures longwave radiation data, so longwave data from NLDAS-2 were used in the SUMMA forcing dataset. With the help of Mark Raleigh, the data were downloaded using Google Earth Engine at 1/8th degree resolution, then downscaled to the UPLMET site using the Meteo-IO library in C++ using a Matlab wrapper (Bavay & Egger, 2014). The longwave radiation from the NLDAS-2 model were compared to longwave radiation data measured by meteorological station at a similar elevation in the Andrews, the Vanilla Leaf Meteorological Station (1275m) (VANMET). Using a qualitative/visual analysis of yearly, cumulative sums, it was concluded that the longwave radiation outputs from NLDAS were underestimated compared to longwave radiation measured at VANMET. To bring modeled longwave data closer to that measured at a comparable meteorological station, a uniform addition of 40 W/m² was added to the longwave radiation forcing used for model forcing.

The SUMMA model was run using default model decisions from the original test cases (M. P. Clark et al., 2021), except in three cases (Table 5). Those decisions are explained below.

The canopy interception of snow decision, 'stickysnow' was selected for model simulation because it includes the interception parameterization that was designed from empirical measurements collected in a climate similar to that of the study area, the Umpqua National Forest, by Storck et al. (2002) (Andreadis et al., 2009). The other snow interception decision, 'lightsnow', includes a canopy interception parameterization that was designed from measurements collected in boreal forests in southwest Canada (Hedstrom & Pomeroy, 1998). Interception modeling equations are described in greater detail in Section 3.3.3. This study assumed that the Andreadis et al. (2009) parametrization was best suited for the study site. The decisions for canopy shortwave radiation (canopySrad) and thermal conductivity of snow (thCondSnow) were selected by conducting sensitivity analyses on a test dataset, WY 2014, to determine which model decision replicated measured snow depth and SWE at UPLMET.

3.3.2 Sensitivity analysis, presence of conifer forest

SUMMA has a structural core of conservation equations that is built up of routines from other models, such as the Noah-multiparameterization (Noah-MP) land surface model (LSM) (Clark et al., 2015a, 2015b). A LSM is a numerical model that simulates the partitioning, absorption, and transfer of water, radiation, and carbon between the atmosphere and the land surface (Pal & Sharma, 2021). LSMs include land surface characteristics that impact atmospheric processes such as albedo, surface roughness, and energy/moisture partitioning on the surface on the Earth. The Noah-MP LSM is an addition to the Noah LSM (Clark, Nijssen, Lundquist, Kavetski, Rupp, Woods, Freer, Gutmann, Wood, Gochis, et al., 2015; Niu et al., 2011).

The model decision 'vegeParTbl' within SUMMA determines which LSM vegetation scheme is used in model simulations (Table 5). This decision has five options, corresponding to vegetation category datasets originating from five different LSMs. The vegetation decision selected for this study is called 'MODIFIED_IGBP_MODIS_NOAH', which uses the vegetation category dataset from the Noah-MP LSM. Within pySUMMA, the Noah-MP model includes land surface characteristics grouped into sixteen vegetation category datasets that can be included in model simulations. Each vegetation category dataset has fifteen vegetation categories that create physical boundary conditions using functions for vegetation roughness length, albedo, emissivity, LAI, stomatal resistance, radiation stress, and vapor pressure deficit that control water and energy fluxes between the land surface and the atmosphere. This study used two of the vegetation category datasets; 'Barren or Sparsely Vegetated' to represent canopy characteristics of the UPLMET clearing and 'Evergreen Needleleaf Forest' to represent an adjacent forest. The LAI constraints in the 'open' category are a minimum of 0.1 and maximum LAI of 0.75 and the constraints in the 'forest' category are a minimum LAI of 5.0 and a maximum LAI of 6.4. However, Marshall and Waring (1986) estimated leaf area indices of 8 to 16 for a Douglas-fir dominated 450-yr-old stand (Reference stand 2) in the Andrews Forest, although they believe that the LAI of 16 is an overestimate. Nevertheless, the LAI of old-growth forests in the Andrews Forest may exceed those included in the SUMMA model (Marshall & Waring, 1986). Using the two vegetation category datasets from the Noah-MP LSM a sensitivity

analysis was used to simulate snowpack response to the presence of conifer forest canopy cover.

Model performance was evaluated using the Nash-Sutcliffe Efficiency (NSE) for periods of snow accumulation and ablation for each of the five years of simulation (Table 6). Overall, SUMMA predicted SWE with a NSE value of 0.93 and snow depth with a NSE value of 0.71. The model was compared to quality checked data for water years 2014-2015 and provisional data for water years 2016-2018.

Table 6. Nash-Sutcliffe efficiency (NSE) values for SUMMA simulation output of snow depth and SWE for water years 2014 to 2018. NSE values are calculated separately for the accumulation and ablation seasons, defined as before and after peak measured snow depth or SWE. – indicates no measured data are available.

Water year	Snow depth		SWE		QA/QC completed
	accumulation	ablation	accumulation	ablation	
2014	0.96	0.51	0.98	0.42	Yes
2015	0.90	0.90	–	–	Yes
2016	0.26	0.90	0.98	0.35	No
2017	0.68	0.85	0.92	0.86	No
2018	0.41	0.46	0.98	0.75	No

3.3.3 Sensitivity analysis, snow interception parameterization

The SUMMA framework was further used to investigate the effect of model representation of canopy interception of snow on seasonal snowpack depth and SWE. A sensitivity analysis was conducted using the SUMMA decision, called 'snowIncept', that controls which interception model is used within SUMMA (Table 6).

SUMMA includes two decisions for canopy interception of snow, following the two most widely used canopy interception models in snow modeling, Hedstrom and Pomeroy (1998) (HP98) and Andreadis et al. (2009) (Figure 13). These two models of canopy interception of snow were developed from empirical measurements of snow interception amounts in two distinctly different climates. HP98 was developed from empirical measurements of snow interception amounts in a southern boreal forest of western Canada (Hedstrom & Pomeroy, 1998). The interception model developed by Andreadis et al. (2009) was created using empirical measurements from Storck et al. (2002). These two parameterizations have been validated in these individual settings and are widely used in global models (Lundquist et al., 2021). The effect of forest canopy on snow accumulation and ablation changes depending on which of the two canopy interception representations is used.

The Andreadis et al. (2009) parameterization for snow interception describes canopy interception efficiency increasing rapidly as temperatures warm above -3°C , due to increasing cohesiveness of snow at warmer temperatures (Figure 13). The Andreadis et al. (2009) snow interception parameterization was developed from observations of snow interception made by Storck et al. (2002) in the Umpqua National Forest, Oregon, at a site with an elevation of 1200 m. Storck et al. (2002) conducted a 3-year field study with the goal of observing processes that control snow accumulation and ablation in a maritime snow climate. The work of Storck et al. (2002) provides a unique contribution to snow interception modeling, as many empirical equations that drive current snow interception models are derived from observations made in colder, drier snow climates such as those of boreal or continental sites (Lundquist et al., 2021). Using cut ponderosa pine, Douglas-fir, white fir, and lodgepole pine placed on lysimeters to monitor snow interception amounts, Storck et al. (2002) showed that conifer forests in snow climates similar to the Andrews Forest can intercept up to 60% of snow in a given storm.

The second of the two options in SUMMA for the representation of canopy interception of snow is formulated by Hedstrom & Pomeroy (1998) and describes the maximum snow load that can be retained by the forest canopy given current canopy structure and temperature conditions, or the maximum snow interception capacity, decreasing as temperature warms above $-3\text{ }^{\circ}\text{C}$ due to decreased branch stiffness. The HP98 snow interception model was developed from observations of interception in the southern boreal forest of western Canada (Lundquist et al., 2021). The two canopy interception models behave differently from -3 to $0\text{ }^{\circ}\text{C}$ (Figure 13). Technical descriptions of model equations are outside the scope of this paper but can be found in the SUMMA Technical Description 1.0 (M. Clark, Nijssen, Lundquist, Kavetski, Rupp, Woods, Freer, Gutmann, Wood, Brekke, et al., 2015).

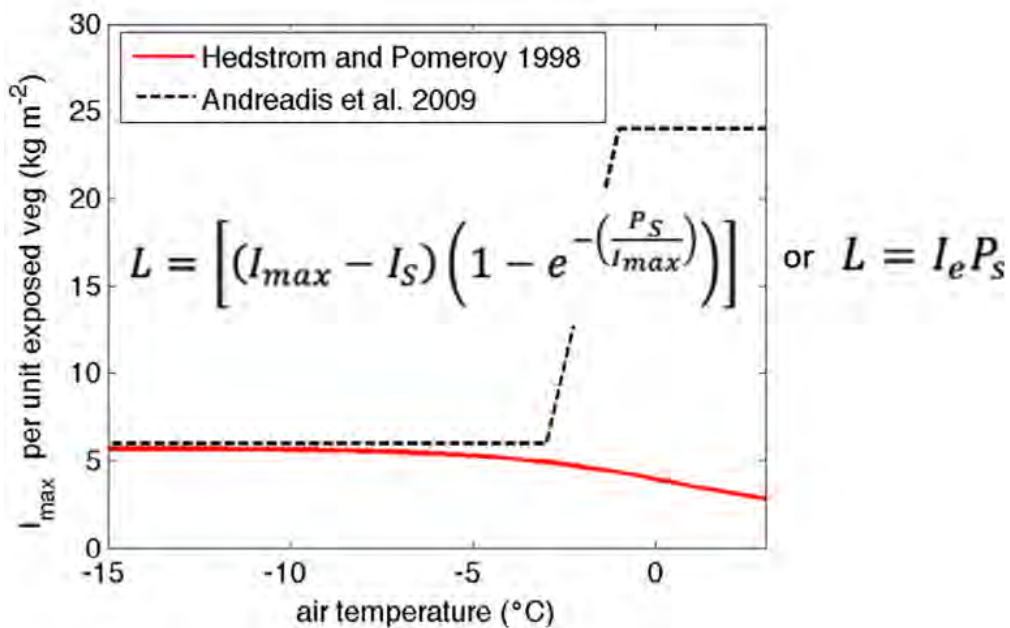


Figure 13. Canopy interception of snow model equations, where L is the amount of snow intercepted by the canopy depending on HP98 (left hand side equation) or Andreadis et al. (2009) (right hand side equation) (Lundquist et al., 2021).

4. Results

4.1 Field comparisons

Snow depth and SWE on March 16, 2022 were greatest in openings and least under mature/old-growth forest, with intermediate values under planted forest (Table 4, Figure 4). The March 2022 sites were not paired sites, so significant variation in elevation was associated with each sample group. For example, every snow sample in the mature/old-growth forest group was taken at a lower elevation than the minimum elevation of the planted forest group. This may have contributed to the significantly lower snow depth observed at the mature/old-growth forest sites. Otherwise, snow depth at the open sites increased with elevation, with a maximum snow depth measured in the clearing for the Upper Lookout meteorological station. There were also high snow depth values measured in the planted forest stand upslope of the UPLMET station, which has sparse canopy (Figure 3) and high snow depth shown in the lidar image (Figure 4). However, these values are thought to be overestimates by the avalanche probe digging into underlying soils.

In March 2022 the average snow depth was 1,192 mm with an avalanche probe and 983 mm with a Federal sampler at 14 open sites, which ranged in elevation from 965 to 1305 meters and had an average elevation of 1173 meters (Table 4, Figure 4). The average SWE was 463 mm with a bulk snow density of 45% at the open sites. In contrast, snow depth was 740 mm using an avalanche probe and 674 mm using a Federal sampler under six planted forest stands with an average elevation of 1277 m (Table 4, Figure 4). The average SWE in the planted forest stands was 324 mm and the average density was 48%. Snow depth was 273 mm using an avalanche probe and 155 mm using a Federal sampler, with a SWE of 68 mm, and density of 44% under three mature/old-growth forest stands with an average elevation of 1127 m (Table 4, Figure 4). Snow density was greatest in the planted forests and lowest in the mature/old-growth forests, but there was no significant difference between these values.

March 1 and 2, 2023 snow depth in four planted forest stands L703, L704A, L305, and L306, ranging from elevation 988 to 1379 meters generally increased with elevation (Table 7), except in the L305 stand which had an open, short canopy (Photograph 3). Snow depth was

more responsive to canopy cover and topographic factors, rather than increases in elevation.

Snow depth was lowest beneath the stand at 988 m and highest in the stand at 1379 m but was responsive to canopy closure and canopy height in the four planted stands sampled.

Table 7. Variation of snow depth by elevation, measurement type, and distance from road at four planted forest stands, March 1 and 2, 2023. Samples were collected along two, 30 meter transects approximately 20 and 100 meters away from the road.

Planted stand ID	L703	L704A	L305	L306
Snow stake pair	506F5/O5	506F6/O6	350F3/O3	350F4/O4
Mean elevation of snow stakes (m)	988	1145	1248	1379
20 m from road (Federal sampler)				
number of samples	3	3	3	1
Mean depth (mm)	504	1444	897	2057
SE	43	52	157	
20 m from road (avalanche probe)				
number of samples	10	10	10	10
Mean depth (mm)	697	1828	946	2315
SE	55	70	84	78
100 m from road (Federal sampler)				
number of samples	--	--	1	1
Mean depth (mm)	--	--	1245	2311
SE	--	--	--	--
100 m from road (avalanche probe)				
number of samples	10	10	10	10
Mean depth (mm)	923	2388	1126	2216
SE	48	116	78	42

4.2 Validation of lidar derived snow depth with data from field sampling, meteorological stations, and snow stakes

The lidar-derived snow depth values were validated by comparing them to snow depth based on field surveys, acoustic snow depth sensors, and snow stake photographs by automated cameras at the MS00701 snow stakes. These three validation datasets enabled comparisons of the lidar-derived snow depth values to measured values in the open, in planted forests, and in mature/old-growth forests at elevations ranging from 800 to 1300 meters. Comparisons included both lidar-derived snow depths, which had been corrected by addition of 295 mm of elevation, and uncorrected lidar-derived snow depths, which had subtracted the 295 mm elevation correction factor (Table 9). Overall, the lidar-derived snow depths exceed field measurements, indicating that the elevation correction applied to the lidar survey (295 mm of height added) may not be appropriate.

Snow depth measured in field sampling varied from 210 to 1,920 mm on March 16, 2022, in 23 sites ranging in elevation from 965 to 1305 meters (Table 9). Snow depth in open sites increased with elevation. Snow depth in openings was 1.6 times deeper than under planted forest and 4.4 times deeper than under mature/old-growth forest.

Based on field sampling conducted on March 16, 2022, lidar-derived snow depths from the elevation-corrected lidar data were not significantly different from field measured data in openings, but significantly greater than field measurements in forests (Table 9). In the comparisons and those that follow in this section, “significance” is based on non-overlapping standard error bars, which assume normally distributed data. Lidar-derived snow depths from elevation-corrected lidar data at 3, 5, and 10 m resolutions were on average 120 ± 54 , 58 ± 55 , and 142 ± 63 mm deeper, respectively, than field measurements for the 23 sites sampled in the field on March 16 (Table 9). Lidar-derived snow depths from elevation-corrected lidar data in openings at 3, 5, and 10 m resolutions were on average 47 ± 61 , 40 ± 62 , and 35 ± 69 mm deeper, respectively, than field measurements for the fourteen open sites sampled in the field on March 16 (Table 9). Lidar-derived snow depths from elevation-corrected lidar data in planted forest and mature/old-growth forest at 3, 5, and 10 m resolutions were on average 232

± 91 , 84 ± 105 , and 309 ± 98 mm deeper, respectively, than field measurements for the nine subcanopy sites sampled in the field on March 16 (Table 9).

Table 8. Lidar snow depth at 3 m, 5 m, and 10 m resolution on March 17, 2022, compared to snow depth data collected in the field using snow pits, a Federal sampler, and an avalanche probe on March 16, 2022. Site: T = transect, SP = snow pit, UPL = UPL met station, 1506 = 1506 road. Cover = P = planted forest, M = mature/old-growth forest, F = forest (both M and P), O = opening. Elev = Elevation, Field = field measured snow depth by IW (all methods), lidar = lidar-derived snow depth at 3, 5, and 10m spatial resolution to account for spatial variability in snow and including a +295 mm correction imposed by NCALM, lidar uncorr = lidar-derived snow depth at 3, 5, and 10m spatial resolution subtracting the 295 mm correction imposed by NCALM, field – lidar = field measured snow depth minus lidar-derived corrected snow depth, Field – lidar uncorr = field measured snow depth minus lidar derived uncorrected snow depth. SD = standard deviation, n = number of sites, SE = standard error. All snow depth measurements are in mm.

Site	Cover	Elev (m)	Field	Lidar (3 m)	Lidar (5 m)	Lidar (10 m)	Lidar uncorr (3 m)	Lidar uncorr (5 m)	Lidar uncorr (10 m)	Field – lidar (3 m)	Field – lidar (5 m)	Field – lidar (10 m)	Field – lidar uncorr (3 m)	Field – lidar uncorr (5 m)	Field – lidar uncorr (10 m)
T 3	P	1163	760	1021	1060	695	726	765	400	-261	-300	65	34	-5	360
SP	P	1298	680	1170	561	1423	875	266	1128	-490	119	-743	-195	414	-448
UPL 6	P	1300	670	675	654	816	380	359	521	-5	16	-146	290	311	149
UPL7	P	1301	610	677	720	874	382	425	579	-67	-110	-264	228	185	31
UPL8	P	1300	840	822	417	800	527	122	505	18	423	40	313	718	335
UPL9	P	1303	880	870	654	1587	575	359	1292	10	226	-707	305	521	-412
1506 6	M	1136	210	891	819	634	596	524	339	-681	-609	-424	-386	-314	-129
1506 6	M	1128	360	421	545	507	126	250	212	-61	-185	-147	234	110	148
1506 6	M	1117	250	804	589	702	509	294	407	-554	-339	-452	-259	-44	-157
1506 5	O	965	380	563	669	592	268	374	297	-183	-289	-212	112	6	83
1506 5	O	966	390	461	396	592	166	101	297	-71	-6	-202	224	289	93
1506 5	O	967	220	386	391	159	91	96	-136	-166	-171	61	129	124	356
1506 6	O	1120	750	256	391	311	-39	96	16	494	359	439	789	654	734
1506 6	O	1122	830	1160	1049	684	865	754	389	-330	-219	146	-35	76	441
1506 6	O	1122	910	717	615	694	422	320	399	193	295	216	488	590	511
T 1	O	1187	1100	767	644	619	472	349	324	333	456	481	628	751	776
T 2	O	1157	1210	1340	1362	1436	1045	1067	1141	-130	-152	-226	165	143	69

UPL4	O	1299	1680	1757	1757	1899	1462	1462	1604	-77	-77	-219	218	218	76
UPL5	O	1299	1850	2043	1996	2113	1748	1701	1818	-193	-146	-263	102	149	32
UPL1	O	1302	1830	1949	1984	1963	1654	1689	1668	-119	-154	-133	176	141	162
SP	O	1304	1830	1951	1980	1934	1656	1685	1639	-121	-150	-104	174	145	191
UPL 2	O	1305	1790	2035	1952	2000	1740	1657	1705	-245	-162	-210	50	133	85
UPL 3	O	1305	1920	1964	2069	2186	1669	1774	1891	-44	-149	-266	251	146	29
Ave-all			954	1074	1012	1097	779	717	802	-120	-58	-142	175	237	153
SD			586	592	619	649	592	619	649	259	263	300	259	263	300
n			23	23	23	23	23	23	23	23	23	23	23	23	23
SE			122	123	129	135	123	129	135	54	55	63	54	55	63
Ave-F			584	817	669	893	522	374	598	-232	-84	-309	63	211	-14
SD			251	215	186	366	215	186	366	274	317	295	274	317	295
n			9	9	9	9	9	9	9	9	9	9	9	9	9
SE			84	72	62	122	72	62	122	91	106	98	91	106	98
Ave-O			1192	1239	1233	1227	944	938	932	-47	-40	-35	248	255	260
SD			622	699	702	763	699	702	763	230	233	260	230	233	260
n			14	14	14	14	14	14	14	14	14	14	14	14	14
SE			166	187	188	204	187	188	204	61	62	69	61	62	69

On average, at all sites (blue bars), field measured snow depth on March 16, 2022 was significantly less than corrected lidar-derived measurements and significantly greater than uncorrected lidar-derived measurements, based on non-overlapping standard errors (Figure 14). On average, in the forest (orange bars), field measured depth was significantly less than corrected lidar-derived measurements at 1 m and 10 m resolutions but not at 3 m resolution, and significantly greater than uncorrected lidar-derived measurements at 5 m resolution but not 3 m or 10 m. On average, in the open (gray bars), field measured depth was not significantly different from corrected lidar-derived measurements, and it was significantly greater than uncorrected lidar-derived measurements. These results show that corrected lidar was closer to field measurements in all sites on average, and in openings, but uncorrected lidar was closer to field measurements in the forest at 1 and 10 m spatial resolutions.

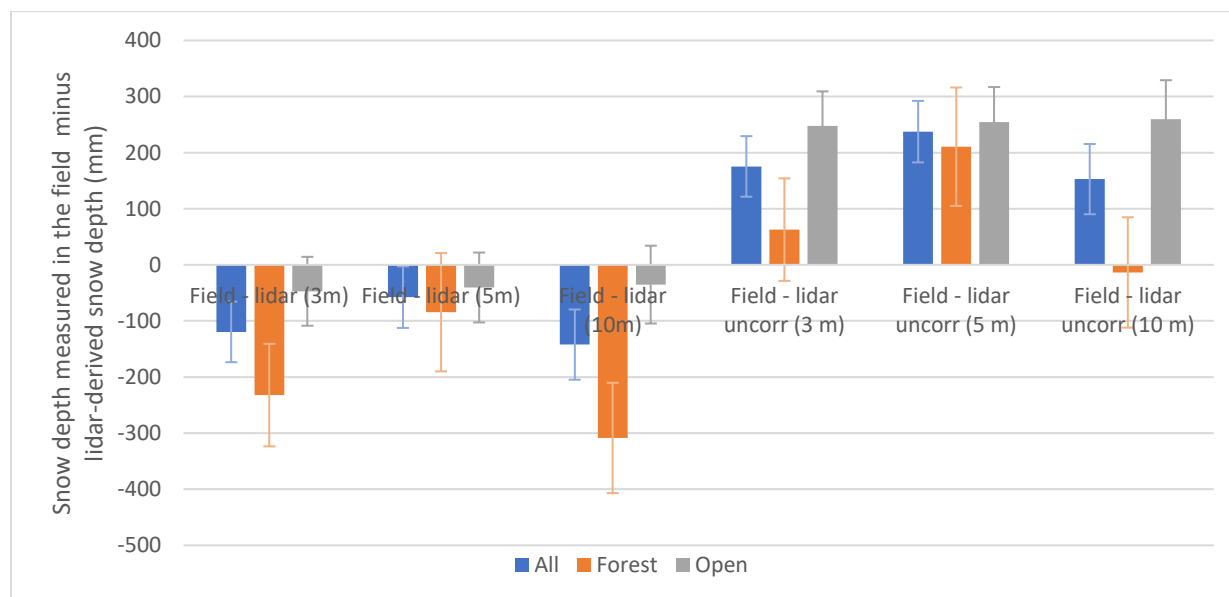


Figure 14. Effect of lidar spatial resolution and forest cover type on difference between field-measured and lidar-derived snow depth.

Snow depth from the acoustic snow depth sensors varied from 164 to 1,564 mm on March 17, 2022 in the clearings of four meteorological stations ranging in elevation from 1028 to 1300 meters (Table 9). Snow depth increased with elevation in these clearings. Snow depth differences between snow sensor measurements and lidar-derived measurements ranged from -474 mm (UPLMET, 5 m resolution) to 272 mm (VARMET, 5m resolution).

Based on snow depth measured by acoustic snow depth sensors in openings at four meteorological stations on March 17, 2022, lidar-derived snow depths from elevation-corrected lidar data were significantly less than field measured data, but lidar-derived snow depths from uncorrected lidar data were significantly greater than field measurements in forests (Table 9). Lidar-derived snow depths from elevation-corrected lidar data at 1, 3, and 5m resolutions were on average 110 ± 95 , 166 ± 86 , and 8 ± 186 mm deeper, respectively, than field measurements for the four snow depth sensors at meteorological stations on March 17 (Table 9). Lidar-derived snow depths from uncorrected lidar data from at 1, 3, and 5m resolutions were on average 185 ± 95 , 129 ± 86 , and 303 ± 186 mm shallower, respectively, than field measurements for the four snow depth sensors at met stations on March 17 (Table 9).

Table 9. Lidar snow depth at 1,3, and 5 m resolution compared to snow depth data measured by an acoustic snow depth sensor at sites of the MS001 meteorological stations.

Station	Elev (m)	Field	Lidar (1 m)	Lidar (3 m)	Lidar (5 m)	Field – lidar (1 m)	Field – lidar (3 m)	Field – lidar (5 m)	Field – lidar uncorr (1 m)	Field – lidar uncorr (3 m)	Field – lidar uncorr (5 m)
CENMET	1028	164	302	296	261	-138	-132	-97	157	163	198
UPLMET	1284	1354	1679	1761	1828	-325	-407	-474	-30	-112	-179
VANMET	1268	831	945	831	501	-114	-1	329	181	294	624
VARMET	1300	1546	1407	1671	1274	139	-125	272	434	170	567
average						-110	-166	8	185	129	303
SD						190	172	372	190	172	372
n						4	4	4	4	4	4
SE						95	86	186	95	86	186

The average snow depth measured at the acoustic snow depth sensors at the four meteorological stations was significantly less than corrected lidar-derived snow depths at 1 m and 3 m, but not significantly different at 5 m resolution (Figure 15). The average snow depth at snow depth sensors at four meteorological stations was greater than uncorrected lidar-derived snow depths at 1 m, 3 m, and 5 m resolution. These findings indicate that the uncorrected lidar underestimated snow depth (field > lidar) and the corrected lidar overestimated snow depth (field < lidar).

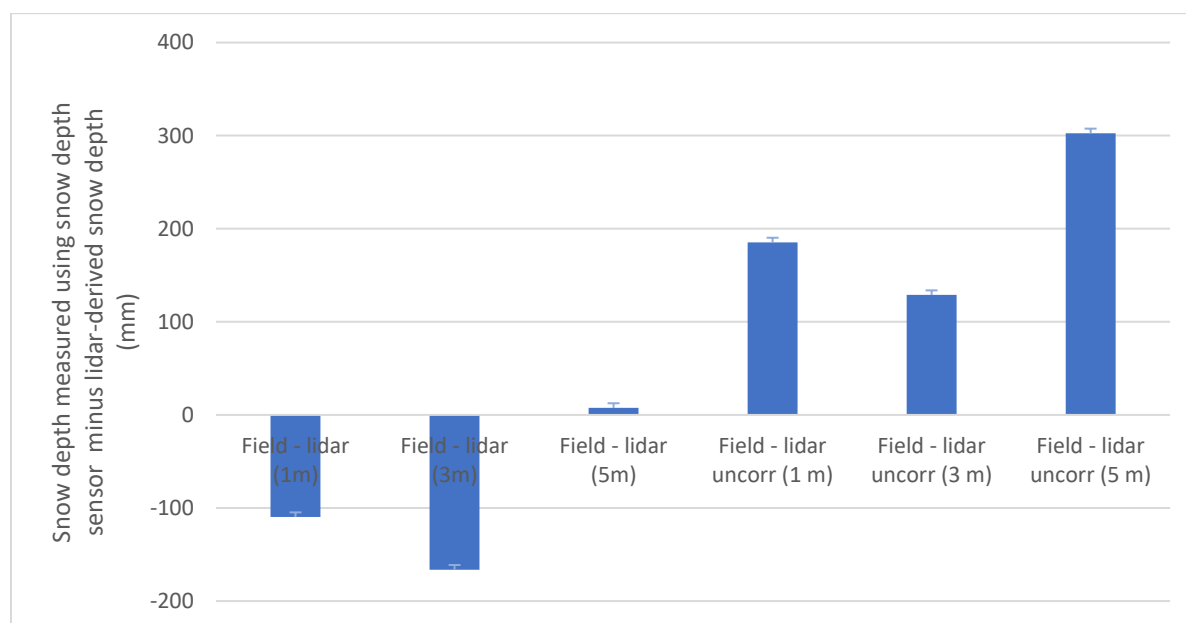


Figure 15. Effect of lidar spatial resolution on difference between snow depth from a snow depth sensor and lidar-derived snow depth.

Snow depth measured by avalanche probe and Federal sampler varied from 680 to 1,920 mm in openings and forest sites at the UPLMET meteorological station on March 16, 2022 (Table 10). Lidar-derived snow depths from elevation-corrected lidar data were significantly greater than these field measured data in openings, but not significantly different from field-measured snow depth in the forest (Table 10). Lidar-derived snow depths from elevation-corrected lidar data were deeper than field measurements on average by 183 ± 39 in the open, 62 ± 89 under forest, and 128 ± 47 mm overall (Table 10, Figure 16). Both field-measured and lidar-derived snow depths in the opening were 2.5 times deeper than in the forest (Table 10).

Table 10. Lidar snow depth at 1 m resolution on March 17, 2022, compared to snow depth data collected in the field using an avalanche probe, two snow pits, and a Federal sampler at Upper Lookout meteorological station clearing and adjacent forest, March 16, 2022. Field = field measured snow depth with 16 points in a 3x3m plot using an avalanche probe, lidar = lidar-derived snow depth at 1m spatial resolution and including a +295-mm elevation correction imposed by NCALM, field – lidar = field measured snow depth minus lidar-derived corrected snow depth. SD = standard deviation, n = number of sites, SE = standard error. All snow depth measurements are in mm. Snow depth measure by acoustic depth sensor at UPLMET on this date was 2,200 mm.

Cover	Field	Lidar	Field – lidar
Open	1790	2050	-260
Open	1920	2050	-130
Open	1830	2150	-320
Open	1830	1980	-150
Open	1680	1730	-50
Open	1850	2040	-190
Forest	880	650	230
Forest	610	750	-140
Forest	670	630	40
Forest	840	1000	-160
Forest	680	960	-280
All			
Mean	1325	1454	-128
SD	572	645	157
n	11	11	11
SE	172	195	47
Forest			
mean	736	798	-62
SD	117	173	199
n	5	5	5
SE	52	77	89
Open			
mean	1817	2000	-183
SD	79	143	96
n	6	6	6
SE	32	58	39

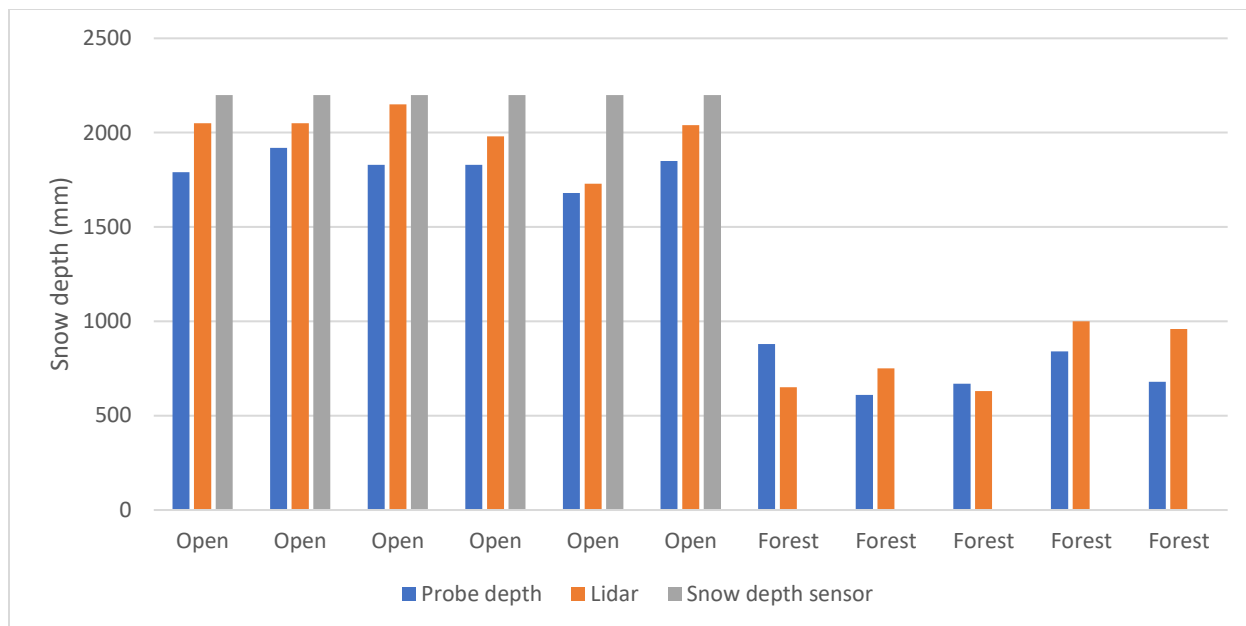


Figure 16. Lidar validation using a 1-meter resolution snow height model with snow depth collected in the UPLMET clearing and beneath the surrounding planted forest on March 16, 2022.

At the MS00701 snow stakes, snow depths ranged from 0 to 1,372 mm at ten pairs of the snow stakes in openings and under forest ranging in elevation from 793 to 1408 m on March 17, 2022 (Table 11). Snow depths at snow stakes in openings were on average five times greater than in forests, and there was no snow under the forest at six of the ten forest stakes (Table 11). Lidar-derived snow depths from elevation-corrected lidar data at 3 m, 5 m, and 10 m in the open were on average 196 ± 93 , 215 ± 58 , and 239 ± 49 mm respectively deeper than snow stake data (Table 11, Figure 16).

Based on snow depths from the MS00701 snow stakes on March 17, 2022, lidar-derived snow depths from elevation-corrected lidar data were significantly greater than snow stake measurements in openings and in forests. However, lidar-derived snow depths from uncorrected lidar data were significantly less than snow stake measurements in openings, but not significantly different from snow stake measurements in forests (Table 11).

Table 11. Lidar snow depth at 3, 5, and 10 m resolution compared to snow depth data measured at snow stakes (MS00701), March 17, 2022. ID: Snow stake identification. Cover: F = forest, O = opening, Elev = Elevation, Field = field measured snow depth, lidar = lidar-derived snow depth at 3, 5, and 10m spatial resolution to account for spatial variability in snow and including a +295 mm correction imposed by NCALM, lidar uncorr = lidar-derived snow depth at 3, 5, and 10m spatial resolution subtracting the 295 mm correction imposed by NCALM, field – lidar = field measured snow depth minus lidar-derived corrected snow depth, Field – lidar uncorr = field measured snow depth minus lidar derived uncorrected snow depth. SD = standard deviation, n = number of sites, and SE = standard error. All snow depth measurements are in mm.

ID	Cover	Elev (m)	Field	lidar (3 m)	lidar (5 m)	lidar (10 m)	Lidar uncorr (3 m)	Lidar uncorr (5 m)	Lidar uncorr (10 m)	Field - lidar (3 m)	Field - lidar (5 m)	Field - lidar (10 m)	Field - lidar uncorr (3 m)	Field - lidar uncorr (5 m)	Field - lidar uncorr (10 m)
R320F2	F	805	0	268	237	388	-27	-58	93	-268	-237	-388	27	58	-93
R350F1	F	919	0	327	439	275	32	144	-20	-327	-439	-275	-32	-144	20
R320F3	F	935	0	207	207	247	-88	-88	-48	-207	-207	-247	88	88	48
R320F4	F	978	0	298	358	370	3	63	75	-298	-358	-370	-3	-63	-75
R506F5	F	1006	0	313	263	225	18	-32	-70	-313	-263	-225	-18	32	70
R350F2	F	1057	0	361	339	433	66	44	138	-361	-339	-433	-66	-44	-138
R506F6	F	1164	15	421	335	352	126	40	57	-406	-320	-337	-111	-25	-42
R507F4	F	1193	30	498	262	264	203	-33	-31	-468	-232	-233	-173	63	62
R350F3	F	1233	61	476	443	444	181	148	149	-415	-382	-383	-120	-87	-88
R350F4	F	1408	853	954	970	1030	659	675	735	-100	-116	-176	195	179	119
R320O2	O	793	30	443	472	420	148	177	125	-412	-442	-390	-117	-147	-95
R320O3	O	916	183	160	226	252	-135	-69	-43	23	-43	-70	318	252	225
R506O5	O	970	686	808	773	720	513	478	425	-122	-87	-35	173	208	260
R320O4	O	997	61	263	281	201	-32	-14	-94	-202	-220	-140	93	75	155
R350O1	O	892	0	336	300	374	41	5	79	-336	-300	-374	-41	-5	-79
R350O2	O	1063	213	899	644	432	604	349	137	-685	-430	-219	-390	-135	76
R506O6	O	1125	686	582	622	839	287	327	544	104	64	-153	399	359	142
R507O4	O	1180	--	1216	1216	650	921	921	355	--	--	--	--	--	--
R350O3	O	1263	1006	1335	1312	1354	1040	1017	1059	-329	-306	-348	-34	-11	-53

R35004	O	1387	1372	1176	1545	1798	881	1250	1503	196	-174	-427	491	121	-132
Ave-all			274	567	562	554	272	267	259	-259	-254	-275	36	41	20
SD			424	364	399	417	364	399	417	210	139	121	210	139	121
n			19	20	20	20	20	20	20	19	19	19	19	19	19
SE			63	127	126	124	61	60	58	-59	-58	-63	8	9	5
Ave-F			96	412	385	403	117	90	108	-316	-289	-307	-21	6	-12
std			267	211	220	234	211	220	234	108	96	86	108	96	86
n			10	10	10	10	10	10	10	10	10	10	10	10	10
SE			84	67	70	74	67	70	74	34	30	27	34	30	27
Ave-O			471	722	739	704	427	444	409	-196	-215	-239	99	80	56
SD			490	427	468	512	427	468	512	279	173	148	279	173	148
n			9	10	10	10	10	10	10	9	9	9	9	9	9
SE			163	135	148	162	135	148	162	93	58	49	93	58	49

On average, snow depth values captured on the ground by the cameras at the MS00701 snow stakes were significantly less than elevation-corrected lidar-derived measurements and not significantly different than uncorrected lidar-derived measurements, regardless of lidar image spatial resolution (Figure 17, all, blue bars). On average, in the forest, field measured depths at snow stakes were significantly less than corrected lidar-derived measurements, and not significantly different than uncorrected lidar-derived measurements (Figure 17, forest, orange bars). On average, in the openings, depths measured at snow stakes were significantly less than corrected lidar-derived measurements, and greater than uncorrected lidar-derived measurements (Figure 17, openings, grey bars). The results presented show that the uncorrected lidar was closer than the elevation-corrected lidar to snow stake measurements at all sites on average and in the forest, but field measurements from snow stakes exceeded uncorrected lidar estimates in openings.

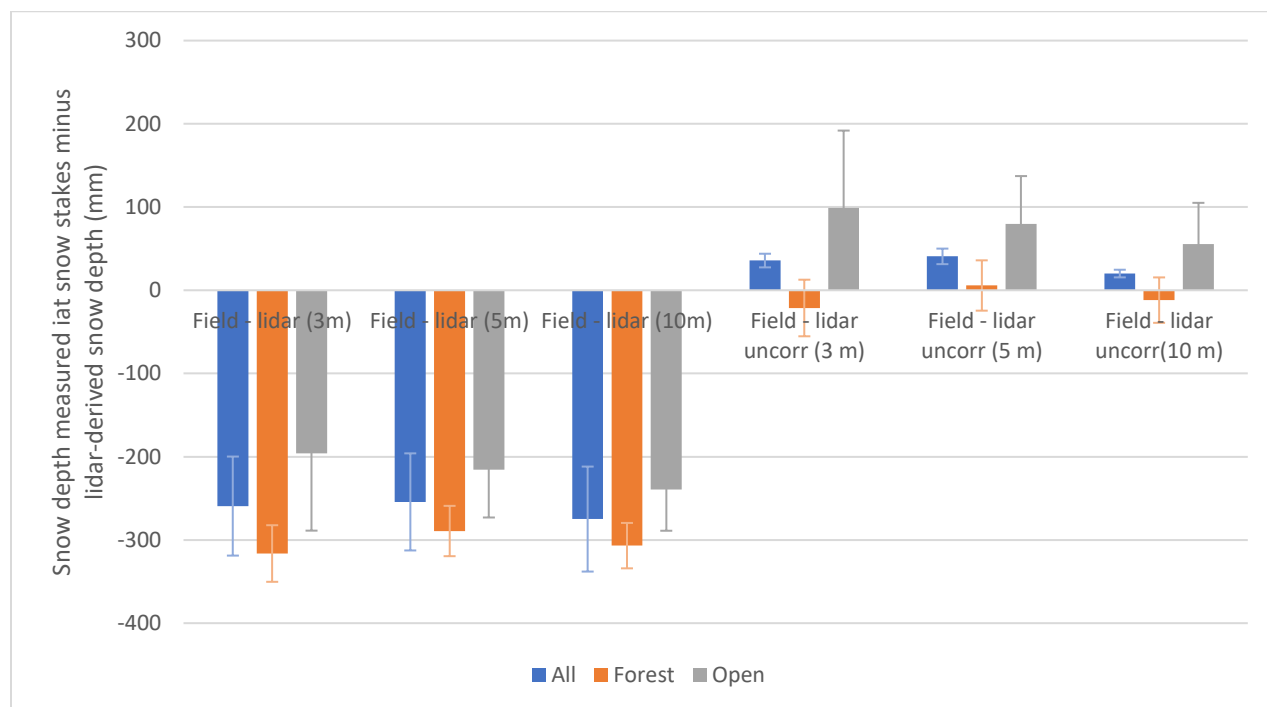


Figure 17. Effect of lidar spatial resolution and forest cover type on difference between snow depth measured at snow stakes and lidar-derived snow depth.

4.2 Data analysis

4.2.1 Lidar comparisons between different forest cover types

To investigate differences in lidar-derived snow depth between paired sites of planted and unharvested forests, zonal statistics were extracted from the raster and compared to one another (Table 13). Mean values of lidar-derived snow depth were obtained for ten pairs of 60-60 m polygons in planted forest and adjacent mature/old-growth forest. Elevation of the polygons ranged from 814 to 1361 m, with a mean of 1067 m (Table 13). Canopy height in polygons (based on the canopy height model, Figure 2 and Figure 6) ranged from 6 to 43 m, with an average of 35 ± 6 m in the mature/old-growth forest polygons, and an average of 23 ± 9 m in the planted forest polygons. Average snow depth in the snow height model ranged from 166 to 905 mm, with an average of 373 ± 28 in the mature/old-growth forest polygons and an average of 412 ± 66 in the planted forest polygons (Table 13). At these forested sites snow depth did not increase with elevation.

Table 12. Characteristics of 60x60 m plots sampled for lidar-derived snow depth and canopy height in planted and mature/old forest stands. SD = standard deviation, SE = standard error, Cover = canopy cover type; M = mature and P = planted.

Planted stand ID	Snow stake ID	Cover	Mean elevation (m)	Canopy height (m)	Canopy SD (m)	Snow depth (mm)	Snow SD (mm)
L503	320F2	M	815	35	21	507	273
L522	320F3	M	947	33	12	302	98
WS6	320F4	M	958	41	10	253	80
L701	350F1	M	890	23	14	302	92
L303/L371	350F2	M	1036	37	13	405	117
L305	350F3	M	1220	31	17	508	183
L306	350F4	M	1352	38	13	425	177
L703	506F5	M	948	38	14	281	109
L704A	506F6	M	1275	43	12	367	119
L209	507F4	M	1230	30	9	383	195
L503	320F2	P	814	34	6	282	80
L522	320F3	P	914	26	7	494	203
WS6	320F4	P	967	20	4	166	68
L701	350F1	P	878	30	6	320	117
L303/L371	350F2	P	1082	24	6	299	102
L305	350F3	P	1217	22	7	571	177
L306	350F4	P	1361	6	5	907	425
L703	506F5	P	925	31	5	311	146
L704A	506F6	P	1280	11	6	453	301
L209	507F4	P	1227	25	4	318	125
ave - all			1067	29		393	
SD			184	10		158	
n			20	20		20	
SE			41	2		35	
ave - M			1067	35		373	
SD			186	6		90	
n			10	10		10	
SE			59	2		28	
ave - P			1067	23		412	
SD			192	9		210	
n			10	10		10	
SE			61	3		66	

Lidar-derived snow depth in 60x60 m polygons was greater beneath the mature/old-growth forest in five instances and greater beneath the planted forest in the other five instances, suggesting no clear relationship of snow depth to canopy cover type (planted vs. mature/old-growth) (Table 13). The mean difference of snow depth between mature/old-growth forests and planted forests was -39 ± 61 mm, indicating no significant difference. Canopy height in mature/old-growth polygons was 12 ± 4 m greater than in the planted polygons. Overall, there was no difference in the lidar-derived snow depth between planted forest and adjacent mature/old-growth forests, which are on average only 10 m taller than the planted forest.

Table 13. Results of differencing the canopy height model and snow height model between planted and mature/old-growth forests using 60x60 m polygons, 1-meter raster. Sites were selected that were near long-term snow stakes.

Snow stake ID	Elevation	Mature/old minus planted snow depth	Mature/old minus planted canopy height (m)
320F2	815	225	1
320F3	947	-192	7
320F4	958	87	21
350F1	890	-18	-7
350F2	1036	106	13
350F3	1220	-63	9
350F4	1352	-482	32
506F5	948	-30	7
506F6	1275	-86	32
507F4	1230	65	5
Average		-39	12
SD		194	13
n		10	10
SE		61	4

At the ten paired 60x60 m sites, lidar-derived snow depth at elevations ranging from 830 to 1360 meters in March 2022 was weakly positively related to elevation under planted forest, but not related to elevation under mature/old-growth forest, and there was no significant difference in snow depth between planted and mature/old-growth forests (Figure 18).

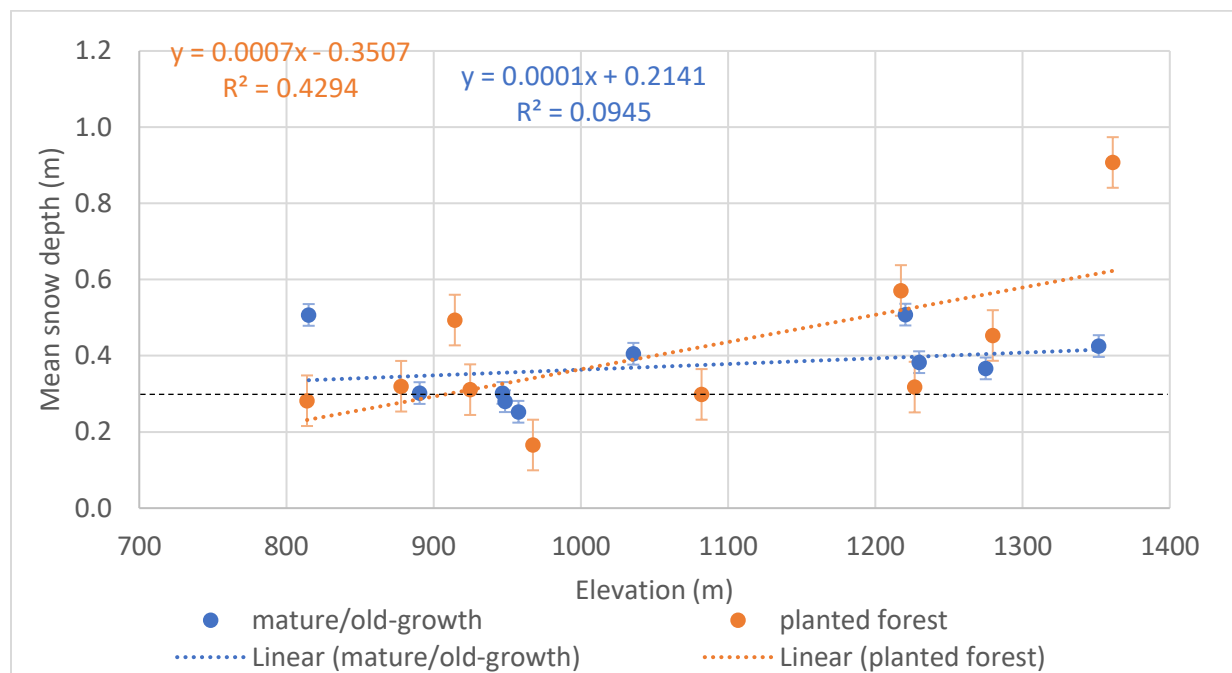


Figure 18. Mean and standard error (SE) of lidar-derived snow depth (1-meter raster) by elevation in ten pairs of polygons of 60x60 m in planted and mature/old-growth forest. Horizontal dashed line at 30 cm indicates uncertainty in lidar snow depth estimates based on comparisons with field measurements; snow depth at or below this line may not be greater than zero.

With the exception of one outlier, snow depth was not related to canopy height (i.e. in post-clearcut regenerating stands vs. mature/old-growth stands) (Figure 19). Over this range of canopy heights (20 to 43 m), increasing canopy height did not necessarily lead to shallower snowpack, suggesting that canopy structural characteristics such as leaf area index (LAI) and bole density control snow interception rates and amounts, rather than canopy height.

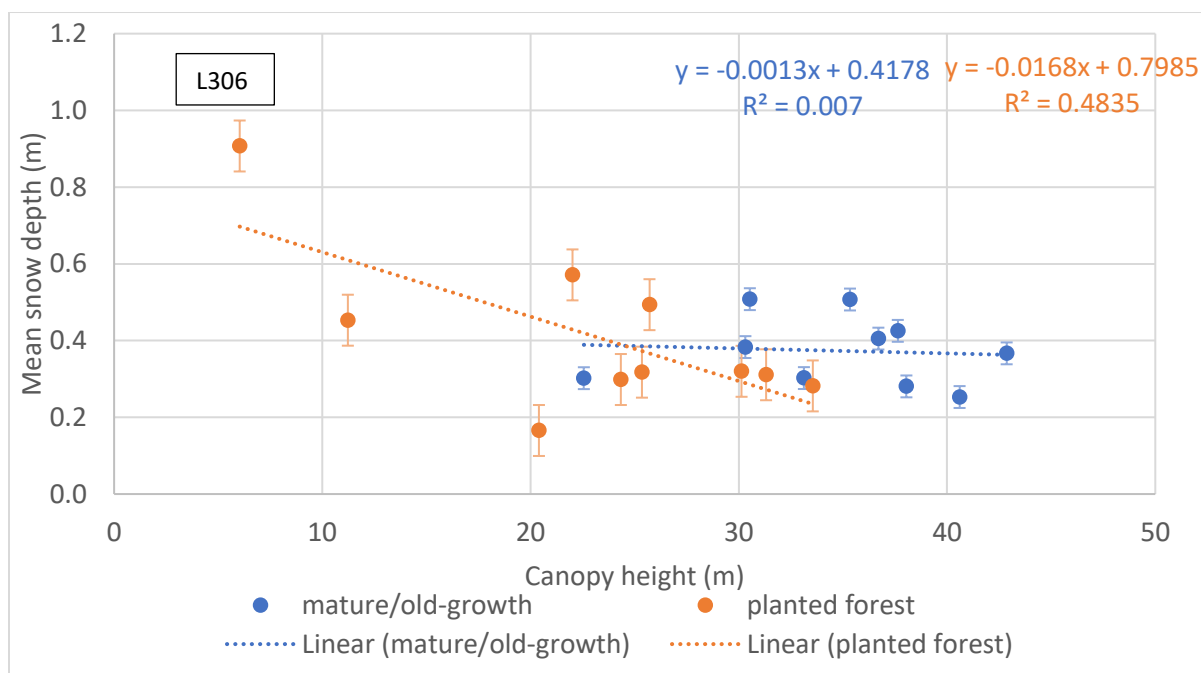


Figure 19. Mean and standard error (SE) of snow depth in lidar image by forest cover type, ten paired sites.

The difference in lidar-derived snowpack depth (mature/old-growth minus planted forest) was not significantly related to the difference in canopy height between planted forests and mature/old-growth forests, based on ten 60x60 m polygons (Figure 20). Over the range of canopy heights sampled (20 to 43 m), snow depth was unrelated to canopy height. The L306/350F4 site has an open, sparse stand, creating an outlier with a large difference (>25 m) in canopy height.

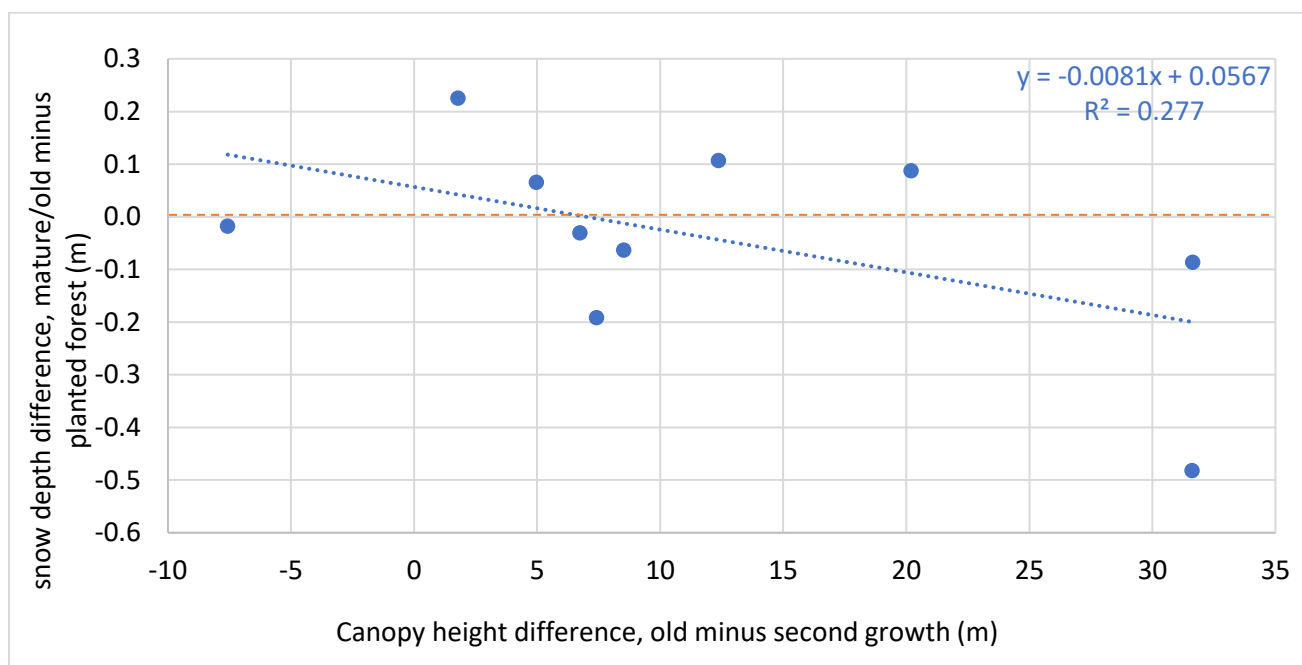


Figure 20. Difference of canopy height, mature/old-growth minus planted forest, vs. difference in snow depth in lidar image, 1-meter raster.

4.2.2 Meteorological station snow analysis

Snow depth and SWE data from Upper Lookout, Vanilla Leaf, and Central meteorological stations from 1997 to 2014 were used to calculate mean snowpack bulk density values and their standard errors on each day of the year (Figure 21). Over the period 1997 to 2014, average snowpack density increased gradually from 0.25 to 0.4 g/cc (25 to 40% or 250 to 400 kg/m³) from mid-November to the end of January, was constant at 0.4 g/cc from February 1 until mid-March, then increased until May 1. By May 1, snow is typically absent from CENMET (1028 m), but at UPLMET (1298 m) and VANMET (1268 m), density declined in May and then increased by the end of May. The decrease in density of snow in May during the melt period was unexpected. This decrease may be due to loss of water from within the melting snowpack.

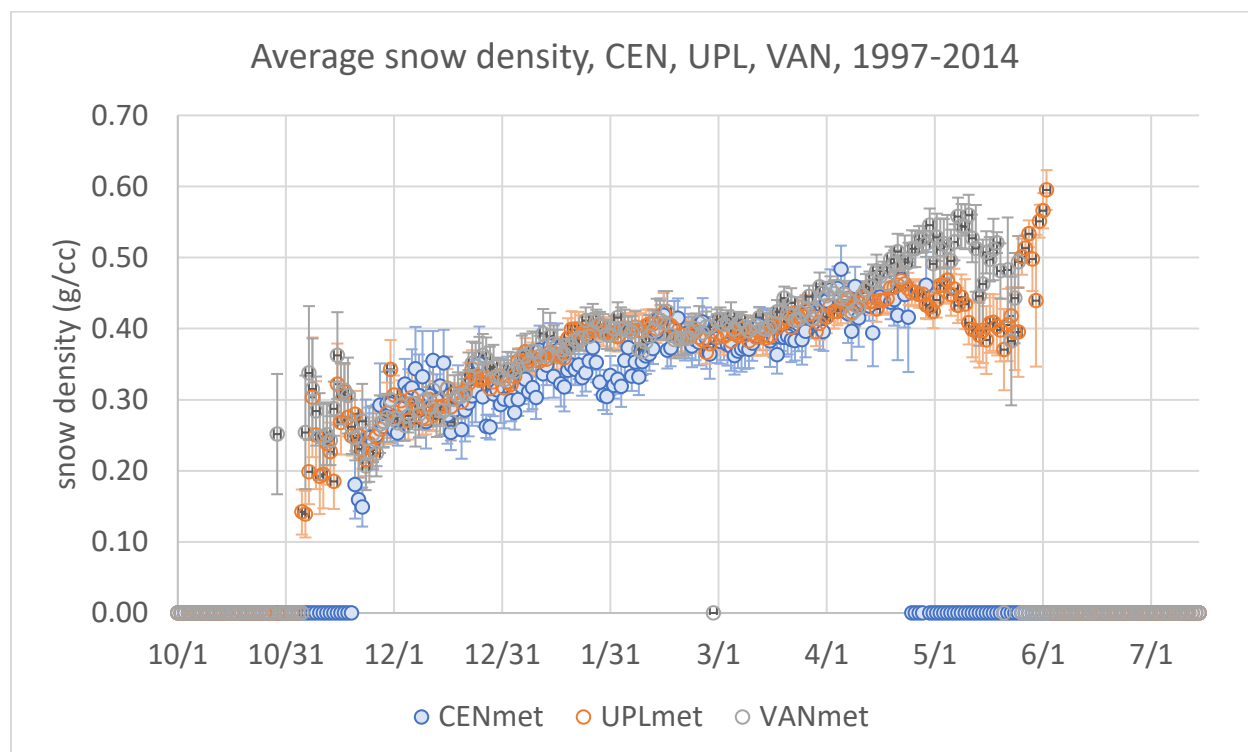


Figure 21. Average snow density from 1997 to 2014 at Upper Lookout, Vanilla Leaf, and Central meteorological stations. Snow density was calculated for days with density < 0.7 and snow depth > 100 mm. The acoustic depth sensor is not considered to be reliable at depths < 100 mm, and values > 0.7 may be artefacts of patchy snow (M. Schulze, personal communication). These criteria omitted < 3% of observations. Averages are for days of the year with more than three years of snow density data meeting these criteria.

Maximum snow water equivalent at the Upper Lookout meteorological station ranged from 200 to 1,500 mm from 1994 to 2014 (Figure 22). Snow water equivalent ranged from 10 to 78% of cumulative precipitation in the 1994 to 2014 water years (Figure 23). In some years, such as 1995 and 2004, SWE only briefly exceeded 30% of cumulative precipitation.

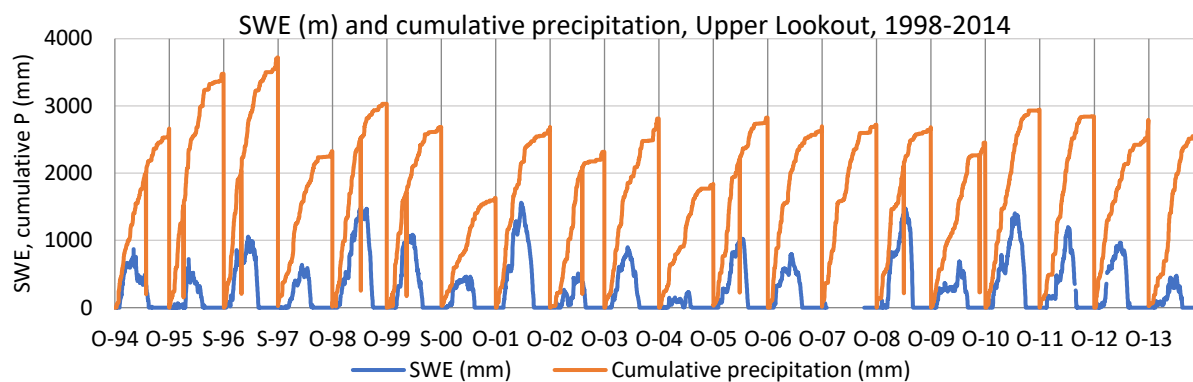


Figure 22. SWE and cumulative precipitation, 1998-2014, Upper Lookout.

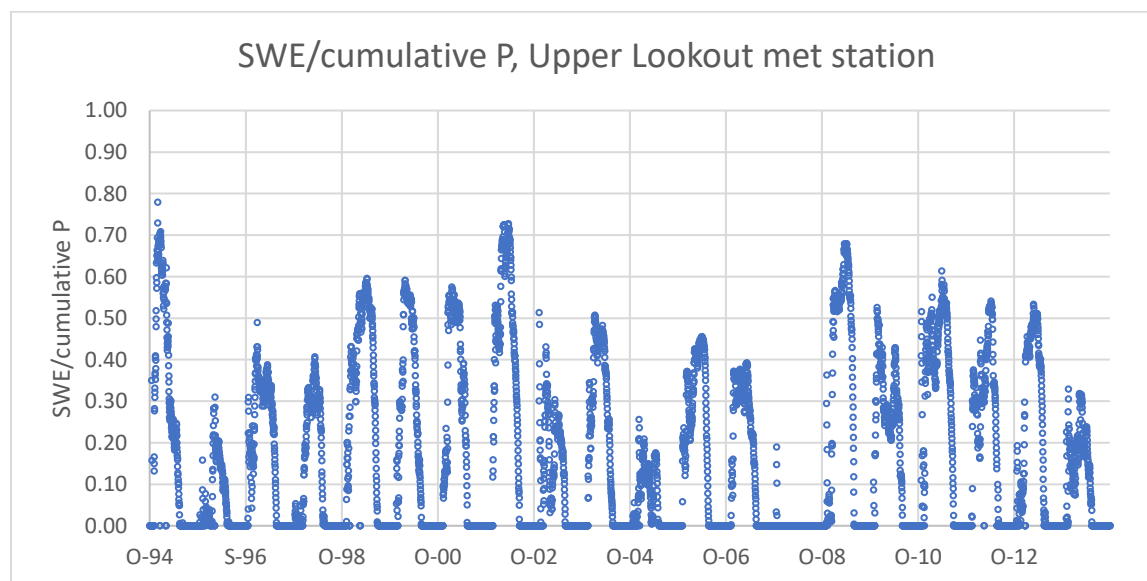


Figure 23. Ratio of SWE to cumulative precipitation within each water year (Oct 1 – Sept 30), 1994-2014, Upper Lookout meteorological station.

The relationship between SWE and snow density is complex (Figure 24). The lowest values of snow density occur at very low levels of SWE (shallow snowpacks), whereas snow density approached 0.5 g/cm^3 in the deepest snowpacks (1 to 1.5 m of SWE) (Figure 24). Calculated values of snow density >0.7 occur at SWE values ranging from zero to 1 m, but these may be artefacts of patchy snow. Hence, snow densities in Figure 21 were calculated only for snow depths $>100 \text{ mm}$, and densities > 0.7 were excluded.

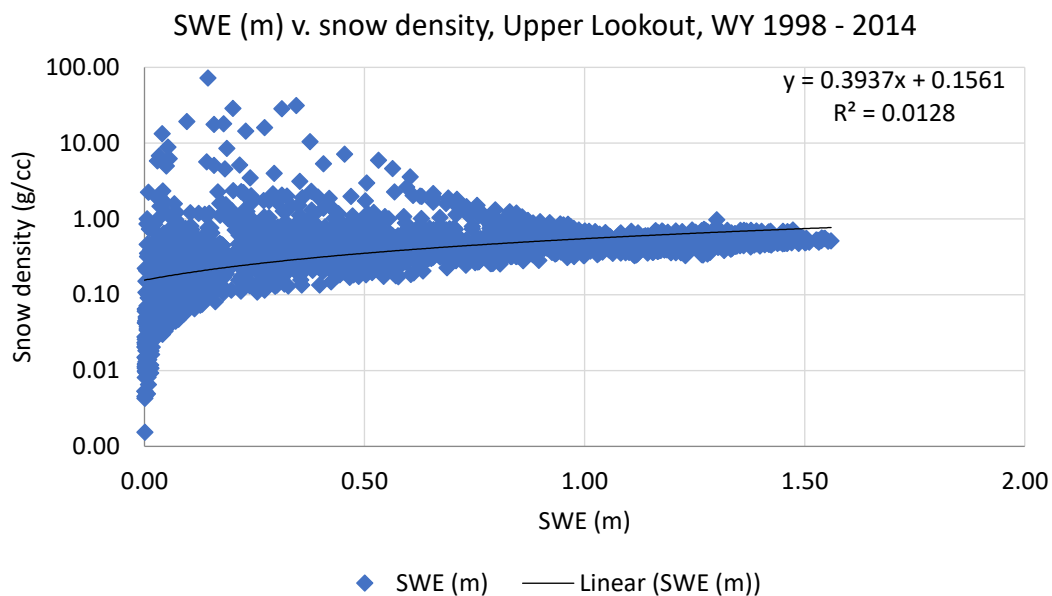
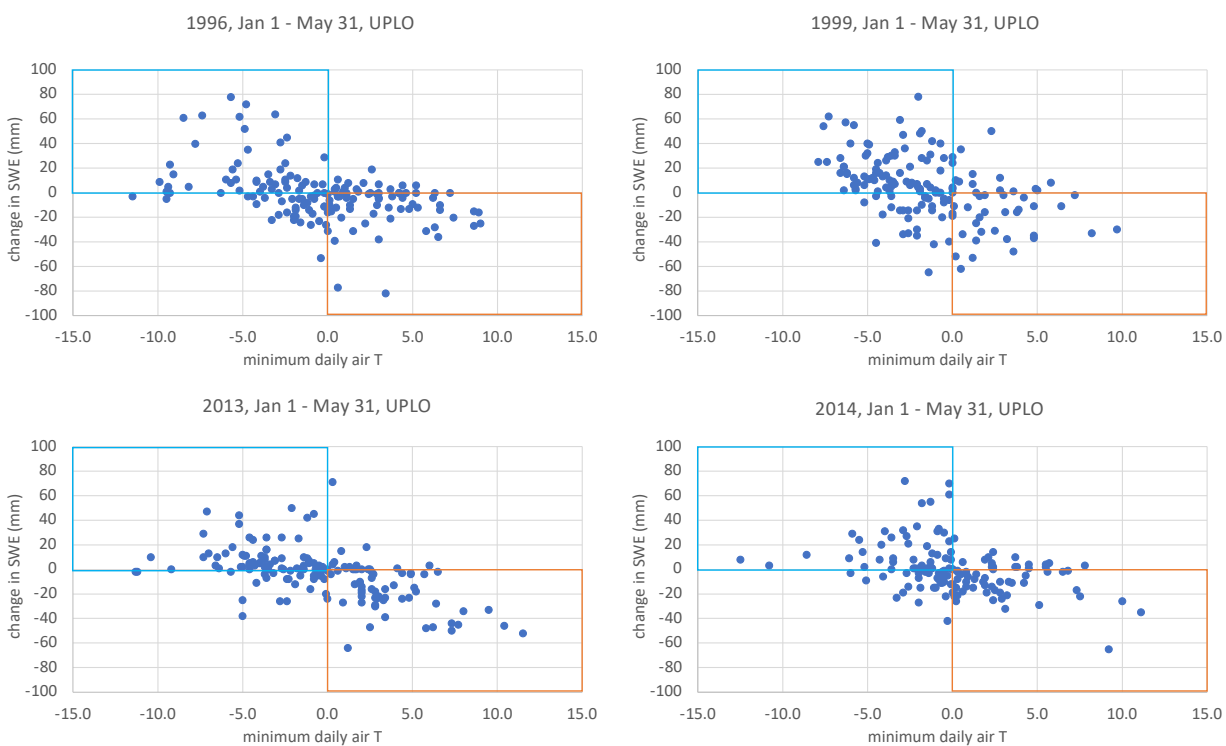


Figure 24. SWE (m) vs. snow density (g/cc), 1998-2014, Upper Lookout.

A visual analysis indicated that changes in SWE were related to minimum air temperature at UPLMET (Figure 25). Generally, when minimum daily air temperature was > 0 °C, SWE decreased and vice-versa. However, SWE increased on some days when the daily minimum air temperature was > 0 °C, and SWE decreased on some days when the daily minimum air temperature was < 0 °C. Increases in SWE when minimum daily air temperature was > 0 °C could be caused by rain on snow, while decreases in SWE when minimum temperature was < 0 °C may be due to sublimation or drainage of water from the base (basal discharge) of the snowpack when soils are > 0 °C.



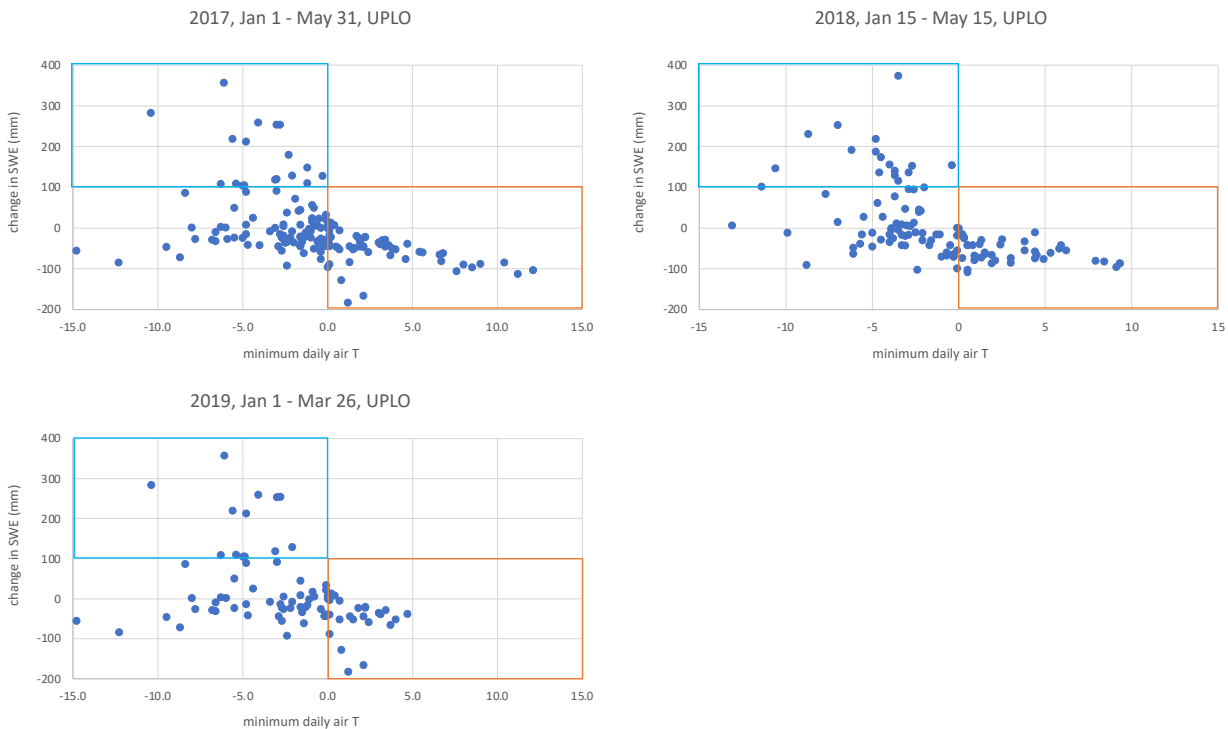


Figure 25. Relationship of daily change in SWE to daily change in minimum T, Upper Lookout, for 1996-2019.

4.2.3 Snow survey stake analysis

At paired snow stakes, 2014 to 2022, snow disappeared earlier under the forest than in openings, but on average, the snow melt rate was faster in openings than under the forest. The average (2014 to 2022) difference in snow disappearance dates (SDDs) varied from 10 to 43 days between the forest stake and the open stake at the ten MS00701 snow stake sites that are within the lidar survey extent (Table 14). This difference comes with some error associated with interpretation of SDD. For example, open stakes may have an SDD that is earlier than the SDD in the center of the road where the snowpack has been compacted more, or forest sites may have a SDD that occurs before all of the patches of snow in the surrounding area have been completely melted. These errors are associated with the sub-meter horizontal variability of seasonal snowpack and produce errors in SDD differences on the magnitude of ~2–4 days.

Table 14. Average snow disappearance date, 2014-2022, open minus forest, and mean snow depth loss rate at ten MS00701 sites with paired snow stakes beneath the forest and in the open (on the road).

Site	Elevation (m)	Delta SDD (days)	Forest snow depth loss rate (mm/day)	Opening snow depth loss rate (mm/day)	Opening minus snow rate (mm/day)
R320F2	799	11	26	25	-1
R350F1	907	10	22	25	3
R320F3	935	12	28	25	-3
R320F4	988	24	19	36	17
R506F5	1006	43	16	27	11
R350F2	1060	36	24	25	1
R506F6	1145	29	19	25	6
R507F4	1187	38	23	32	9
R350F3	1248	31	32	28	-4
R350F4	1379	10	20	39	19
ave					5.8
SD					8.1
SE					2.6

Snow was deeper in openings than in the forest and the SDD was significantly later in openings than in forests despite variability among years (Figure 26). The difference in snow disappearance date (in days) visually increases with elevation, but the effect of elevation on SDD was not tested.

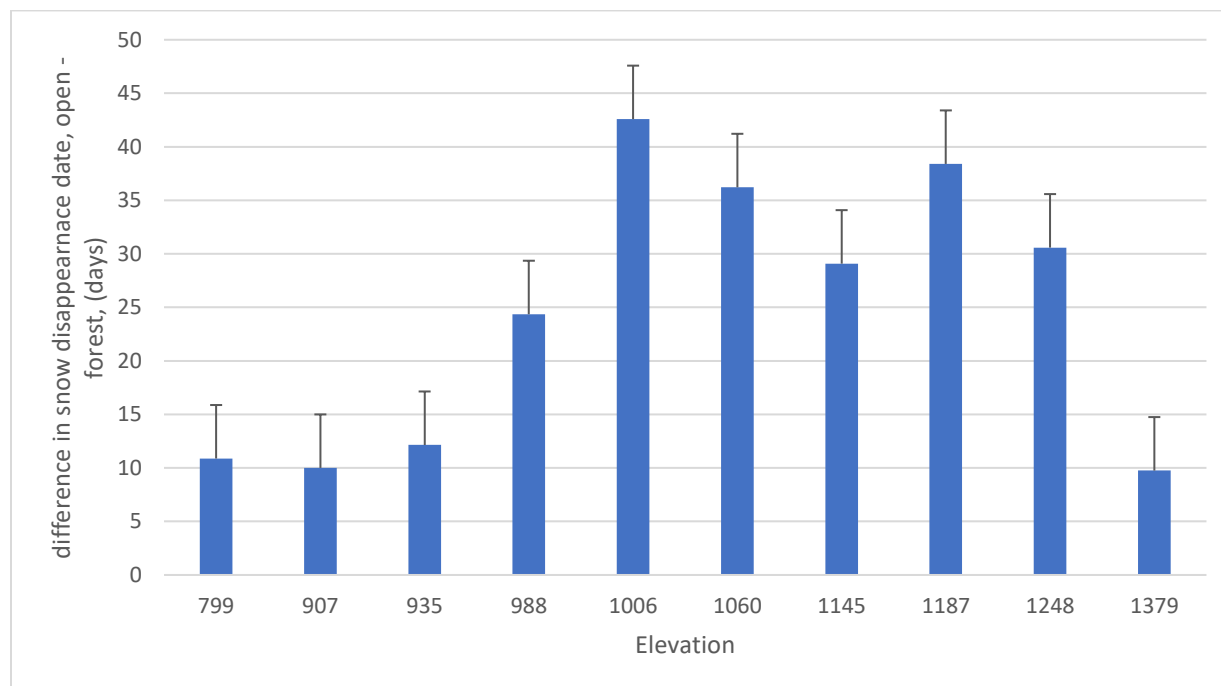


Figure 26. Difference in snow disappearance date, open – forest, 2014-2022.

Using the peak snow depth date, peak snow depth amount, and SDD, mean snow depth loss rates were calculated for the period of record that has continuous snow depth data, 2014 to 2022. Snow depth loss rates varied from 19 to 32 mm/day under forest and from 25 to 39 mm/day in openings (Table 14, Figure 26). On average, snow depth loss rates were 6 mm/day faster in openings than under the forest (Table 14). At seven of the ten sites mean snow depth loss rates for the melt season were more rapid at the stake in the opening than at the stake under the forest (Table 14, Figure 27, Figure 28).

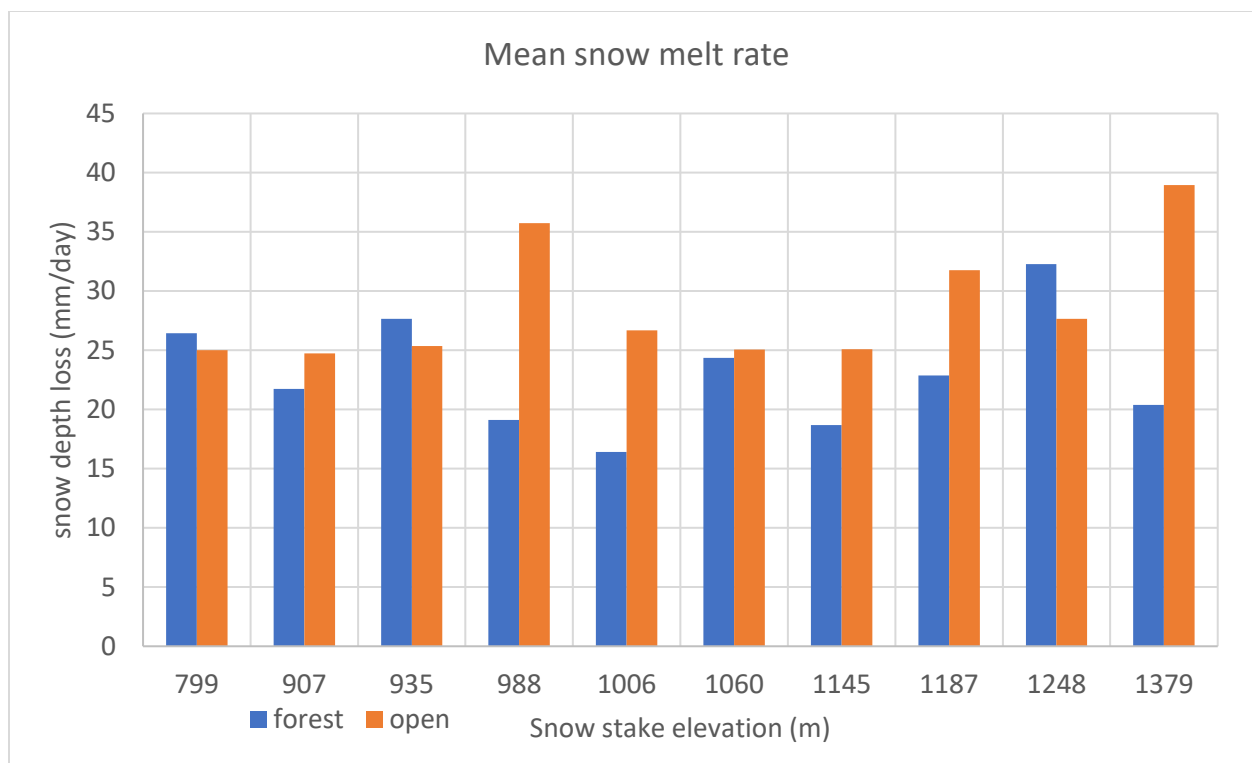


Figure 27. Mean snow depth loss rate using peak snow depth date, amount, and snow disappearance date, 2014-2022.

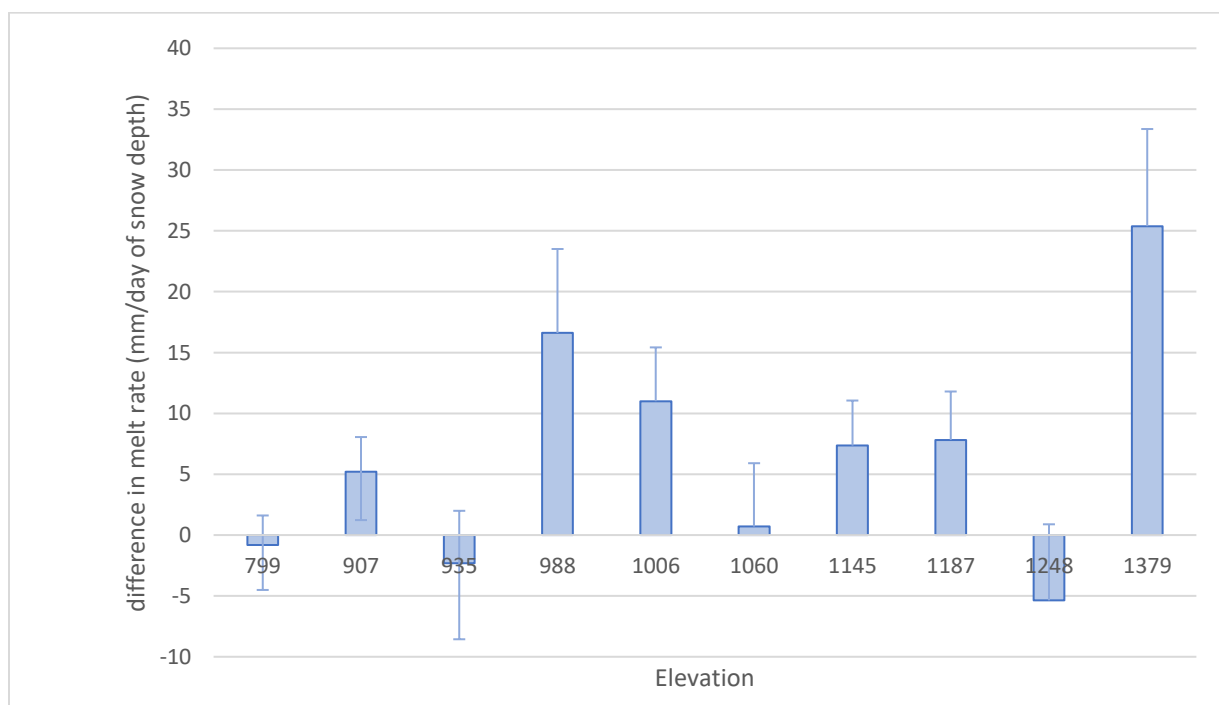


Figure 28. Difference in snow depth loss rate, open – forest, 2014–2022.

Mean snow density from 1994 to 2016 (Table 15, Figure 29) at ten snow stake pairs ranging in elevation from 668 meters to 1379 meters varied by site type and elevation. At site 320F1 the mean snow density at the forest stake was significantly greater than at the open stake (Table 15, Figure 29). At the other eight of the sites density values were not significantly different from one another and at the 350F4 open site snow density was significantly greater than the forest site. Calculating the annual, mean snow density across all 138 snow tube measurements in the forest and 213 measurements in the open from 1994 to 2016 revealed snow densities were similar at all elevations, except the sites at the minimum (668 m) and maximum (1379) elevation (Figure 29). The mean snow density across all elevations was $364 \pm 28 \text{ kg/m}^3$ ($36.4 \pm 2.8\%$) in the forest and $366 \pm 18 \text{ kg/m}^3$ ($36.6 \pm 1.8\%$) in the open (Table 15). Annual, mean snow density across all elevations ranged from 318 to 413 kg/m^3 (32 to 42%) in the forest and 337 to 426 kg/m^3 (34 to 43%) in the open. Prior to the installation of the cameras at the snow stakes in 2014, the MS00701 dataset includes density measurements at ~3-12 times per year. In 2014, cameras were installed at the snow stakes and the frequency of SWE samples was reduced to once a year, so the change in frequency and timing of measurements may affect density means.

Table 15. Snow density (%) at ten pairs of snow survey stakes in forested sites over the period 1994-2016. SE = standard error.

Site	Elevation	Forest n	Mean	SE	Open n	Mean	SE
320F1	668	6	41	2	11	34	3
320F2	799	15	31.8	3.2	24	33.7	2
320F3	926	15	32.3	3.1	24	33.9	2
320F4	978	12	35.5	2.7	21	34.5	2
506F5	988	13	39.5	5.9	25	36.1	2
350F2	1060	11	36.9	2.4	24	36	2
506F6	1145	20	35.5	2.6	29	38.3	1
507F4	1187	12	36.7	3.1	14	38.9	2
350F3	1248	15	35.3	2.4	22	37.9	1
350F4	1379	19	39.9	1	19	42.6	1
Total		138			213		
Average			36.4	2.8		36.6	1.8

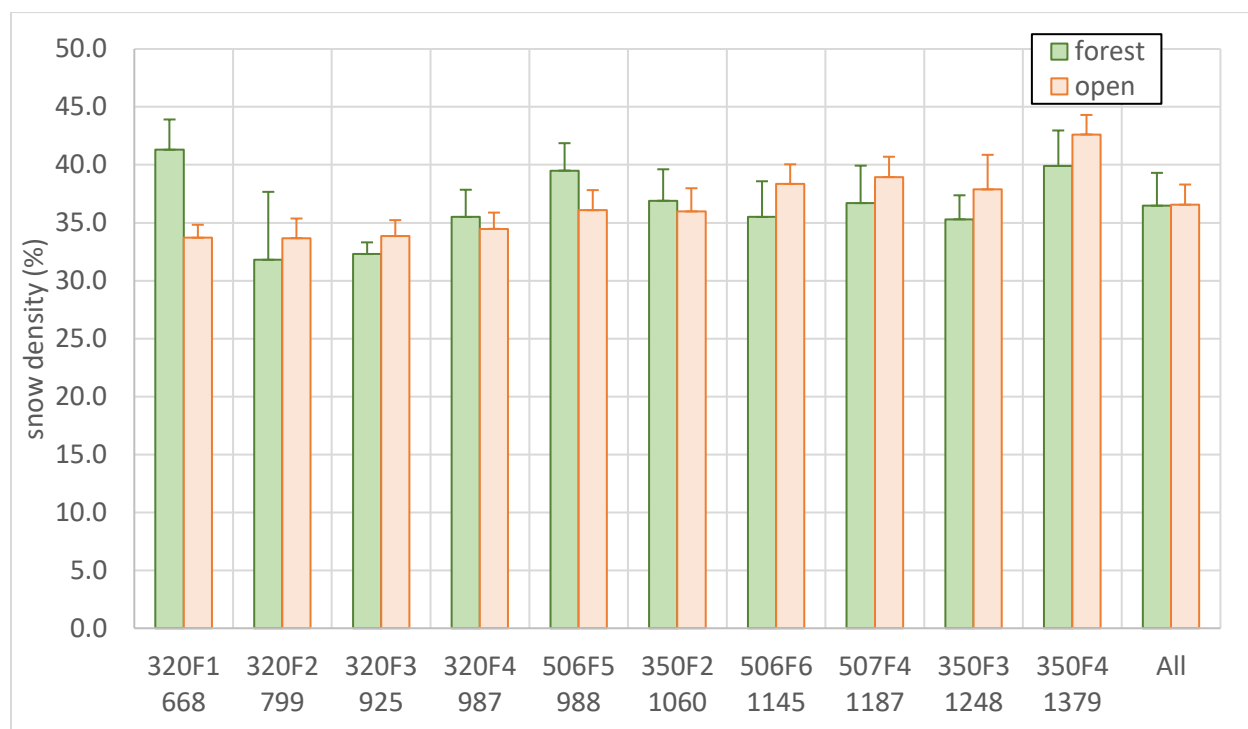


Figure 29. Snow density (%) at 10 paired forest and open sites sampled from 1994 to 2016. See Table 7.

Overall, snow depth in the forest was $38 \pm 3\%$ of the snow depth in the open at nine snow stakes with continuous data from 2015 to 2022 ranging in elevation from 805 to 1370 m (Table 16). Cumulative snow depth in the forest relative to open sites on April 1 ranged from 4 to 120%. Mean values across the nine snow stakes ranged from 30 to 55% among the eight years, with the highest percent in 2019 and the lowest percent in 2021. Mean values across the eight years ranged 29 to 66% among the nine snow stakes, with the lowest percent at 1006 m and the highest percent at 805 m, and no clear pattern relative to elevation (Table 16). These results indicate that the presence of the forest canopy decreases net snow accumulation (i.e., accumulation minus melt) over the snow season by 62%.

Table 16. Cumulative snow depth on April 1, forest as percent of open, at nine snow stakes with continuous (daily) records from 2015 to 2022. This value was calculated by summing snow depth over the days in each snow season and calculating the cumulative snow depth in the forest site as a percent of the cumulative snow depth in the open site on April 1. The ID and elevation of each snow stake are provided. No data were available on April 1 for the 2020 year.

	R350F4	R350F3	R507F4	R506F6	R350F2	R506F5	R320F4	R320F3	R320F2	mean	n	SD	SE
Year	1370 m	1233 m	1180 m	1164 m	1057 m	1006 m	978 m	935 m	805 m				
2015	33	53	--	46	23	12	36	33	65	38	8	17	6
2016	--	51	--	35	20	14	25	43	58	35	7	16	6
2017	--	--	--	43	18	18	18	--	56	31	5	18	8
2018	45	--	54	50	26	23	32	51	47	41	8	12	4
2019	23	73	53	--	52	--	51	70	61	55	7	17	6
2020	--	--	--	--	--	--	--	--	--				
2021	15	35	35	23	10	4	10	15	120	30	9	36	12
2022	--	--	--	44	34	14	27	47	53	37	6	14	6
mean	29	53	47	40	26	14	28	43	66	38	50	21	3
n	4	4	3	6	7	6	7	6	7				
SD	13	16	11	10	14	6	13	18	25				
SE	6	8	6	4	5	3	5	8	9				

Mid-March to early April marks the typical end of snow accumulation. The mean cumulative snow depth in the forest relative to open sites in mid-March to early April ranged from 21 ± 6 to 32 ± 3 % over the period 1994 to 2022 at five snow stakes with periodic data from 1994 to 2014, and continuous data from 2015 to 2022 (Table 17). The mean cumulative snow depth in the forest relative to open sites in mid-March to early April ranged from 26 ± 5 to 64 ± 10 % during the period of periodic sampling (1994 to 2014), whereas it ranged from 21 ± 2 to 40 ± 4 % during the period of continuous sampling (Table 17). The analysis used April 1 for all years with continuous data (2015 to 2022), and the periodic sampling data that was closest to April 1 for the periodically sampled data (1994 to 2014). A visual analysis indicated that the mean cumulative snow depth in the forest relative to open sites from 1994 to 2014 was not related to elevation across the five sites (Table 17).

Table 17. Relationships of snow depth under forest and in openings at snow survey stakes, 1994-2022, by elevation. Cumulative snow depth, forest as percent of open.

Snow survey stake ID	R320F2	R350F2	R506F6	R507F	R350F3
Elevation	800	1050	1150	1150	1250
1994-2014					
ave	31	19	32	21	32
stdev	13	11	13	15	17
count	20	17	20	7	17
SE	3	3	3	6	4
2014-2022					
ave	64	26	40	56	54
stdev	26	14	12	71	13
count	7	7	6	7	5
SE	10	5	5	27	6
1994-2022					
ave	40	21	34	39	37
stdev	22	12	13	53	18
count	27	24	26	14	22
SE	4	2	3	14	4

Snow depth, forest as percent of open, was greater during the period of record prior to the installation of automated cameras at the snow stakes (Figure 30). The higher values of forest as a percent of open depth in the two periods may be due to differences in sampling: the snow depth measurements during the 1994–2014 period were taken with a Federal sampler, whereas depths for the 2015–2022 record were based on a camera reading of the snow stake. The higher values of forest as a percent of open depth in the two periods may be due to differences in dates used: data during the 1994-2014 period were obtained on April 1 plus or minus three weeks, whereas the measurements in the 2015-2022 period were all from April 1. A visual analysis of this data suggests the ~3-week sampling intervals before 2014 produced lower snow depth estimates (Figure 30).

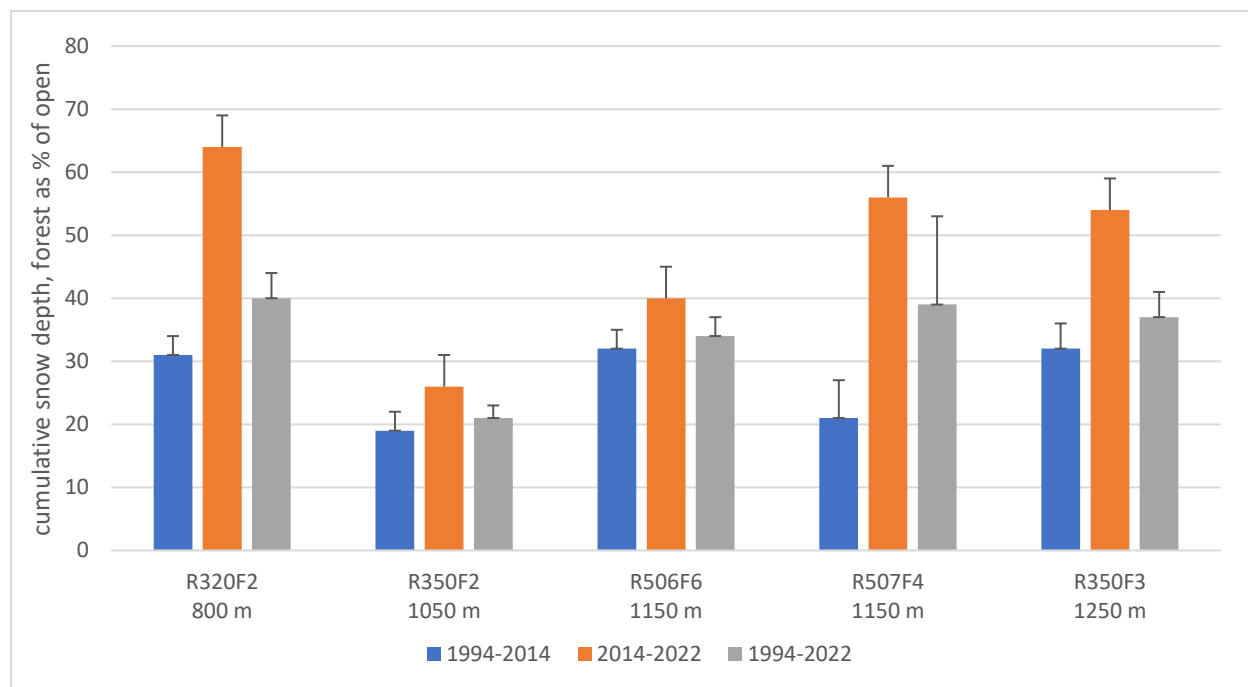


Figure 30. Cumulative snow depth, forest as % of open.

4.3 Snow modeling

To assess model performance, the SUMMA simulation output for the open site at UPLMET was compared to measured snow depth and SWE values at the meteorological station. The SUMMA model simulation predicted snow depth in the open site with a Nash Sutcliffe Efficiency (NSE) value of 0.71 and snow water equivalent with a NSE value of 0.93 over the period of WY 2014 to 2018 (Table 7). Using the years that have QA/QCed snow data, WY 2014 and 2015, NSE values were calculated for the seasonal snowpack accumulation and ablation seasons. For snow depth, the accumulation and ablation periods are delineated by peak snow depth date, and for SWE the periods are delineated by peak SWE date. The NSE values for snow depth and SWE were 0.96 and 0.98 in the accumulation season and 0.67 and 0.52 in the ablation season of the 2014 water year. The NSE value for snow depth was 0.9 in the accumulation season and 0.91 in the ablation season of the 2015 water year (Table 7). The years WY 2014 and 2015 were selected because reliable, QA/QCed snow data were only available during the two of five years of model simulations. The snow data from WY 2016-2018 are provisional and not suitable for statistical comparison. This affects the NSE performance across all years and should be considered.

For snow depth, the modeled value (blue line) is close to the measured value (red line) during periods of increasing snow depth but exceeds the measured value during periods of decreasing snow in all years, 2014 to 2018 (Figure 31, top panel). In 2016, the measured values of snow depth appear to be erroneous. In 2017, modeled snow depth exceeds the measured value during the period of increasing snow (Figure 31, top panel).

For SWE, the modeled value (blue line) is close to the measured value (red line) during periods of increasing SWE in all modeled years, but the modeled value (blue line) exceeds the measured value (red line) during periods of decreasing snow in all years except 2015, when no data was available (Figure 31, bottom panel). Modeled SWE is less than the measured value during the early part of the snow season in 2016 and much of the snow season in 2017 (Figure 31, bottom panel).

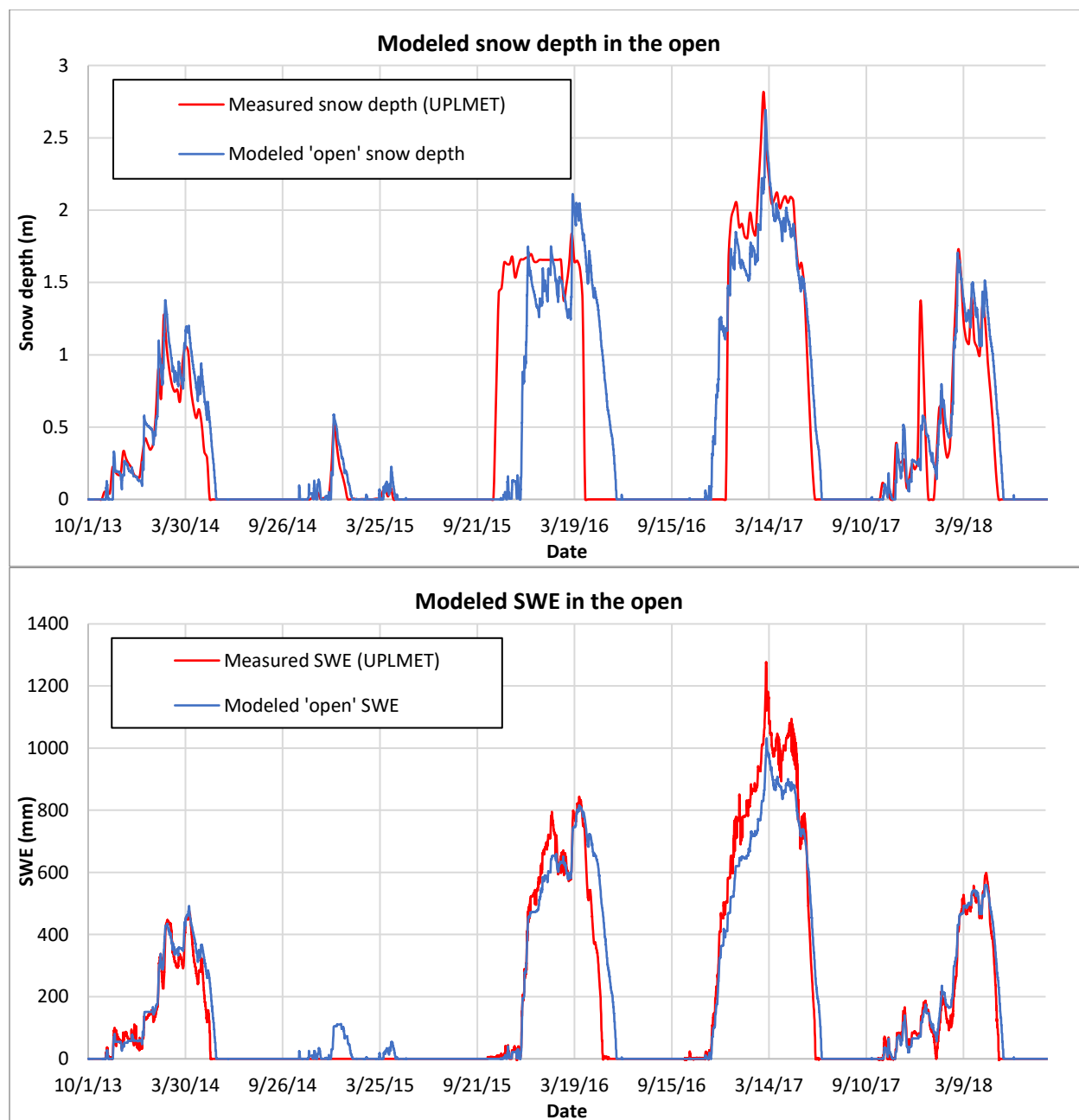


Figure 31. Simulated snow depth (top) and SWE (bottom) output over a five-year period, covering water years 2014-2018, based on SUMMA model forced with data from the Upper Lookout benchmark meteorological station. Measured, provisional snow depth data by the acoustic snow depth sensor was resampled to 5-day median for better visual comparison. All other data is at a one-hour resolution.

The modeled snowpack temperature profile in the open, which is based on simulated energy and water exchange between five layers of the snowpack at a 1-hour resolution, shows periods of persistent cold layers at the surface of the snowpack in the mid-winter (blue and green colors in the middle panel of Figure 32), but generally the snowpack is predicted to be isothermal and near 0°C throughout the winter season (yellow colors in the middle panel of Figure 32).

Water year 2015 was a year of anomalously low snowpack despite near normal precipitation (top panel, Figure 32). Low snow during this year was caused by warm minimum daily air temperature, particularly in the early winter (bottom panel, Figure 32). Water year 2017 was a deep snow year with cold (dark blue) simulated near surface snow temperatures. Early winter minimum and maximum daily temperature were particularly low in WY 2017 (bottom panel, Figure 32), which could have contributed to greater cold content and a deeper snowpack that year.

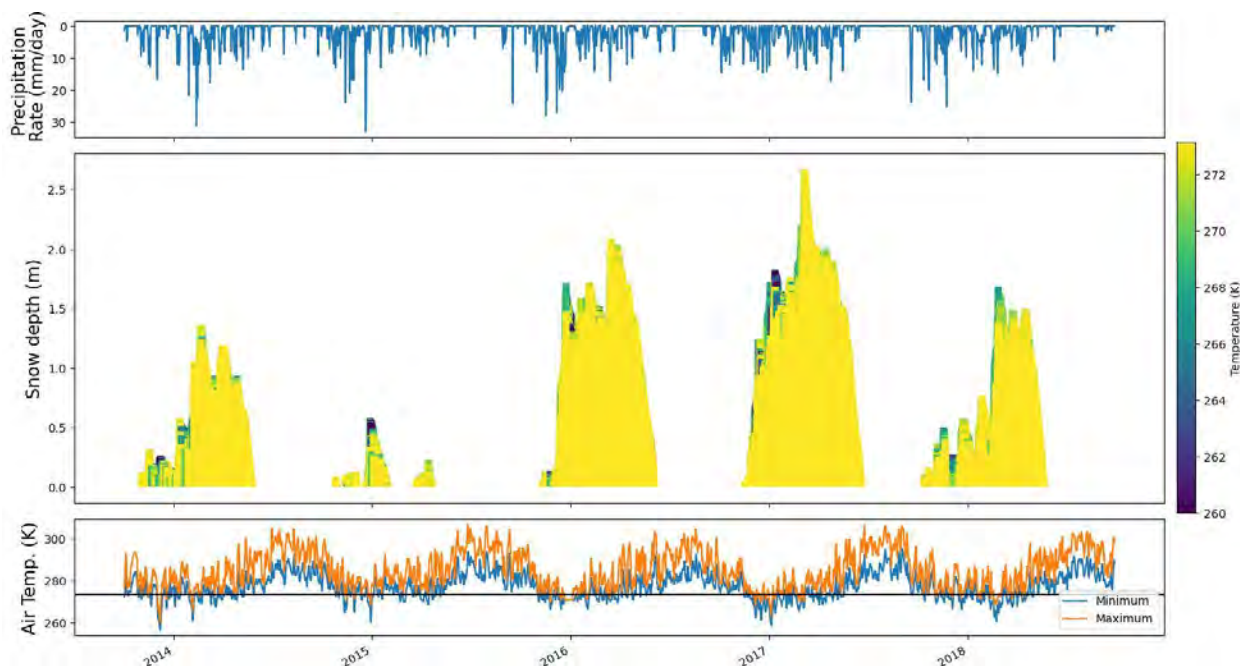


Figure 32. Measured precipitation (top), simulated snow depth and snowpack temperature (middle), and measured minimum and maximum daily temperature for water years 2014-2018.

Using the vegetation category dataset for an open site and a conifer forest site (see Methods section 3.3.2), SUMMA model output predicted delayed snow accumulation, less

snow depth, less SWE, and delayed melt under the conifer forest (green line) compared with the opening (blue line) (Figure 33). Model performance appeared to be similar across all years and canopy types, regardless of anomalously warm or cold winter seasons. The modeled snow depth under forest was 69% of the modeled snow depth in the opening on average on April 1 across the five simulated years, and 66% of the modeled snow depth in the opening on average on all days across the five simulated years. These percentages are considerably larger than the observed snow depth under forest as a percent of the opening at snow stakes in the Andrews Forest (Figure A-1, Appendix A; Table 16).

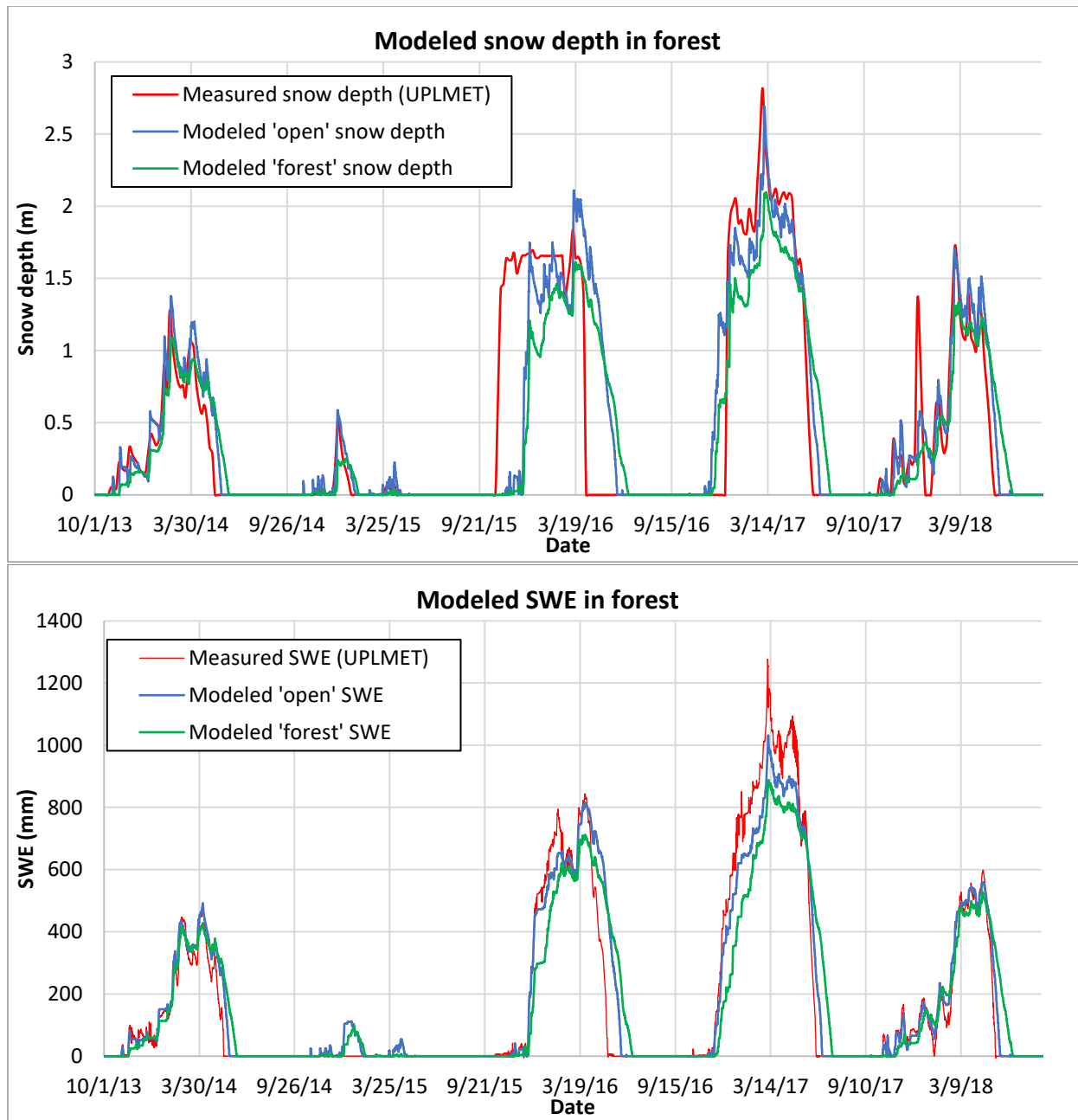


Figure 33. SUMMA snow depth and SWE output over a five-year period, covering water years 2014-2018.

Simulated snow depth and SWE using the HP98 canopy interception of snow model are considerably greater than simulated snow depth and SWE using the interception model developed from empirical data measured in Oregon by Storck et al. (2002) and represented in a model by Andreadis et al. (2009) (Figure 34). The simulated snow depth using the HP98 model on average was 10 to 20% of the modeled snow depth using the Andreadis et al. (2009) model on April 1 across the five simulated years. The simulated SWE using the HP98 model on average was 199% of the modeled SWE using the Andreadis et al. (2009) model on all days across the five simulated years. The different models for canopy interception of snow produce different results as they were developed from empirical measurements taken in different snow climates. Using the HP98 parametrization produces a deeper snowpack than Andreadis et al. (2009) because less snow is intercepted by the forest canopy as storm temperatures get colder due to the cohesiveness of snow and other factors.

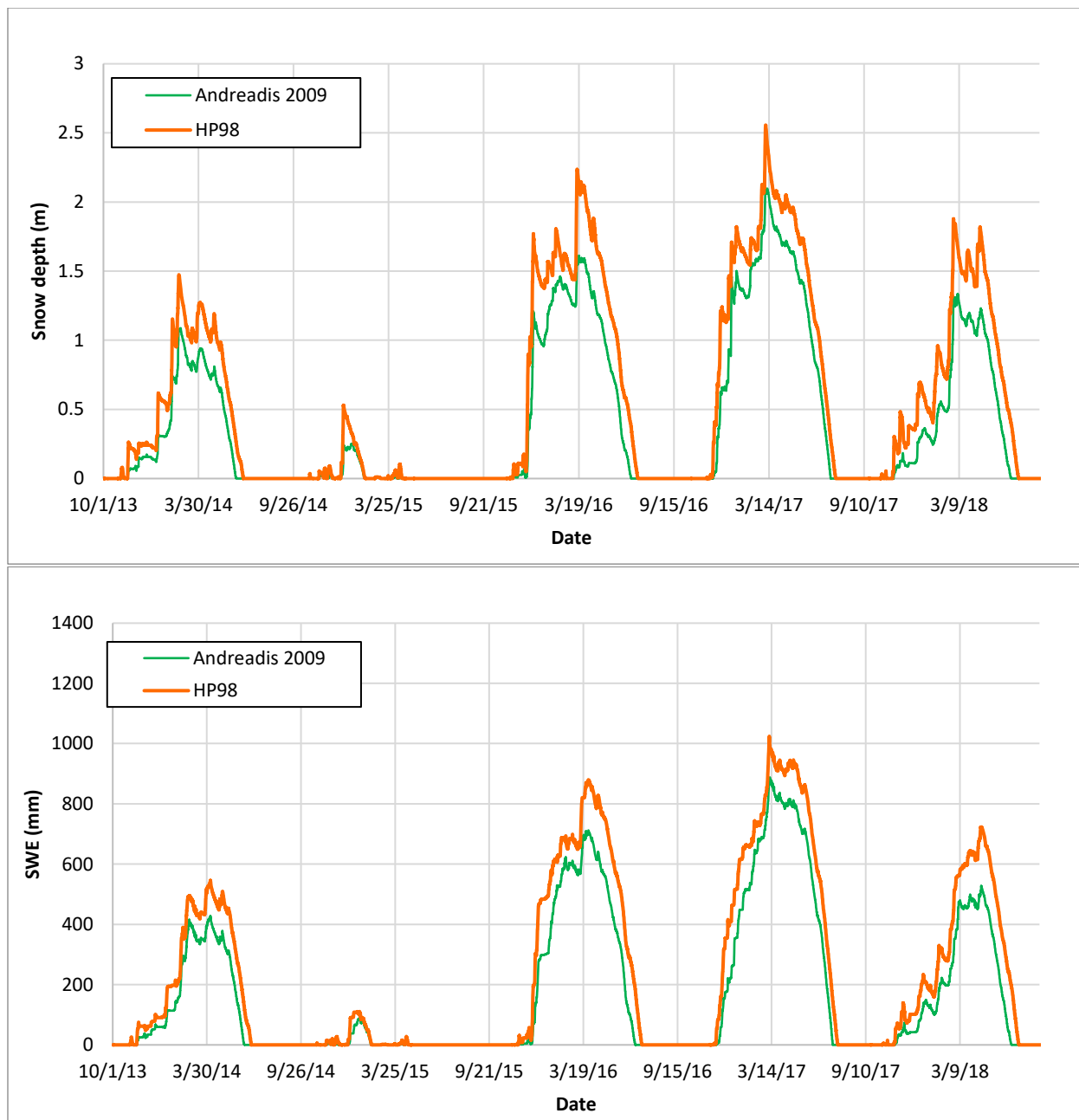


Figure 34. Snow depth and SWE output from a sensitivity analysis with the canopy interception of snow option

5. Discussion

The goal of this study was to explore the application of contemporary snow measurement and modeling tools to investigate how conifer forests may influence seasonal snowpack dynamics in a maritime snow climate. Results indicate that multiple factors operating at many spatial scales influence snow depth, SWE, and duration in the H.J. Andrews Experimental Forest, located in the Willamette National Forest, western Oregon, USA. Lidar imagery provided a synoptic view of the snowpack on a single date, but there was considerable uncertainty ($\pm 200\text{-}300$ mm) in lidar-derived snowpack depth values compared to field measurements, and snow depth was not consistently related to lidar-derived canopy height. Simulated snow depth and SWE using the SUMMA model reproduced measured snow variables over the 2014 to 2018 snow seasons with a Nash-Sutcliffe efficiency of 0.7 to 0.93 in the opening at a meteorological station at 1300 m elevation, when forced by data from that station. However, simulated snow depth and SWE under forests, using a parameterization for canopy interception of snow based on empirical studies in the nearby Umpqua National Forest, were much higher than indicated by long-term snow stake surveys and other field sampling.

5.1 Effects of forest structure and topographic factors on snow

Snow depth and density data collected with snow surveying, remote sensing, and estimated with snow modeling indicated that the spatial variability of snow in the H.J. Andrews Experimental Forest was not controlled by any single factor, but is influenced by elevation and landscape position, as well as vegetation cover type and forest structure.

Snow, especially the effect of forests on snow, was expected to have different characteristics in the maritime climate of the Andrews Forest than in a continental climate, because of winter climate conditions that bring warm air temperatures, low wind, and high surface-ground interface temperatures (Sturm et al., 1995). Prior literature has explored the effect of maritime climate (Dickerson-Lange et al., 2015), elevation (Molotch & Meromy, 2014), aspect (Hinckley et al., 2014), and forest cover (Dickerson-Lange et al., 2021) on seasonal snowpack. The characteristics of seasonal mountain snowpack in a maritime climate are distinctly different from those of a continental or boreal snow climate (Sturm et al., 1995). The

relative strength of the effect of forests on snowpack accumulation and ablation is determined by snow climate (see Introduction) (Dickerson-Lange et al., 2021). In both maritime and continental snow climates, the effect of canopy interception of snow on snowpack accumulation is controlled by air temperature and snow event size. Warmer air temperature creates canopy conditions that are more efficient at intercepting snow than colder air temperature (Roth & Nolin, 2019). Forests effects on snow accumulation in the Pacific Northwest are enhanced because the land area of the region consists of 80% forest cover (Alig et al., 2000).

5.1.1 Maritime climate effects

Results of this study indicated that snow density at the meteorological stations ranged from 250 kg/m^3 to 550 kg/m^3 , was on average 400 kg/m^3 , and was 250 kg/m^3 at the beginning of the snow season and 550 kg/m^3 at the end of the snow season. In addition, average snow densities were 365 kg/m^3 at long-term snow stakes, with little change with elevation or vegetation cover type (forest vs. opening). These snow densities compare to reported snow densities at SNOTEL site in maritime temperate climates of 400 kg/m^3 on average, 250 kg/m^3 at the beginning, and 600 kg/m^3 at the end of the snow season (Mizukami & Perica, 2008). In contrast, reported snow densities at a SNOTEL site in a continental climate were 350 kg/m^3 on average, 150 kg/m^3 at the beginning, and 550 kg/m^3 at the end of the snow season (Mazurkiewicz et al., 2008). The higher average snow densities in the maritime climate of the Andrews Forest compared to continental climates are due to warmer winter temperatures and deeper snowpack in the maritime climate. Modeled snow density values of canopy delivered snow by Bonner et al. (2022) suggested that snow sloughed from the canopy in continental climates is $150\text{-}240 \text{ kg/m}^3$, while the density of snow sloughed from the canopy in maritime climates is as great as 500 kg/m^3 . This process highlights just one of many ways canopy dominates snow processes in a maritime climate.

5.1.2 Effects of elevation

Snow characteristics were expected to be related to elevation, because air temperature and precipitation change with elevation. Snow depth generally increases with elevation despite differences in canopy cover, climate, or topography (Tennant et al., 2017). It was expected that snow depth, SWE, and snow disappearance date would increase with elevation because of declining air temperature with elevation, while snow density would be greater in the open compared to beneath forests because snow is deeper in openings, causing compaction, and more longwave emission occurs in forests, which contributes energy to both snow on the ground and snow stored in the canopy. The study site included the transition from the ephemeral to maritime seasonal snow zone, two classes within which snowpack varies considerably in depth, extent, and metamorphism in maritime climates (Sturm et al., 1995;

Sturm & Liston, 2021). This study examined snow over the range of elevation of 600 to 1400 m, which is considered to be part of the transient (350-1100 m) snow zone (Harr, 1986). The study spanned forests of the Douglas-fir/western hemlock zone (below 1000 or 1200 m), transition zone, and subalpine true-fir forest zone (above 1200 m) (Zobel et al., 1976).

A visual analysis of snow depth over the long-term at paired open/forest sites showed increases in depth with elevation at both the open and forest stakes (Figure A-1, Appendix A), but snow depth sampled in the field in March of 2022 and 2023 (Table 4), and in 60x60 polygons in the lidar image was not related to elevation (Figure 17). Also, snow density beneath forests was not related to elevation at the MS00701 forest snow stakes (Table 11). Daily snow density at the meteorological stations increased as the winter season progressed, but sample size was too limited to comment on differences in snowpack density in the open across elevations. Differences in landscape position, slope orientation, and/or forest cover and structure (see below) probably account for the lack of relationships of snow depth and density to elevation in short-term sampling.

5.1.3 Effects of slope orientation

Snow characteristics were expected to differ based on aspect, because aspect in the rain-snow transition zone —where snow accumulates and persists near 0 °C— plays a particularly important role in accumulation and ablation (Hinckley et al., 2014). Shading of surfaces by adjacent terrain and exposure to prevailing winds leads to melting and compaction. In the northern hemisphere, slopes with south aspects have much more incident solar than north facing slopes, causing higher melt rates (Dewalle, 2008). Snow depth in the March 2022 lidar image was qualitatively greater on N and E-facing slopes, but this effect was not tested statistically (Figure 9). In a limited sampling of a ridge line at 1500 m in the snow height model, the N aspect had a mean value of 2.3 m snow depth, and the adjacent S aspect had a mean depth value of 0.6 m. The bottom of Lookout Creek had 1.3 m. The average depth of the whole snow height model was 0.54 m.

5.1.4 Effects of landform position and air drainage

Snow characteristics were expected to differ based on landform position (hillslopes vs. valleys), as differences in slope and aspect cause temperature inversions and cold air flows (Malek, 2019; Rupp et al., 2020). In the Andrews Forest, temperature inversions occur during most months out of the year (Rosentrater, 1997; Rupp et al., 2021). Visual inspection of the lidar image in this study indicated deeper snowpack in the valley floor of upper Lookout Creek, but this effect was not tested statistically (Figure 9). Open canopy in the upper, west facing slopes of the L704A and L704C strip clearcuts (Figure 7) may facilitate cold air drainage and pooling in the valley floor, preserving deeper snow (Figure 9, Table 4, Table 7).

5.1.5 Effect of vegetation cover type

Snow characteristics were expected to differ in openings vs. forest, because forests intercept snow and emit longwave, decreasing snowpack accumulation. Reduction of snow accumulation from canopy interception of snow is expected to dominate over canopy shading and protection from wind, which could increase snow depth, in the Oregon maritime climate (Dickerson-Lange et al., 2017). Results from long-term paired snow stakes under forest and in openings indicate that forest canopies intercepted forty to sixty percent of snow over the study period (Appendix A, Figure A-1). The ratio of snow depth under the forest to snow depth in the open generally decreased with elevation.

Many studies have investigated the effect of mature/old-growth forests on microclimate (Chen et al. 1993; Gray et al., 2002). Microclimate can be influenced by vegetation, micro-topography, and elevation, but quantifying it requires fine spatial resolution measurements (Frey et al., 2016, Wolf et al. 2020). Comparing snow in “forest” vs. “open” sites along roads revealed large differences in snow characteristics. Snow depth under forest was much less than in openings at field-measured sites (Table 10) and at long-term snow stakes (Table 11, Figure 17).

Snow disappeared earlier and snow depth loss rates (a measure of melt rate) were less rapid at forest snow stakes than paired open snow stakes (Table 14). However, mean winter snow density was not different at forest snow stakes compared with paired open snow stakes

(Table 15). The Hedstrom and Pomeroy (1998) snow interception model used in this study focuses on event size and forest structure as the drivers of interception, rather than air temperature. In contrast, the Andreadis et al. (2009) parameterization is almost entirely dependent on air temperature but produces simulated snow depth and SWE (Figure 33) that is slightly less under forest than in the open. Although designed from empirical measurement of snow interception in Umpqua National Forest, the Andreadis interception model does not replicate interception amounts at Upper Lookout. Omission of air temperature or canopy structure considerations could contribute to model underestimates of interception (Roth & Nolin, 2019). Martin et al. (2013) also found that the VIC model underpredicted forest canopy interception by 33%, illustrating the prevalence of this issue in the snow modeling community.

5.1.6 Effects of forest structure

Snow characteristics were expected to differ based on forest structure differences between mature/old-growth forests versus planted forests, including edges, gaps, canopy height, and canopy density. The term 'forest structure' generally refers to the essential attributes of a forest stand such as structural type, size, and spatial distribution of vegetation components (Spies, 1998). The structural characteristics of planted and mature/old-growth forests influence microclimate (Frey et al., 2016). In this study, forest structure was categorized as 'planted forests' and 'mature/old-growth forests' to investigate differences in snow depth. The 'planted forest' class refers to forest that was harvested and planted 50-70 years ago. Mature/old-growth forests regenerated after wildfires circa 1500 CE and the mid 1800s CE. The structural components of old-growth forests include a diverse range of tree heights and crown diameters, a deep, dense overstory canopy, snags of varying size classes, and abundant downed and dead wood (Spies & Franklin, 1991). In contrast, planted stands have shorter canopies, denser stands, less species diversity, and less dead and down wood. The Andrews Forest (Figure 2) is typical of National Forests across the western United States, which are a mosaic of patches of plantations and remnant old growth, intersected by a network of linear openings along forest roads and a network of edges between patches and between roads and adjacent forests.

In contrast, private industrial forest land has younger intensively managed plantations, and fresh clearcuts.

Snow was expected to differ between forest and openings, depending on distance from an edge, or the size of the canopy gap. Chen et al. (1993) found that the transitions from forest to clearcut opening create microclimate influences on incoming radiation, relative humidity, vapor pressure, and air temperature, creating gradients across edges. The orientation of forest edges particularly influences air temperature and relative humidity in the summer (Chen et al 1993). However, edge orientation was not associated with differential patterns of snow depth in the winter in maritime snow climates (Currier & Lundquist, 2018). Snow stakes are located along logging roads that were constructed in the 1950s and 1960s (see e.g., Jones and Grant 1996). When they were constructed, the road width (“right of way”) was about 20 m including the cut slope, fill slope, and road surface. However, in the ensuing 60 years, trees have established on the road cut and road fill and the branches of neighboring trees have extending into the light gap above the road, so canopy gaps above current roads may be as little as ~5-8 meters wide. Forest gap formation, size, and distribution is highly variable and depends on species composition within the stand. The width of the road gap is not dissimilar from sizes of naturally formed forest gaps, which range from ~4 to 9 m in diameter in mature (140 year) and old growth (400-500) Douglas-fir stands in the Cascade Range (Spies et al., 1990). Gap widths of 5-10 m diameter are a small fraction of the height of neighboring trees, including 50 to 60-yr-old planted forests (30+ m tall) or mature/old-growth forest (60 – 80 m tall), so they are highly affected by edges. Snow intercepted along the forest-opening edge may reduce snow in the road opening, or it may cascade onto the road gap, increasing snow in the road gap and potentially reducing snow within the forest along the forest-road edge.

Snow also was expected to differ between planted and mature/old-growth forest based on differences in canopy height and canopy density. Across all snow climates, the dominant effect of conifer forests on snow accumulation and melt is the formation of tree wells (Musselman et al., 2008). Using DHSVM to model snowpack response to canopy density across multiple snow climates, Sun et al. (2022) found that increased canopy density was associated with reduced peak SWE and earlier snow disappearance date. A forest canopy density of 25 to

40% was associated with maximum snow accumulation based on field sampling and modeling in a continental climate by Veatch et al. (2009). Generally, across all climates, peak SWE decreases as the density of the forest canopy increases. In warm maritime climates, the effect of canopy density depends on the counteracting effects of interception versus exposure to solar radiation (Sun et al., 2022).

The results of this study showed that snow depth sampled in the field in March, 2022 was significantly greater in planted forest stands than in nearby mature/old-growth stands (Table 4). However, lidar-derived snow depth of mature/old-growth forest stands, with an average canopy height of 35 m, was not significantly different than lidar-derived snow depth in adjacent planted forests, with an average canopy height of 23 m (Table 13). Furthermore, canopy height was not related to lidar-derived snow depth in ten pairs of 60x60 m polygons (Figure 19).

This lack of a clear relationship between canopy height and snow depth may be explained by the effects of stand density. Stand density and canopy closure were higher in planted forests than in adjacent mature/old-growth sampled in this study, but canopy height was greater in the mature/old-growth forest. A greater number of tree boles creating tree wells combined with the high canopy closure in the planted forests may explain the low snow depths measured in field sampling in March 2022 (Table 4) and March 2023 (Table 7). Also, sparse canopies in some planted forest stands (Photograph 3) are associated with deeper snowpacks than in planted stands with dense canopies (Photograph 4, Photograph 7). The shorter, denser canopy of the planted forests and the taller, less dense canopy of the mature/old-growth forests could have counteracting effects on snow accumulation, explaining the similar March snow depths between the two canopy types observed in this study. The ten pairs of sites used in the lidar analysis provided only limited information about the spatial variability of snow beneath forests. Further work using lidar-derived snow depths, lidar-derived canopy structure, and lidar bare earth models could help to identify forest structural characteristics and other factors that explain differences in snow depth.

5.2 Implications and relevance

Forecasting and measuring snow depth, SWE, and snow disappearance date is important to water supply, the surface energy balance, and soil moisture in mountain ecosystems. Snow metrics such as SWE and SDD of seasonal mountain snowpack help inform water management decisions, such as spring discharge estimates, that are critical to summer water supply. The Pacific Northwest has a Mediterranean summer climate with dry, hot summers and the late spring and summer stream discharge is sensitive to late spring/early summer snow water storage (Brooks et al., 2012). This study used lidar imagery to estimate the total snow water volume stored in the Andrews Forest and express it in terms of equivalent days of flow at Lookout Creek, the drainage basin that comprises the Andrews Forest (Table 18). If the average snow depth from the lidar image is accurate, this calculation indicated that the volume of water stored on March 17, 2022 was equivalent to 29 to 31 days of mean daily flow at Lookout Creek, or 3.6 to 3.7 days of continuous high flow at a rate of the 1-year return period peak discharge. This volume does not represent peak SWE, so the amount of water contributed to discharge from the snowpack may have been greater than this estimate. On the other hand, this estimate may be too high, because the lidar snow depth may have been overestimated when using the 29.5 cm correction.. Furthermore, the lidar-derived snow depth does not include losses to basal discharge, a process that contributes water to the underlying soils throughout the winter, particularly in the ablation season. Contributions to soil moisture and run-off from basal discharge are not included in the lidar-derived SWE estimate and likely cause the estimated SWE volume to be lower than the actual water contribution from the snowpack to spring discharge, especially when considering the porosity of the soils in the Andrews Forest.

Table 18. Lidar-derived snow depth on March 17, 2022 as a volume of water based on average daily SWE measured 1997-2014 at the three meteorological stations and expressed in terms of equivalent streamflow at the mouth of Lookout Creek.

	SWE = 0.38	SWE = 0.4
average snow depth (m)	0.544	0.544
snow density (%)	0.380	0.400
snow water depth (m)	0.207	0.218
Snow water volume (m ³ /m ²)	0.207	0.218
m ² per ha	10000	10000
Snow water volume (m ³ /ha)	2067	2176
n of hectares	4204	4204
Snow water volume (m ³ in 4204 ha)	8690175	9147553
mean daily flow at Lookout Creek, WY 1950-2018 (cfs)	122	
m ³ /s per cfs	0.028316847	
mean daily flow at Lookout Creek, WY 1950-2018 (m ³ /s)	3.45	
seconds per day	86400	
Lookout Creek, m ³ per 24 hours of mean daily flow, WY 1950-2018 (m ³ /s)	298482	
N of days of mean daily flow of Lookout Creek equivalent to snow stored on March 17, 2022	29	31
~1-year return flow at Lookout Creek (cfs)	1000	
m ³ /s per cfs	0.028316847	
~1-year return flow at Lookout Creek (m ³ /s)	28.32	
seconds per day	86400	
Lookout Creek, m ³ per 24 hours at ~1-yr return period	2446576	
N of days of 24-hour flow of Lookout Creek at 1-yr-return period rate equivalent to snow stored on March 17, 2022	3.6	3.7

In addition to contributing to water supply, seasonal mountain snowpack plays an important part in the surface energy balance by increasing land surface albedo. The snow disappearance date, i.e. the day that snow disappears from the land surface, marks a shift in surface albedo. This study showed that snow disappeared on average 6 days earlier under forest than in openings created by roads.

Tools such as lidar and automated snow stakes can help assess the spatiotemporal variability of snow and its response to forest cover and forest structure. Understanding how trees influence snowpack in this relatively warm, wet winter environment may influence how forests are managed, both on public and private lands. Results of this study confirm prior findings that forest management decisions such as clearcutting, selective thinning, and salvage logging, which create openings, have an impact on seasonal snowpack in the Cascades. The paired MS00701 snow stake data from 1994–2022 revealed that forests reduce snow accumulation by 62% on average when compared to openings (Table 16). However, this study also showed quite varied impacts of past forest management decisions on snow depth, SWE, and SDD in planted forests, depending on forest regeneration and forest structure. Continued research about forest effects on seasonal snowpack is needed as forested landscapes continue to change in response to forest management decisions and anthropogenic climate change.

Remote sensing and modeling of snow enable snow metrics to be measured and estimated in areas where field measurements are rare or difficult to obtain. Measuring and modeling of snow in the transient snow zone is complicated by many factors, including precipitation phase partitioning and new snow density (Wayand et al., 2016). Much of the lower elevation seasonal snowpack is expected to shift to transient snowpack in the face of future climate warming. The snow simulation modeling in this study showed that snow accumulation and melt were quite sensitive to early snow season air temperature, suggesting that climate warming in November and December could reduce the snowpack. These findings are consistent with predictions (e.g., Nolin and Daly 2006 and Sproles et al., 2013).

5.3 Limitations and recommendations

5.3.1 Snow surveying

The high spatial variability of snow within forests requires many samples to accurately represent snowpack behavior in space and time. Snow surveying is time consuming and can be dangerous. Mountain slopes are remote, steep, and prone to avalanches. Digging snow pits or using a Federal sampler is a time-consuming task that produces a few point measurements and point measurements in the field may obscure fine scale topographic effects on snow depth and density. Snow depth measurements at the road stakes may be influenced by edge effects with adjacent forests. SWE measurements taken with a Federal sampler are prone to error as snow slides out of the tube, dirt plugs the tube, or snow is melted by friction, while snow depth measurements taken with an avalanche probe frequently overestimate depth by penetrating underlying soils.

Nevertheless, many forested areas have roads that provide access with a good 4WD vehicle and a set of chains, and field snow survey may be the safest, least-cost and most precise and accurate method for these areas. In contrast, long-term snow monitoring sites, such as the meteorological stations in the Andrews Forest or SNOTEL sites, involve expensive equipment that requires frequent maintenance. A snow survey, such as the snow stake surveys in this study that accompany maintenance visits to a monitoring site can be a low-cost way to obtain high quality snow depth and SWE data.

5.3.2. Lidar snow survey

Lidar technology has advanced since the turn of the century, including higher precision, greater accessibility to the public, and lower costs. The technology is widely used. ‘Snow-on’ lidar surveys produce snow depth values at a 1 square meter resolution over a large area at one time. Furthermore, lidar surveys can retrieve data in remote locations that are difficult or dangerous to access. Lidar has potentially high value as a means to extrapolate snow cover from distributed field snow surveys and monitoring stations that collect SWE measurements.

Lidar-derived snow depth measurements had 200 to 300 mm of uncertainty, and sometimes, but not always, over-estimated snow depth measured in the field. Some of these differences may have been due to horizontal uncertainty of GPS coordinates for field sampling locations and/or lidar spatial errors, while others may be related to vertical errors associated with the sensing of the top of the snowpack or the bare earth, which was subtracted from the snowpack lidar image to obtain lidar-derived snow depth. Accuracy of scanning lidar is specified in the horizontal (x, y) and the vertical (z) (Deems et al., 2013). The error in horizontal accuracy is largely determined by errors in altitude measurement and the vertical accuracy is determined largely by errors in range measurement to target. Common sources of error in ALS systems arise from terrain geometry (occlusion), scattering, boresight offset, vegetation, and light absorption in the near surface snow layers in near infrared wavelengths. Sources of error in airborne lidar scanning applications over mountain terrain arise from the geometric relationship between aircraft dynamics, the scanning system, and the complex topography of the ground surface (Deems et al., 2013). One possibility, which deserves further exploration, is how the bare earth DTM for the Andrews Forest senses the top of the forest floor (i.e., the top of the litter and down wood layer) vs. the top of the mineral soil. If the lidar bare earth DTM primarily senses the top of the mineral soil, lidar-derived snow depths may also include forest floor, overestimating the snowpack.

Airborne lidar surveys are expensive. The survey requires an aircraft, a survey team, a data processing team, and all the associated equipment. A 'snow-on' lidar survey produces a measurement at one point in time, but hydrologists are interested in how snow varies from day to day or week to week, and repeating airborne lidar surveys at frequency needed to measure accumulation and melt rates is not feasible.

5.3.3 Snow modeling

The complexity in the spatiotemporal variability of seasonal mountain snowpack is difficult to model. Hydrologic processes vary considerably with climate type. Using a modeling framework that includes commonly employed representations of hydrologic process, such as SUMMA, can help illustrate how each parameterization of a process affects snowpack. This can

help guide model decision selection when modeling snow across different climates and locations.

Errors in a hydrologic simulation model can arise from the model boundary conditions and inputs, error associated with using an approximation of a real process, and error in the measurement of the variable being simulated. Furthermore, the equifinality principle suggests that there is no single correct representation of a system given normal limitations and characterization data, meaning there is no single correct representation of a processes in the hydrologic system (Beven, 2006). In this study, model output was compared to measured data from a provisional snow dataset that had an unknown number of potentially erroneous values. A visual check was made to remove anomalously high or negative values in the provisional dataset for snow depth measured by the acoustic depth sensor, but no formal QA/QC process has been completed on these data. Snow depth data early in WY 2016 were particularly full of errors, making model assessment of modeled snow depth impossible during that period and affecting reported NSE values.

Representations of individual pieces of the hydrologic system within models are, at times, based on measurements from very few studies. For example, the process of canopy interception of snow within hydrologic models is largely based off empirical measurements from only two studies, Hedstrom and Pomeroy (1998) and Storck et al. (2002). A greater effort toward more intensive field campaigns to study forest canopy interception of snow in the maritime climate of the Andrews Forest could help improve equations in the SUMMA model.

6. Conclusion

This study applied contemporary modeling, measuring, and remote sensing of snow techniques to investigate effects of forest cover, topography, and microclimate on the variability of seasonal snowpack in the transient to seasonal snow zones (800 to 1400 m) of the H.J. Andrews Experimental Forest, western Cascade Range, Oregon, US.

Long-term (1994 to 2022) paired snow stake data in openings along roads and under adjacent forests indicated that the canopy of the conifer forests of the Andrews Forest intercepts as much as 60% of snow over a winter season. The ratio of snow depth beneath forests relative to openings decreases with elevation. Mean snow density was similar (364 kg/m³ and 366 kg/m³) across all elevations in forests and openings.

A survey using airborne laser scanning (ALS) captured an image that was used to construct a snowpack surface covering >4000 ha of the upper-elevation portion of the Andrews Forest HUC on March 17, 2022. Lidar-derived snow depths had an error of +/- 200-300 mm compared to field measurements. Shaded slopes and temperature inversions contributed to greater snow depth on north and east facing slopes and along the valley floor of upper Lookout Creek, both in the lidar image and in field sampling during March 2023.

High canopy density and associated interception and tree wells may explain lower snow depth under planted forest stands with closed canopies based on field sampling of snow in March 2023. However, forest canopy height did not explain lidar-derived snow depth in a limited sample of 60x60 m polygons in planted vs. adjacent mature/old-growth forest.

Simulated snowpack using SUMMA somewhat accurately reproduced SWE at the meteorological station (1298 m) but overestimated snow depth beneath conifer forests compared to data from paired snow stakes in forest and openings at similar elevations. Further long-term snow measurement at paired forest/open sites and meteorological stations are needed to improve model snow interception parametrizations. More robust parametrizations of canopy interception of snow are needed for accurate snow simulation modeling in forests in maritime climates.

Overall, long-term observational data indicated that conifer forest canopy in the maritime climate of the H.J. Andrews Experimental Forest is capable of high amounts of interception, producing shallower snowpack under forest that was not replicated using a widely-used snow interception models. At the same time, a lidar-derived image of snow depth spanning elevations of 800 to 1600 m and >4000 ha in the landscape indicated that many other factors, including elevation, landscape position, and slope orientation created complex patterns of snow depth that were not consistently related to forest canopy height. Nevertheless, the lidar-derived estimated volume of water stored in the landscape on March 17, 2022 was equivalent to one month of mean daily flow at the mouth of Lookout Creek, which comprises the H.J. Andrews Experimental Forest.

Overall, this study applies multiple snow measuring and modeling methods to investigate depth and density differences of snow in forests in the transient snow zone in a maritime climate. These findings reveal that multiple factors contribute to snow spatial and temporal variability. Results underscore the need for continued long-term monitoring and additional analysis of observational data from long-term snow stakes, meteorological stations, and process-based studies to develop more robust canopy interception of snow equations in the transient to seasonal snow zones of maritime snow climates.

References

- Ali Malek. (2019). *Empirical Analysis of Processes Affect Drainage Flows and Inversions in a Forested Mountain Landscape*.
<https://andrewsforest.oregonstate.edu/publications/5093>
- Alig, R., Zheng, D., Spies, T., & Butler, B. (2000). Forest Cover Dynamics in the Pacific Northwest West Side: Regional Trends and Projections. *USDA Forest Service - Research Papers RMRS*.
- Andreadis, K., Storck, P., & Lettenmaier, D. (2009). Modeling snow accumulation and ablation processes in forested environments. *Water Resources Research*, 45.
<https://doi.org/10.1029/2008WR007042>
- Berris, S. N., & Harr, R. D. (1987). Comparative snow accumulation and melt during rainfall in forested and clear-cut plots in the Western Cascades of Oregon. *Water Resources Research*, 23(1), 135–142. <https://doi.org/10.1029/WR023i001p00135>
- Beven, K. (2006). A manifesto for the equifinality thesis. *Journal of Hydrology*, 320(1), 18–36.
<https://doi.org/10.1016/j.jhydrol.2005.07.007>
- Brooks, J. R., Wigington, Parker, Phillips, Donald, Comeleo, R., & Coulombe, R. (2012). Willamette River Basin surface water isoscape ($\delta^{18}\text{O}$ and $\delta^2\text{H}$): Temporal changes of source water within the river. *Ecosphere*, 3, 39. <https://doi.org/10.1890/ES11-00338.1>
- Choi, Y. D., Goodall, J., Sadler, J., Bennett, A., Goodall, J., Nijssen, B., Clark, M., Castronova, A., & Tarboton, D. (2018). Prototyping a Python wrapper for the Structure for Unifying Multiple Modeling Alternatives (SUMMA) hydrologic modeling framework. *International Congress on Environmental Modelling and Software*.
<https://scholarsarchive.byu.edu/iemssconference/2018/Stream-A/47>
- Clark, M., Nijssen, B., Lundquist, D., Kavetski, D., Rupp, E., Woods, A., Freer, E., Gutmann, D., Wood, W., Brekke, D., Arnold, R., Gochis, J., Rasmussen, M., Tarboton, G., Mahat, V., Flerchinger, N., & Marks, G. (2015). *The structure for unifying multiple modeling alternatives (SUMMA), Version 1.0: Technical Description*.
<https://doi.org/10.5065/D6WQ01TD>

- Clark, M. P., Hendrikx, J., Slater, A. G., Kavetski, D., Anderson, B., Cullen, N. J., Kerr, T., Örn Hreinsson, E., & Woods, R. A. (2011). Representing spatial variability of snow water equivalent in hydrologic and land-surface models: A review. *Water Resources Research*, 47(7). <https://doi.org/10.1029/2011WR010745>
- Clark, M. P., Nijssen, B., Lundquist, J. D., Kavetski, D., Rupp, D. E., Woods, R. A., Freer, J. E., Gutmann, E. D., Wood, A. W., Brekke, L. D., Arnold, J. R., Gochis, D. J., & Rasmussen, R. M. (2015). A unified approach for process-based hydrologic modeling: 1. Modeling concept. *Water Resources Research*, 51(4), 2498–2514. <https://doi.org/10.1002/2015WR017198>
- Clark, M. P., Nijssen, B., Lundquist, J. D., Kavetski, D., Rupp, D. E., Woods, R. A., Freer, J. E., Gutmann, E. D., Wood, A. W., Gochis, D. J., Rasmussen, R. M., Tarboton, D. G., Mahat, V., Flerchinger, G. N., & Marks, D. G. (2015). A unified approach for process-based hydrologic modeling: 2. Model implementation and case studies. *Water Resources Research*, 51(4), 2515–2542. <https://doi.org/10.1002/2015WR017200>
- Clark, M. P., Zolfaghari, R., Green, K. R., Trim, S., Knoben, W. J. M., Bennett, A., Nijssen, B., Ireson, A., & Spiteri, R. J. (2021). The Numerical Implementation of Land Models: Problem Formulation and Laugh Tests. *Journal of Hydrometeorology*, 22(6), 1627–1648. <https://doi.org/10.1175/JHM-D-20-0175.1>
- Currier, W. R., & Lundquist, J. D. (2018). Snow Depth Variability at the Forest Edge in Multiple Climates in the Western United States. *Water Resources Research*, 54(11), 8756–8773. <https://doi.org/10.1029/2018WR022553>
- Dave Bell. (2023). *2020 HJA Canopy Height Model* [dataset].
- David Dewalle. (2008). *Principles of snow hydrology*. Cambridge University Press.
- Deems, J. S., Painter, T. H., & Finnegan, D. C. (2013). Lidar measurement of snow depth: A review. *Journal of Glaciology*, 59(215), 467–479. <https://doi.org/10.3189/2013JoG12J154>
- Dennis Harr. (1981). *Some characteristics and Consequences of Snowmelt During Rainfall in Western Oregon*. <https://andrewsforest.oregonstate.edu/publications/605>

- Dickerson-Lange, S. E., Lutz, J. A., Gersonde, R., Martin, K. A., Forsyth, J. E., & Lundquist, J. D. (2015). Observations of distributed snow depth and snow duration within diverse forest structures in a maritime mountain watershed. *Water Resources Research*, *51*(11), 9353–9366. <https://doi.org/10.1002/2015WR017873>
- Dickerson-Lange, S. E., Vano, J. A., Gersonde, R., & Lundquist, J. D. (2021). Ranking Forest Effects on Snow Storage: A Decision Tool for Forest Management. *Water Resources Research*, *57*(10), e2020WR027926. <https://doi.org/10.1029/2020WR027926>
- Dickerson-Lange, S., Gersonde, R., Hubbart, J., Link, T., Nolin, A., Perry, G., Roth, T., Wayand, N., & Lundquist, J. (2017). Snow disappearance timing is dominated by forest effects on snow accumulation in warm winter climates of the Pacific Northwest, USA: Forest Effects on Snow Across the Pacific Northwest. *Hydrological Processes*, *31*. <https://doi.org/10.1002/hyp.11144>
- Frey, S. J. K., Hadley, A. S., Johnson, S. L., Schulze, M., Jones, J. A., & Betts, M. G. (2016). Spatial models reveal the microclimatic buffering capacity of old-growth forests. *Science Advances*, *2*(4), e1501392. <https://doi.org/10.1126/sciadv.1501392>
- Goodman, A. C., Segura, C., Jones, J. A., & Swanson, F. J. (2023). Seventy years of watershed response to floods and changing forestry practices in western Oregon, USA. *Earth Surface Processes and Landforms*, *48*(6), 1103–1118. <https://doi.org/10.1002/esp.5537>
- Hannah M. Bonner, Mark S. Raleigh, & Eric E. Small. (2022). *Isolating forest process effects on modelled snowpack density and snow water equivalent*. <https://doi.org/10.1002/hyp.14475>
- Harr, R. D. (1986). Effects of Clearcutting on Rain-on-Snow Runoff in Western Oregon: A New Look at Old Studies. *Water Resources Research*, *22*(7), 1095–1100. <https://doi.org/10.1029/WR022i007p01095>
- Hedstrom, N. R., & Pomeroy, J. W. (1998). Measurements and modelling of snow interception in the boreal forest. *Hydrological Processes*, *12*(10–11), 1611–1625. [https://doi.org/10.1002/\(SICI\)1099-1085\(199808/09\)12:10/11<1611::AID-HYP684>3.0.CO;2-4](https://doi.org/10.1002/(SICI)1099-1085(199808/09)12:10/11<1611::AID-HYP684>3.0.CO;2-4)

- Hinckley, E.-L. S., Ebel, B. A., Barnes, R. T., Anderson, R. S., Williams, M. W., & Anderson, S. P. (2014). Aspect control of water movement on hillslopes near the rain–snow transition of the Colorado Front Range. *Hydrological Processes*, *28*(1), 74–85.
<https://doi.org/10.1002/hyp.9549>
- Jefferson, A., Nolin, A., Lewis, S., & Tague, C. (2008). Hydrogeologic controls on streamflow sensitivity to climate variation. *Hydrological Processes*, *22*(22), 4371–4385.
<https://doi.org/10.1002/hyp.7041>
- Jennings, K., & Jones, J. A. (2015). Precipitation-snowmelt timing and snowmelt augmentation of large peak flow events, western Cascades, Oregon. *Water Resources Research*, *51*(9), 7649–7661. <https://doi.org/10.1002/2014WR016877>
- Jones, J. A., & Perkins, R. M. (2010). Extreme flood sensitivity to snow and forest harvest, western Cascades, Oregon, United States. *Water Resources Research* *46*. W12512. 21 p, 46. <https://doi.org/10.1029/2009WR008632>
- Jones, J., & Grant, G. (1996). Peak Flow Responses to Clear-Cutting and Roads in Small and Large Basins, Western Cascades, Oregon. *Water Resources Research - WATER RESOUR RES*, *32*, 959–974. <https://doi.org/10.1029/95WR03493>
- Largeron, C., Dumont, M., Morin, S., Boone, A., Lafaysse, M., Metref, S., Cosme, E., Jonas, T., Winstral, A., & Margulis, S. A. (2020). Toward Snow Cover Estimation in Mountainous Areas Using Modern Data Assimilation Methods: A Review. *Frontiers in Earth Science*, *8*, 325. <https://doi.org/10.3389/feart.2020.00325>
- Lawrence, D. M., Oleson, K. W., Flanner, M. G., Thornton, P. E., Swenson, S. C., Lawrence, P. J., Zeng, X., Yang, Z.-L., Levis, S., Sakaguchi, K., Bonan, G. B., & Slater, A. G. (2011). Parameterization improvements and functional and structural advances in Version 4 of the Community Land Model. *Journal of Advances in Modeling Earth Systems*, *3*(1).
<https://doi.org/10.1029/2011MS00045>
- Levno, A. B., Schulze, M. D., & Downing, G. (2023). *Snow depth and snow water equivalent measurements along a road course and historic snow course in the Andrews Experimental Forest, 1978 to present* [dataset]. Environmental Data Initiative.
<https://doi.org/10.6073/PASTA/FA08F53ADC1B657B2AA12311E91C8EE7>

- Li, D., Wrzesien, M. L., Durand, M., Adam, J., & Lettenmaier, D. P. (2017). How much runoff originates as snow in the western United States, and how will that change in the future? *Geophysical Research Letters*, *44*(12), 6163–6172.
<https://doi.org/10.1002/2017GL073551>
- Lienkaemper, G., & Schulze, M. (2015). *Vegetation classification, Andrews Experimental Forest and vicinity (1988,1993,1996,1997,2002, 2008)* [dataset]. Environmental Data Initiative.
<https://doi.org/10.6073/PASTA/68296D816C9F4D8FE6E8BC3ED1668A5B>
- Lundquist, J. D., Dickerson-Lange, S., Gutmann, E., Jonas, T., Lumbrazo, C., & Reynolds, D. (2021). Snow interception modelling: Isolated observations have led to many land surface models lacking appropriate temperature sensitivities. *Hydrological Processes*, *35*(7), e14274. <https://doi.org/10.1002/hyp.14274>
- Lynn D. Rosentrater. (1997). *Thermal Climate of the H.J. Andrews Experimental Forest, Oregon*.
<https://andrewsforest.oregonstate.edu/publications/2383>
- Marshall, J. D., & Waring, R. H. (1986). Comparison of Methods of Estimating Leaf-Area Index In Old-Growth Douglas-Fir. *Ecology*, *67*(4), 975–979. <https://doi.org/10.2307/1939820>
- Martin, K. A., Van Stan II, J. T., Dickerson-Lange, S. E., Lutz, J. A., Berman, J. W., Gersonde, R., & Lundquist, J. D. (2013). Development and testing of a snow interceptometer to quantify canopy water storage and interception processes in the rain/snow transition zone of the North Cascades, Washington, USA. *Water Resources Research*, *49*(6), 3243–3256.
<https://doi.org/10.1002/wrcr.20271>
- Mazurkiewicz, A. B., Callery, D. G., & McDonnell, J. J. (2008). Assessing the controls of the snow energy balance and water available for runoff in a rain-on-snow environment. *Journal of Hydrology*, *354*(1), 1–14. <https://doi.org/10.1016/j.jhydrol.2007.12.027>
- Mitchell, K. E., Lohmann, D., Houser, P. R., Wood, E. F., Schaake, J. C., Robock, A., Cosgrove, B. A., Sheffield, J., Duan, Q., Luo, L., Higgins, R. W., Pinker, R. T., Tarpley, J. D., Lettenmaier, D. P., Marshall, C. H., Entin, J. K., Pan, M., Shi, W., Koren, V., ... Bailey, A. A. (2004). The multi-institution North American Land Data Assimilation System (NLDAS): Utilizing multiple GCIP products and partners in a continental distributed hydrological modeling

- system. *Journal of Geophysical Research: Atmospheres*, 109(D7).
<https://doi.org/10.1029/2003JD003823>
- Mizukami, N., & Perica, S. (2008). Spatiotemporal Characteristics of Snowpack Density in the Mountainous Regions of the Western United States. *Journal of Hydrometeorology*, 9(6), 1416–1426. <https://doi.org/10.1175/2008JHM981.1>
- Molotch, N. P., & Meromy, L. (2014). Physiographic and climatic controls on snow cover persistence in the Sierra Nevada Mountains. *Hydrological Processes*, 28(16), 4573–4586. <https://doi.org/10.1002/hyp.10254>
- Mote, P. W. (2003). Trends in snow water equivalent in the Pacific Northwest and their climatic causes. *Geophysical Research Letters*, 30(12). <https://doi.org/10.1029/2003GL017258>
- Musselman, K. N., Molotch, N. P., & Brooks, P. D. (2008). Effects of vegetation on snow accumulation and ablation in a mid-latitude sub-alpine forest. *Hydrological Processes*, 22(15), 2767–2776. <https://doi.org/10.1002/hyp.7050>
- Nash, J. E., & Sutcliffe, J. V. (1970). River flow forecasting through conceptual models part I — A discussion of principles. *Journal of Hydrology*, 10(3), 282–290.
[https://doi.org/10.1016/0022-1694\(70\)90255-6](https://doi.org/10.1016/0022-1694(70)90255-6)
- Nolin, A. W., & Daly, C. (2006). Mapping “At Risk” Snow in the Pacific Northwest. *Journal of Hydrometeorology*, 7(5), 1164–1171. <https://doi.org/10.1175/JHM543.1>
- OpenTopography. (2022). *Linking Snowpack Heterogeneity to Subsurface Storage and Transmissivity, OR 2022*. <https://doi.org/10.5069/G99S1P8W>
- Painter, T., Berisford, D., Boardman, J., Bormann, K., Deems, J., Gehrke, F., Hedrick, A., Joyce, M., Laidlaw, R., Marks, D., Mattmann, C., McGurk, B., Ramirez, P., Richardson, M., Skiles, M., Seidel, F., & Winstral, A. (2016). The Airborne Snow Observatory: Fusion of scanning lidar, imaging spectrometer, and physically-based modeling for mapping snow water equivalent and snow albedo. *Remote Sensing of Environment*, 184.
<https://doi.org/10.1016/j.rse.2016.06.018>
- Pal, S., & Sharma, P. (2021). A Review of Machine Learning Applications in Land Surface Modeling. *Earth*, 2(1), Article 1. <https://doi.org/10.3390/earth2010011>

- Perkins, R. M., & Jones, J. A. (2008). Climate variability, snow, and physiographic controls on storm hydrographs in small forested basins, western Cascades, Oregon. *Hydrological Processes*, 22(25), 4949–4964. <https://doi.org/10.1002/hyp.7117>
- Quantum Spatial. (2020). *Wallowa-Whitman National Forest Lidar Processing Report* [dataset].
- Ralph Alig, Daolan Zheng, Thmas A. Spies, & Brett Butler. (2000). *Forest Cover Dynamics in the Pacific Northwest West Side: Regional Trends and Projections*.
- Roth, T. R., & Nolin, A. W. (2019). Characterizing Maritime Snow Canopy Interception in Forested Mountains. *Water Resources Research*, 55(6), 4564–4581. <https://doi.org/10.1029/2018WR024089>
- Rupp, D. E., Shafer, S. L., Daly, C., Jones, J. A., & Frey, S. J. K. (2020). Temperature Gradients and Inversions in a Forested Cascade Range Basin: Synoptic- to Local-Scale Controls. *Journal of Geophysical Research: Atmospheres*, 125(23), e2020JD032686. <https://doi.org/10.1029/2020JD032686>
- Rupp, D. E., Shafer, S. L., Daly, C., Jones, J. A., & Higgins, C. W. (2021). Influence of anthropogenic greenhouse gases on the propensity for nocturnal cold-air drainage. *Theoretical and Applied Climatology*, 146(1), 231–241. <https://doi.org/10.1007/s00704-021-03712-y>
- Sproles, E., Nolin, A. W., Rittger, K., & Painter, T. H. (2013). Climate change impacts on maritime mountain snowpack in the Oregon Cascades. *Hydrology and Earth System Sciences*, 17, 2581–2597. <https://doi.org/10.5194/hess-17-2581-2013>
- Storck, P., Lettenmaier, D. P., & Bolton, S. M. (2002). Measurement of snow interception and canopy effects on snow accumulation and melt in a mountainous maritime climate, Oregon, United States. *Water Resources Research*, 38(11), 5-1-5–16. <https://doi.org/10.1029/2002WR001281>
- Sturm, M., Holmgren, J., & Liston, G. E. (1995). A Seasonal Snow Cover Classification System for Local to Global Applications. *Journal of Climate*, 8(5), 1261–1283. [https://doi.org/10.1175/1520-0442\(1995\)008<1261:ASSCCS>2.0.CO;2](https://doi.org/10.1175/1520-0442(1995)008<1261:ASSCCS>2.0.CO;2)

- Sturm, M., & Liston, G. E. (2021). Revisiting the Global Seasonal Snow Classification: An Updated Dataset for Earth System Applications. *Journal of Hydrometeorology*, 22(11), 2917–2938. <https://doi.org/10.1175/JHM-D-21-0070.1>
- Sun, N., Yan, H., Wigmosta, M., Lundquist, J., Dickerson-Lange, S., & Zhou, T. (2022). Forest Canopy Density Effects on Snowpack Across the Climate Gradients of the Western United States Mountain Ranges. *Water Resources Research*, 58. <https://doi.org/10.1029/2020WR029194>
- Tennant, C. J., Harpold, A. A., Lohse, K. A., Godsey, S. E., Crosby, B. T., Larsen, L. G., Brooks, P. D., Van Kirk, R. W., & Glenn, N. F. (2017). Regional sensitivities of seasonal snowpack to elevation, aspect, and vegetation cover in western North America. *Water Resources Research*, 53(8), 6908–6926. <https://doi.org/10.1002/2016WR019374>
- Thatcher, C. A., Heidemann, H. K., Stoker, J. M., & Eldridge, D. F. (2017). The 3D Elevation Program national indexing scheme. In *The 3D Elevation Program national indexing scheme* (USGS Numbered Series 2017–3073; Fact Sheet, Vols. 2017–3073). U.S. Geological Survey. <https://doi.org/10.3133/fs20173073>
- Thomas A. Spies. (1998). *Forest Structure: A Key to the Ecosystem*. <https://andrewsforest.oregonstate.edu/publications/2564>
- Thomas A. Spies & Jerry F. Franklin. (1991). *The Structure of Natural Young, Mature, and Old-Growth Douglas-Fir Forest in Oregon and Washington*. <https://andrewsforest.oregonstate.edu/publications/1244>
- Thomas A. Spies, Jerry F. Franklin, & Mark Klopsch. (1990). *Canopy Gaps in Douglas-fir forests of the Cascade Mountains*. <https://andrewsforest.oregonstate.edu/publications/1074>
- USACE, North Pacific Division, Portland, OR. (1956). *Summary report of the snow investigations: Snow hydrology*.
- USACE, South Pacific Division, San Francisco, CA. (1956). *US Army Corps of Engineers, 1951. Hydrometeorological log of the Willamette Basin Snow Laboratory 1947-48 and 1948-49 water years*.

- Veatch, W., Brooks, P. D., Gustafson, J. R., & Molotch, N. P. (2009). 'Quantifying the effects of forest canopy cover on net snow accumulation at a continental, mid-latitude site.' *Ecohydrology*, 2(2), 115–128. <https://doi.org/10.1002/eco.45>
- Wayand, N., Clark, M., & Lundquist, J. (2016). Diagnosing Snow Accumulation Errors in a Rain-Snow Transitional Environment with Snow Board Observations. *Hydrological Processes*, 31, n/a-n/a. <https://doi.org/10.1002/hyp.11002>
- Xia, Y., Mitchell, K., Ek, M., Sheffield, J., Cosgrove, B., Wood, E., Luo, L., Alonge, C., Wei, H., Meng, J., Livneh, B., Lettenmaier, D., Koren, V., Duan, Q., Mo, K., Fan, Y., & Mocko, D. (2012). Continental-scale water and energy flux analysis and validation for the North American Land Data Assimilation System project phase 2 (NLDAS-2): 1. Intercomparison and application of model products. *Journal of Geophysical Research: Atmospheres*, 117(D3). <https://doi.org/10.1029/2011JD016048>
- Zobel, D. B., McKee, A., Hawk, G. M., & Dyrness, C. T. (1976). Relationships of Environment to Composition, Structure, and Diversity of Forest Communities of the Central Western Cascades of Oregon. *Ecological Monographs*, 46(2), 135–156. <https://doi.org/10.2307/1942248>

Appendix A – Long-term snow stake data

Table A-1. Summary of snow depths measured at snow stakes in forest and openings in dataset MS00701 (1994 to 2022).

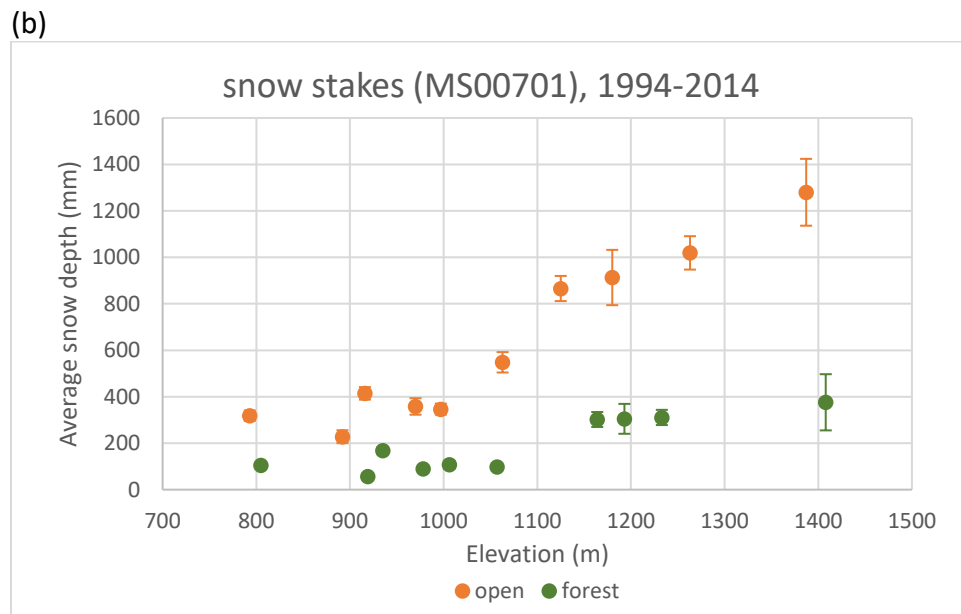
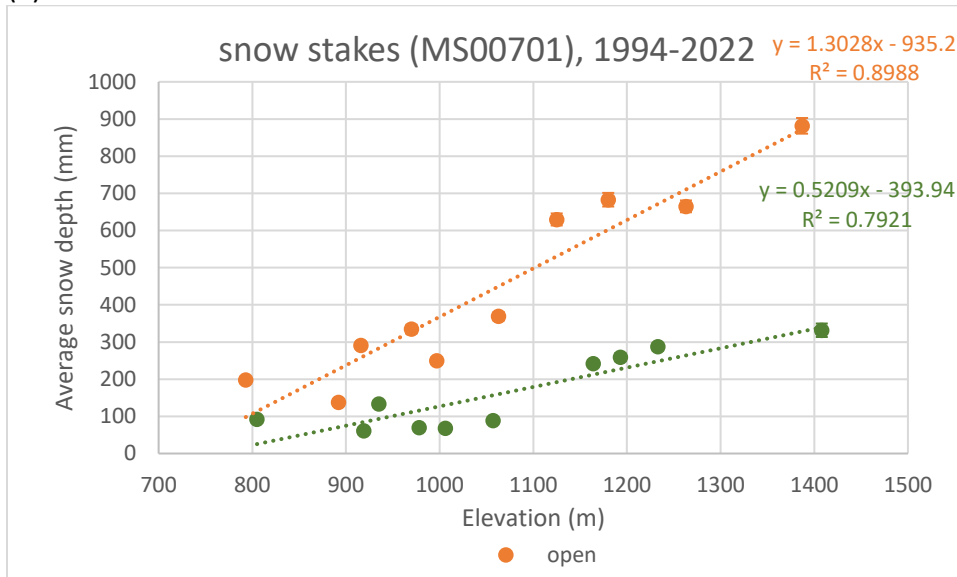
snow stake	Elevation (m)		average snow depth (mm)		SE (mm)		open - forest	forest as % of open
	open	forest	open	forest	open	forest		
<u>1994-2022 (MS00701)</u>								
R506O6/F6	1125	1164	630	242	16	9	388	38
R506O5/F5	970	1006	335	68	12	4	267	20
R350O4/F4/E4	1387	1408	882	332	21	18	550	38
R350O3/F3	1263	1233	665	287	16	10	378	43
R350O2/F2	1063	1057	369	89	11	5	280	24
R350O1/F1	892	919	138	61	7	4	77	44
R320O4/F4	997	978	249	70	9	4	180	28
R320O3/F3	916	935	291	133	10	6	157	46
R320O2/F2	793	805	198	92	8	4	107	46
R507O4/F4	1180	1193	683	259	18	11	424	38
<u>1994-2014</u>								
R506O6/F6	1125	1164	866	302	54	32	564	35
R506O5/F5	970	1006	358	107	35	18	251	30
R350O4/F4/E4	1387	1408	1280	376	144	121	904	29
R350O3/F3	1263	1233	1019	311	72	33	708	30
R350O2/F2	1063	1057	548	97	44	16	451	18
R350O1/F1	892	919	228	56	28	10	172	25
R320O4/F4	997	978	347	89	24	10	257	26
R320O3/F3	916	935	414	168	27	16	247	40
R320O2/F2	793	805	318	104	22	11	214	33

R507O4/F4	1180	1193	913	305	119	64	608	33
<u>2014-2022</u>								
R506O6/F6	1125	1164	598	235	17	9	363	39
R506O5/F5	970	1006	331	63	12	4	268	19
R350O4/F4/E4	1387	1408	870	331	21	18	539	38
R350O3/F3	1263	1233	630	285	16	11	345	45
R350O2/F2	1063	1057	349	88	12	6	262	25
R350O1/F1	892	919	126	60	7	4	66	47
R320O4/F4	997	978	226	65	10	4	161	29
R320O3/F3	916	935	261	125	10	7	136	48
R320O2/F2	793	805	170	89	8	5	81	52
R507O4/F4	1180	1193	679	258	19	11	421	38
1994-2022								
ave			444	163	13	8	281	37
SE			79	33	1	1	48	3
1994-2014								
ave			629	192	57	33	438	30
SE			114	37	13	11	79	2
2014-2022								
ave			424	160	13	8	264	38
SE			80	33	1	1	49	3

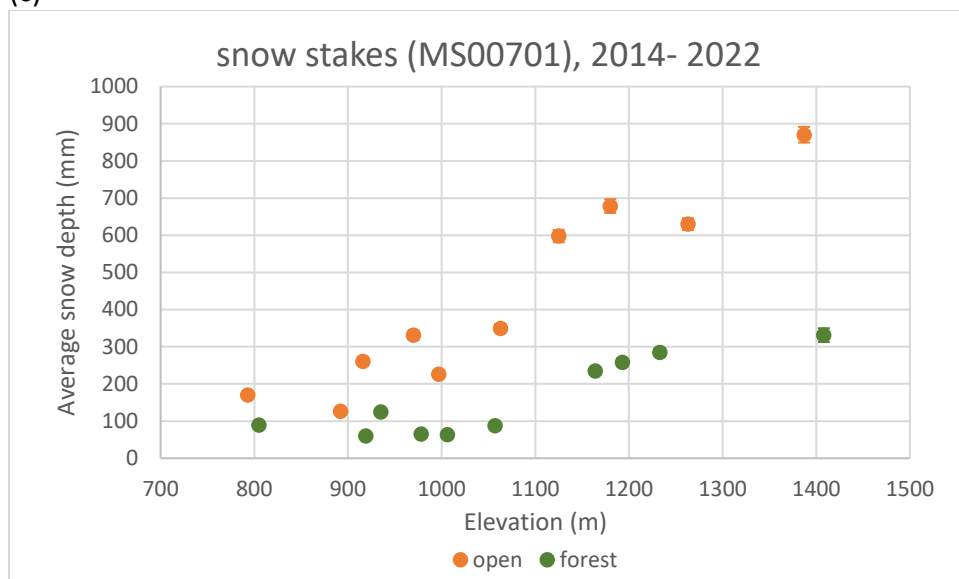
Table A-2. Summary of SWE (mm) measured at snow stakes in forest and openings in dataset MS00702 (1978 to 2003).

snow stake	Elevation (m)		average SWE (mm)		SE (mm)		open - forest	forest as % of open
	open	forest	open	forest	open	forest		
<u>1978-2003 (MS00702)</u>								
RS03_O	978		240		35			
RS12_, RS12_O	987	987	203	108	45	23	95	53
RS26_, RS26_O	1037	1037	199	92	57	17	106	46
RS04_, RS04_O	1307	1307	481	153	38	20	328	32
RS13_, RS13_O	1350	1350	571	211	34	19	360	37
RS14_, RS14_O	1430	1430	485	291	40	24	194	60
<u>1978-2003</u>								
ave			388	171	43	21	217	46
SE			78	36	4	1	55	5

Figure A-1. Snow depth in openings increases significantly with elevation, and is greater relative to under forest based on long-term paired snow stakes in the Andrews Forest. (a) dataset MS00701 (1994-2022), (b) dataset MS00701 (1994-2014), periodic measurements, (c) dataset MS00701 (2013-2022), daily measurements, (d) MS00702 (1978-2003), periodic measurements.



(c)



(d)

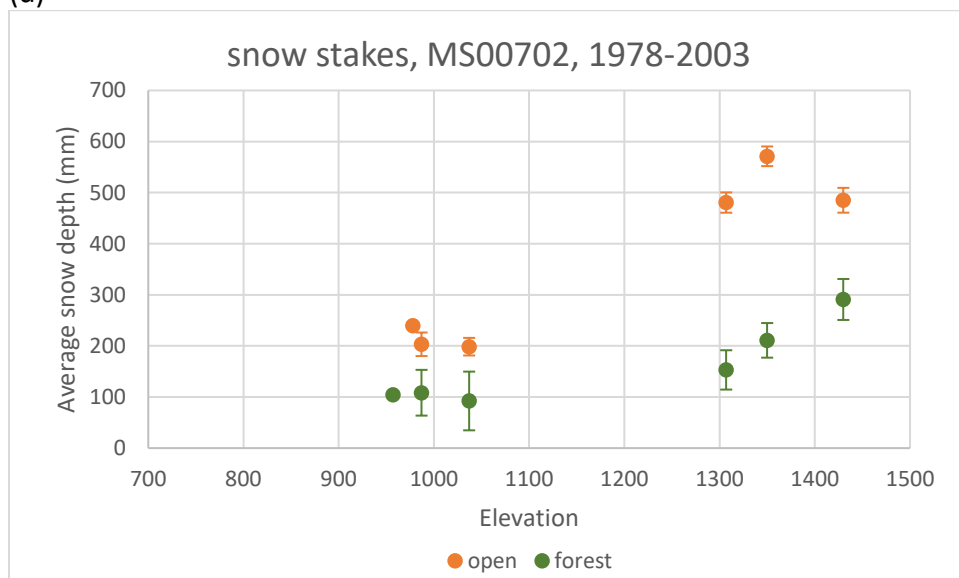
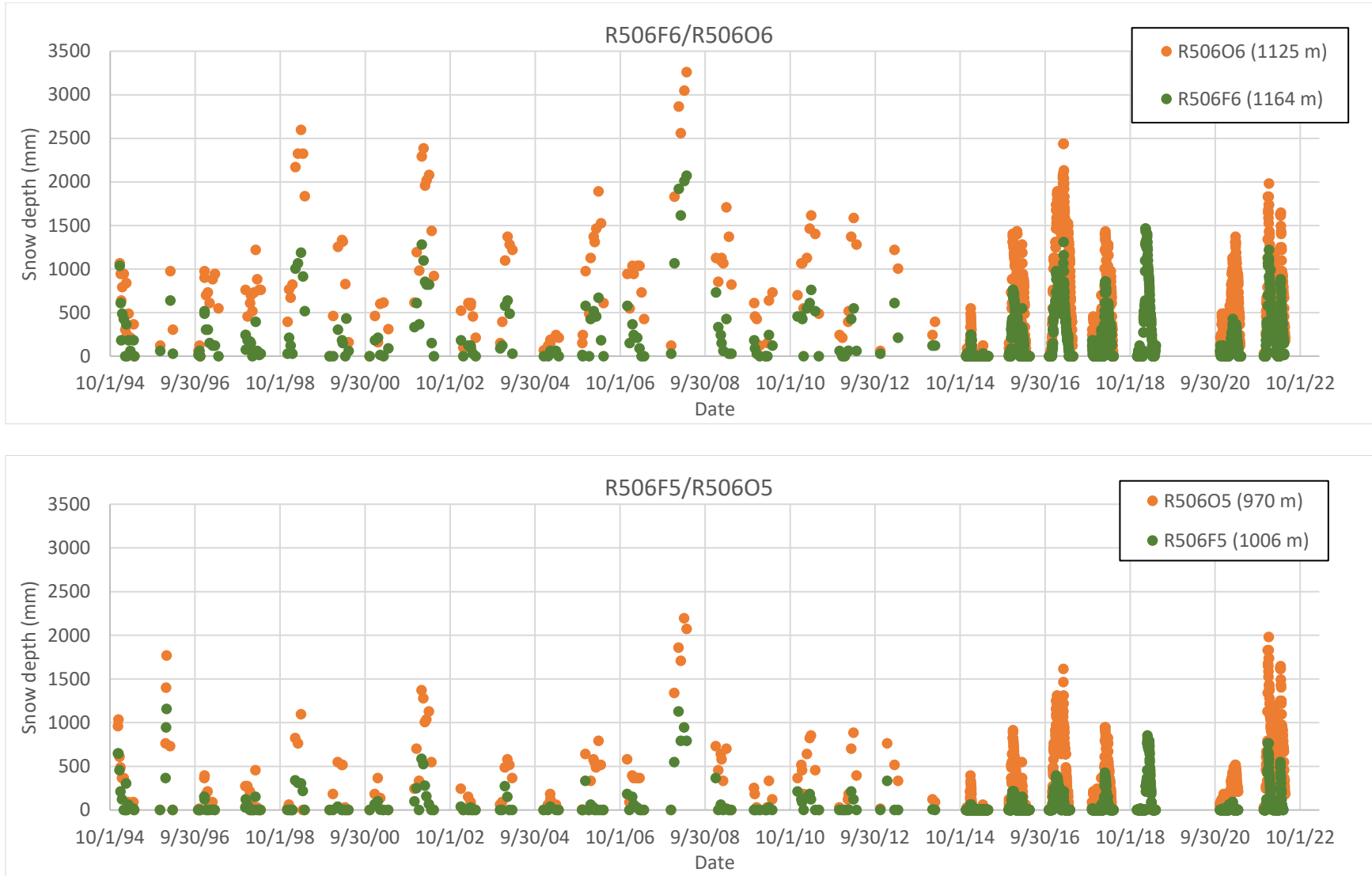
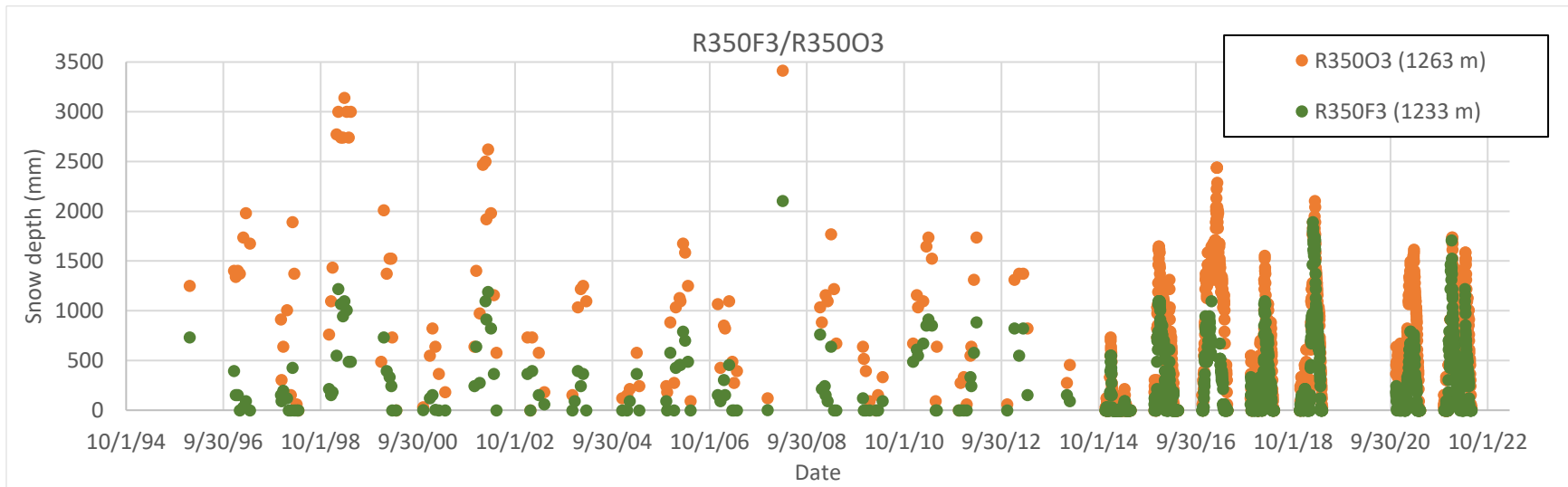
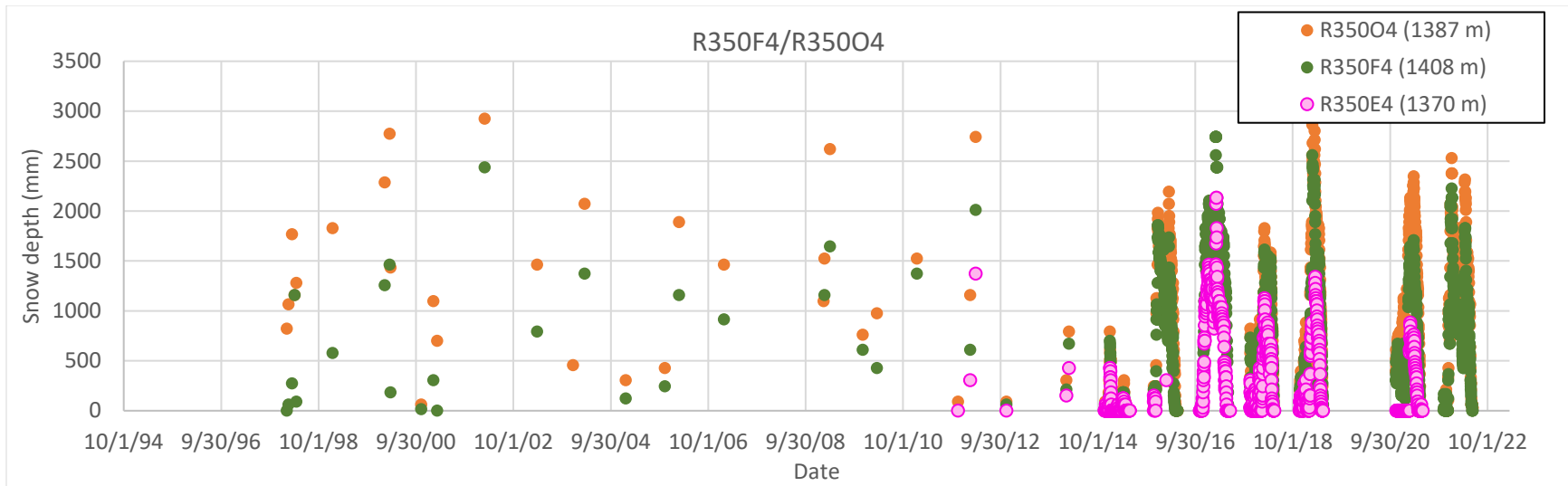
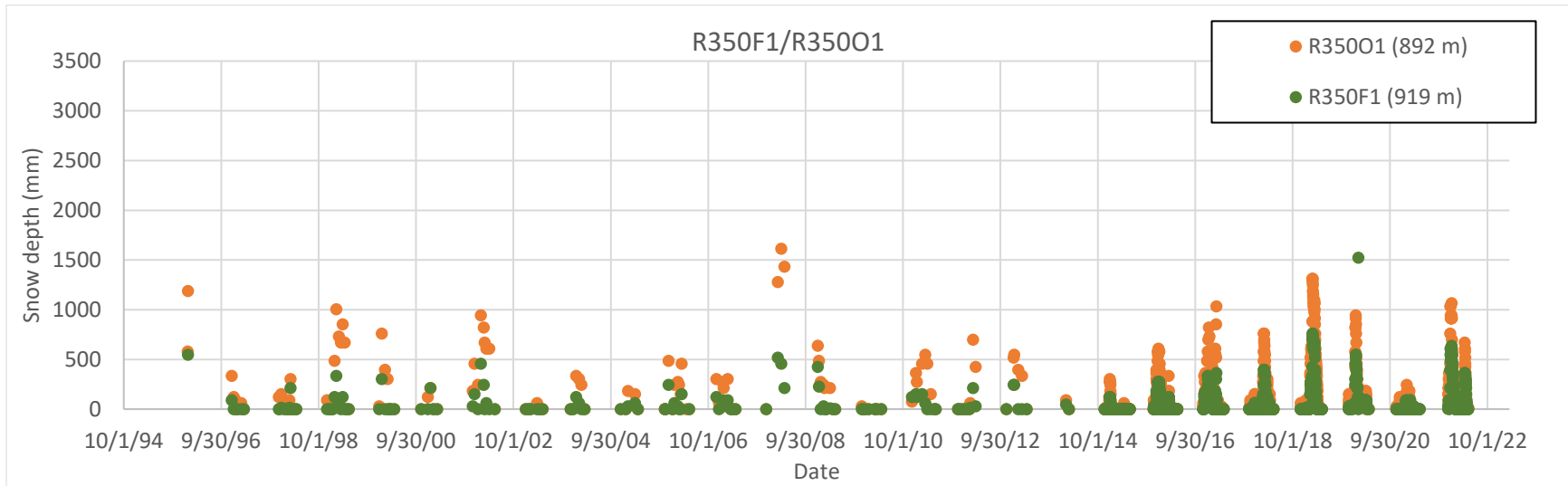
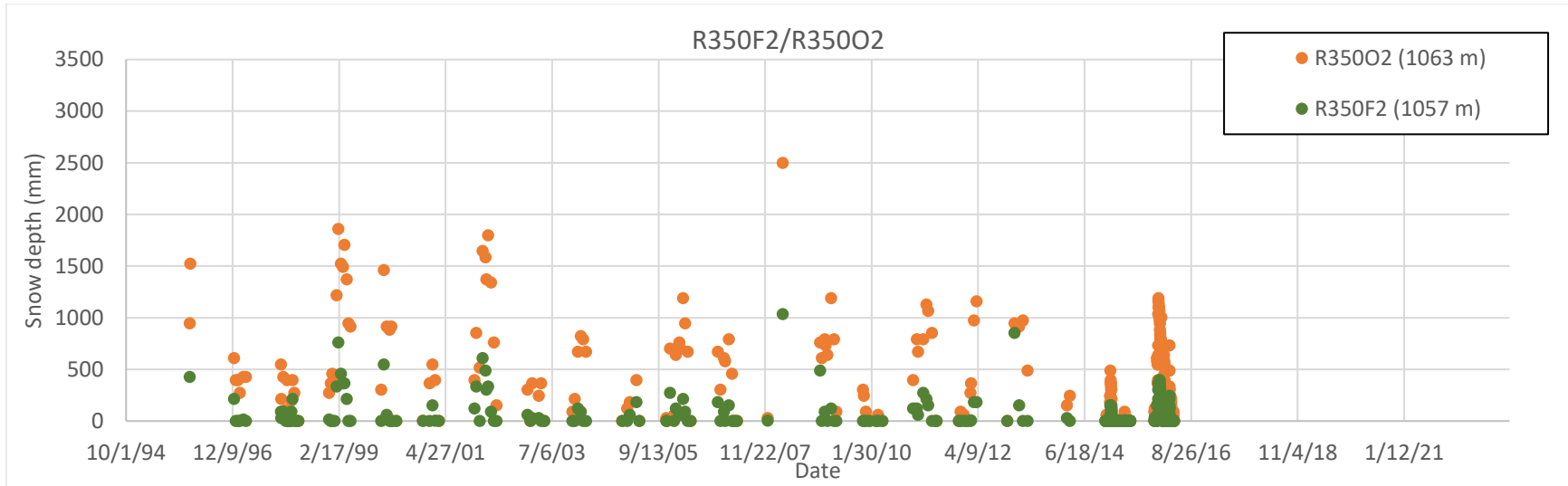
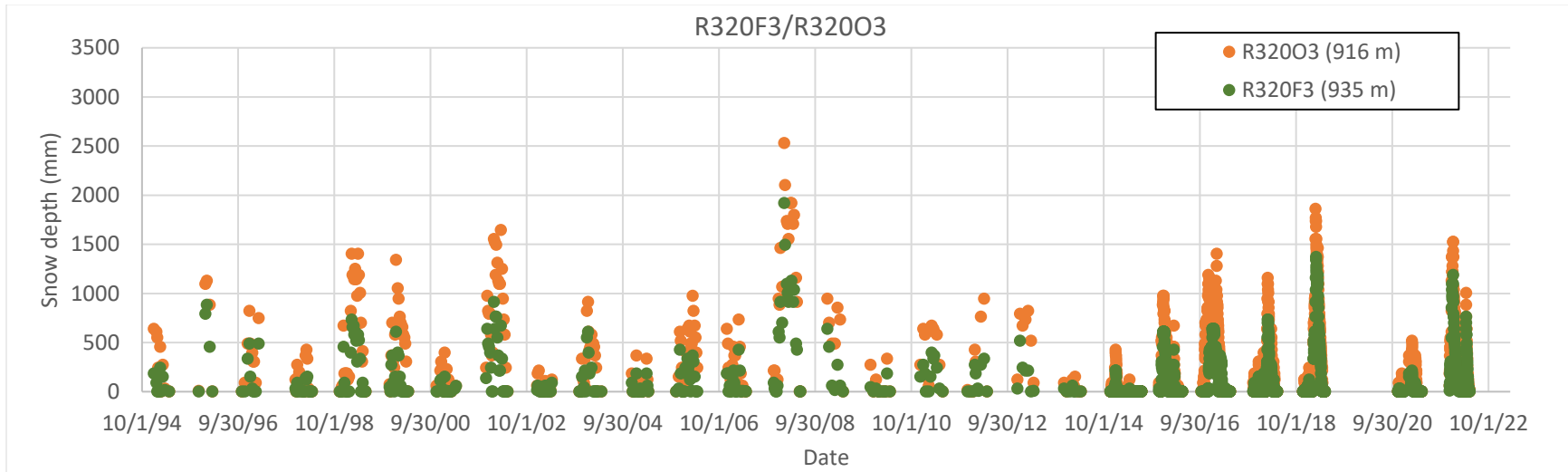
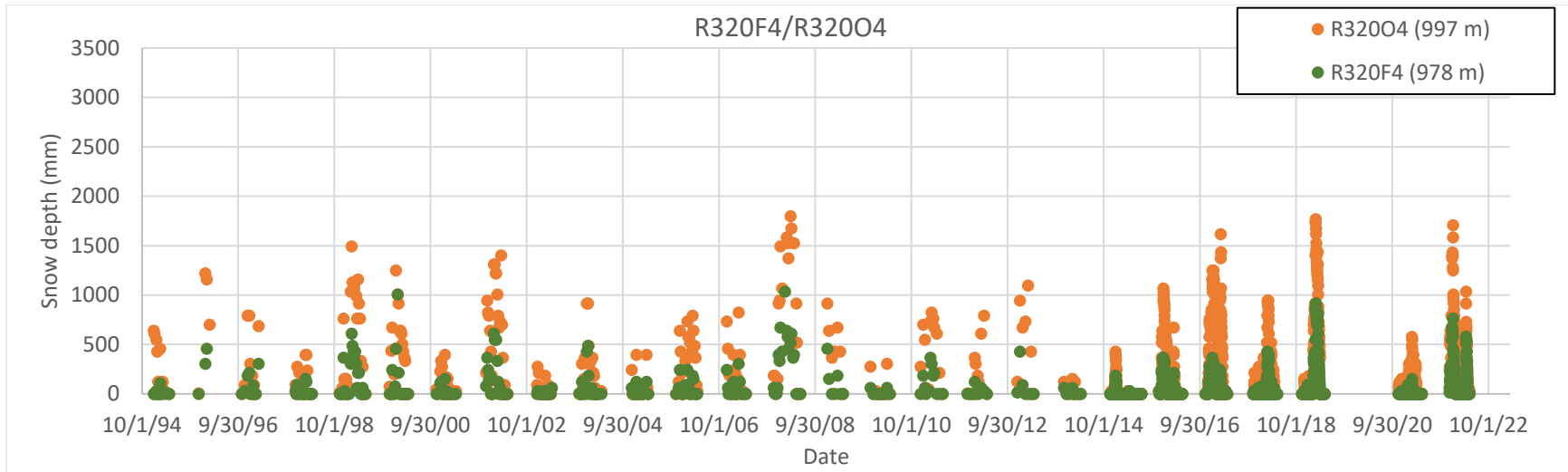


Figure A-2. Complete measurement series of snow depth (mm) in openings and under forest at paired snow stakes, Andrews Forest, dataset MS00701, 1994 to 2022.









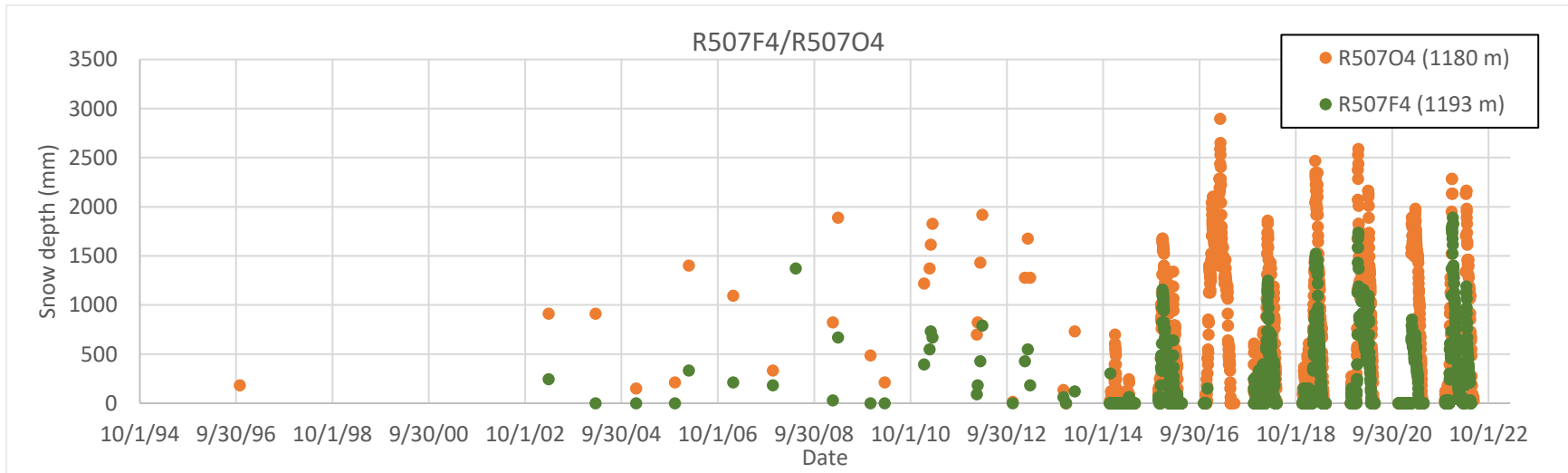
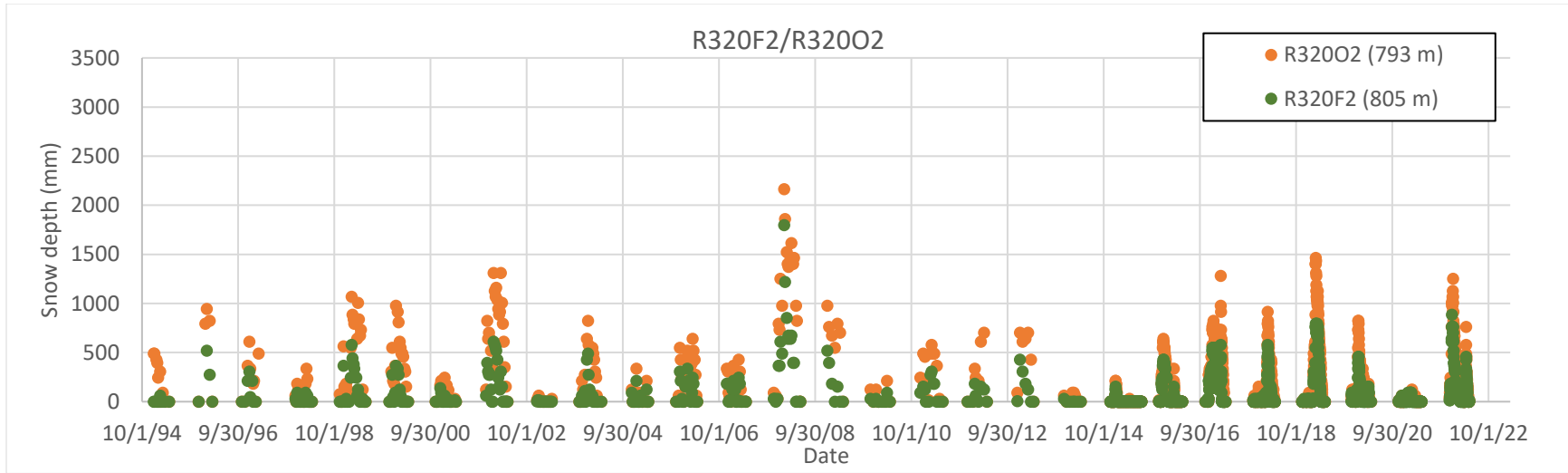
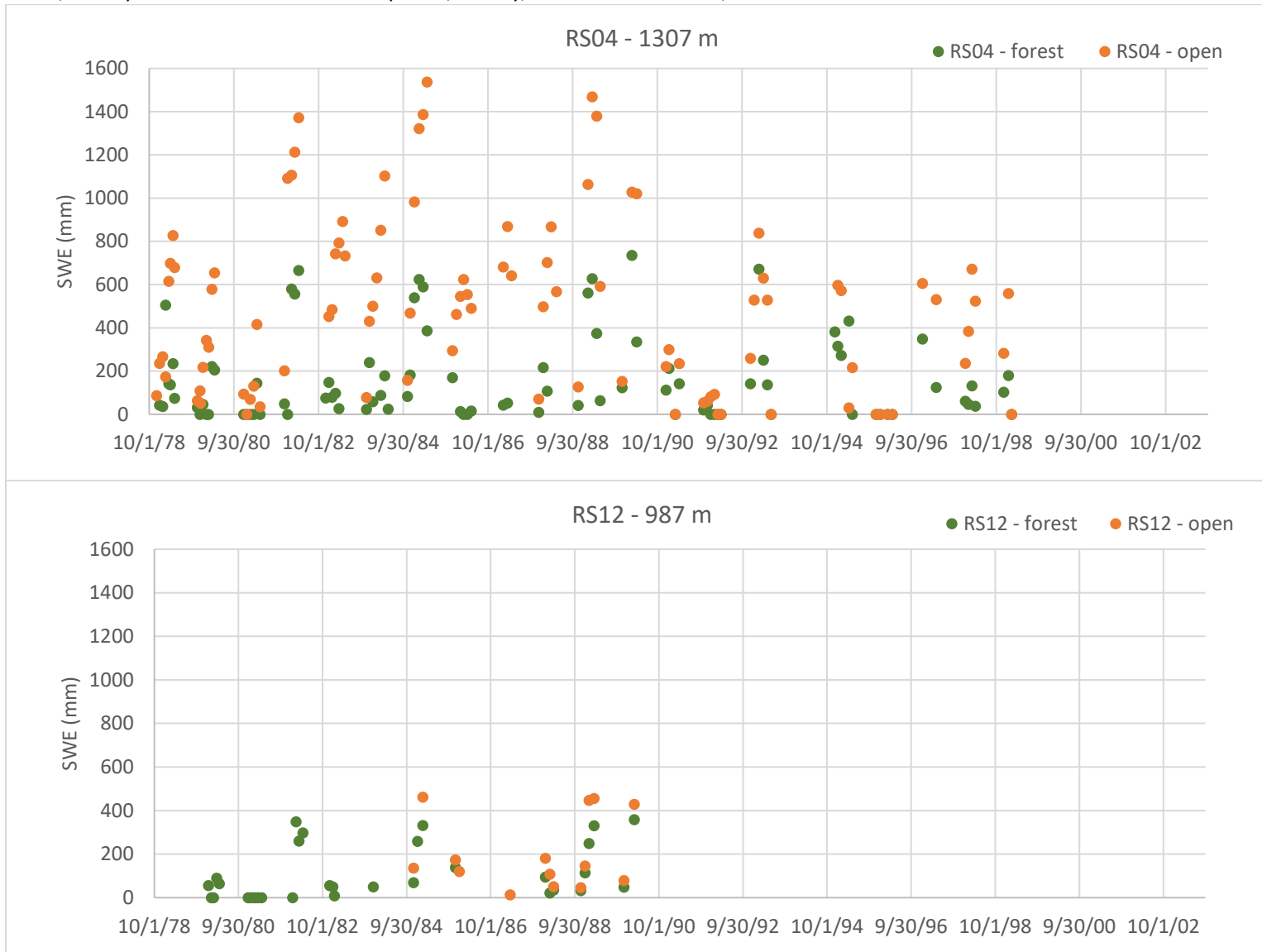
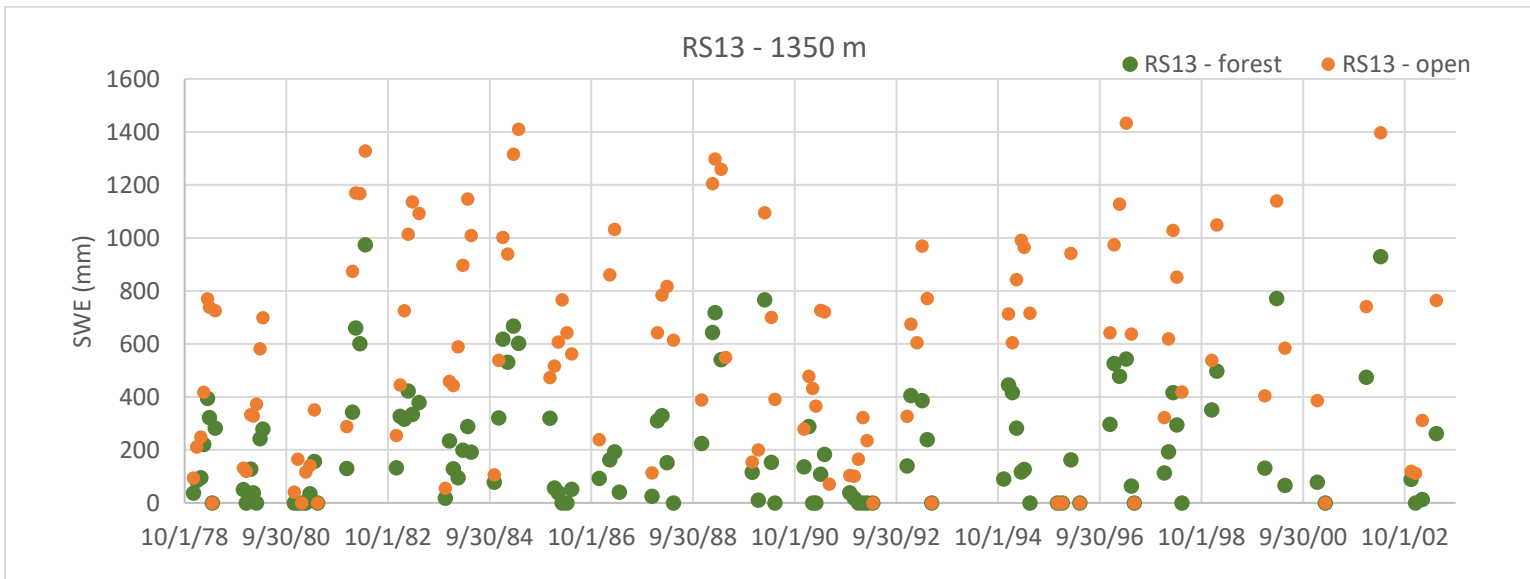
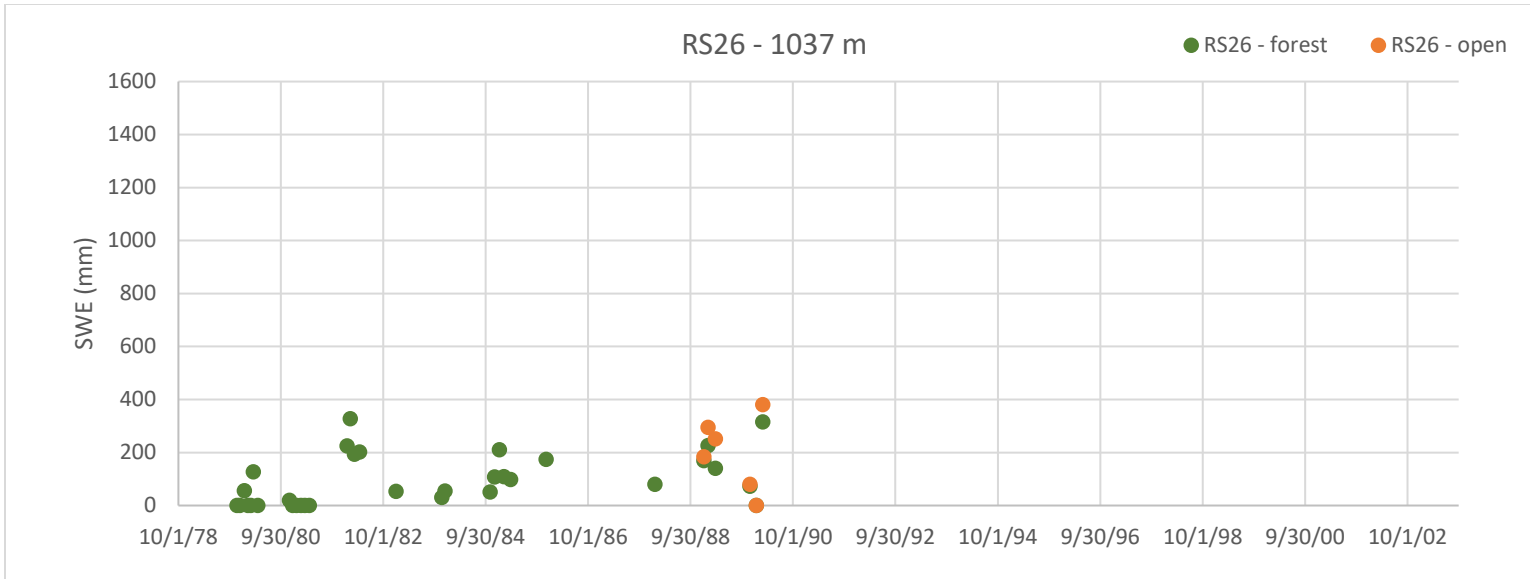
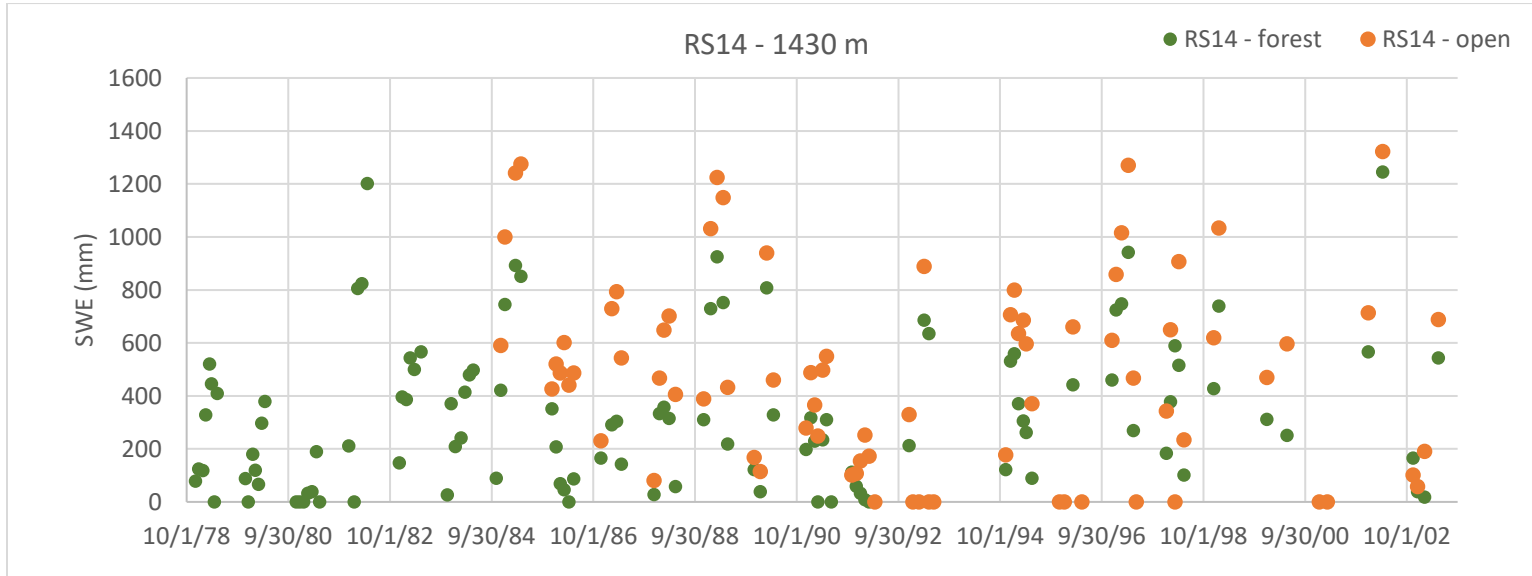


Figure A-3. Complete measurement series of SWE (mm) in openings and under forest at paired snow stakes, Andrews Forest (RS04, RS12, RS26) and Wildcat Mountain (RS13, RS14), dataset MS00702, 1978 to 2003.







Appendix B – Equations

$$spechum = RH * e^{(17.67(T_{air}-T_{frz})/(T_{air}-29.65))}/(0.263*P)$$

Equation 1. Specific humidity for SUMMA forcing calculated by measured relative humidity, pressure, and air temperature (Lumbrazo personal communication).

$$NSE = 1 - \frac{\sum_{t=1}^T (Q_o^t - Q_o^t)^2}{\sum_{t=1}^T (Q_o^t - Q_o^t)^2}$$

Equation 2. Nash Sutcliffe Efficiency (Nash & Sutcliffe, 1970).

$$NSE = 1 - \text{SUMPRODUCT}((B2:B43801-C2:C43801)^2) / \text{SUMPRODUCT}((B2:B43801-H2)^2)$$

Equation 2 continued. Nash Sutcliffe Efficiency Excel formula.

Appendix C – SUMMA code

```

%pylab inline
%load_ext autoreload
%autoreload 2
%reload_ext autoreload
import pysumma.plotting as psp
import seaborn as sns
import matplotlib.pyplot as plt
import sys
import xarray as xr
import numpy as np
import pandas as pd
import pysumma as ps

# function to convert summa
def convert_time_to_summa_string(t):
    return (
        f'{t.dt.year.values[()]:04}'
        f'-{t.dt.month.values[()]:02}'
        f'-{t.dt.day.values[()]:02}'
        f' {t.dt.hour.values[()]:02}'
        f':{t.dt.minute.values[()]:02}'
    )

attrs = {
    'airpres': {'units': 'Pa', 'long_name': 'Air pressure'},
    'airtemp': {'units': 'K', 'long_name': 'Air temperature'},
    'spechum': {'units': 'g g-1', 'long_name': 'Specific humidity'},
    'windspd': {'units': 'Wind speed', 'long_name': 'm s-1'},
    'SWRadAtm': {'units': 'W m-2', 'long_name': 'Downward shortwave radiation'},
    'LWRadAtm': {'units': 'W m-2', 'long_name': 'Downward longwave radiation'},
    'pptrate': {'units': 'kg m-2 s-1', 'long_name': 'Precipitation rate'}
}

name_lookup = {
    'airpres': 'pressure_Pa',
    'airtemp': 'temp_K',
    'spechum': 'spechum',
    'windspd': 'wind_ms',
    'SWRadAtm': 'sw_mean_wm2',
    'LWRadAtm': 'LW_40',
    'pptrate': 'precip_PPT016', }

```

```

df =
pd.read_csv('/Users/ianwhidden/pysumma/pysumma/summa_met_forcing/final_forcing/forci
ng_WY14_18_June.csv')
df.index = pd.DatetimeIndex(df['datetime'], name='time')

forcing_filename = 'uplo_station_forcing.nc'
# Adding 1 hour to account for SUMMA being period-ending
time_idx = df.index + pd.Timedelta('1H')
shape = (len(time_idx), 1, )
dims = ('time', 'hru', )
coords = {'time': time_idx}

met_data = xr.Dataset(coords=coords)
met_data.time.encoding['calendar'] = 'standard'
met_data.time.encoding['units'] = 'hours since 2013-10-01'
for varname, varattrs in attrs.items():
    df_name = name_lookup[varname]
    met_data[varname] = xr.DataArray(
        data=df[df_name].values.reshape(-1, 1),
        coords=coords, dims=dims, name=varname, attrs=varattrs
    )

#met_data['airtemp'] += 273.16 # Convert to Kelvin, not needed if air in K
met_data['pptrate'] /= 3600.0 # Convert to mm/s
met_data['data_step'] = xr.Variable([], 3600.0)
met_data.to_netcdf(f'./forcings/{forcing_filename}')

with open('./forcings/forcing_file_list.txt', 'w') as f:
    f.write(f"{forcing_filename}\n")

lat = 44.2072180256268
lon = -122.119450090239
elev = 1300
local_attrs = xr.open_dataset('./summa_setup_template/params/local_attributes.nc').load()
local_attrs['longitude'].values[:] = lon
local_attrs['latitude'].values[:] = lat
local_attrs['elevation'].values[:] = elev
local_attrs['tan_slope'] = 10.0 #
local_attrs['aspect'] = 72.0
local_attrs['mHeight'] = 6.0
local_attrs['vegTypeIndex'].values[:] = 1 # 1 is 'Evergreen Needleleaf Forest', 16 is 'Barren or
Sparsely Vegetated'

!./install_local_setup.sh

```



```

summa_exe = 'summa.exe'
file_manager = './file_manager.txt'
# INITIATE (instantiate?) simulation object
s = ps.Simulation(summa_exe, file_manager)
# Update file manager with start and end time
s.manager['simStartTime'] = '2013-10-01 00:00'
s.manager['simEndTime'] = '2018-09-29 23:00'

t0 = met_data['time'].isel(time=0)
t1 = met_data['time'].isel(time=-1)
s.manager['simStartTime'] = convert_time_to_summa_string(t0)

# OUTPUT Control , Add additional variables written to the output control file
s.output_control['scalarSnowDepth'] = [1, 0, 1, 0, 0, 0, 0, 0]
s.output_control['scalarSnowAlbedo'] = [1, 0, 1, 0, 0, 0, 0, 0]
#'scalarCanopySnowUnloading' - unloading of snow from the vegetation canopy (kg m-2 s-1)
s.output_control['SWRadAtm'] = [1, 0, 1, 0, 0, 0, 0, 0]
s.output_control['scalarCanopyTemp'] = [1, 0, 1, 0, 0, 0, 0, 0]

s.output_control['upperBoundTemp'] = [1, 0, 1, 0, 0, 0, 0, 0]

# Set decision options
s.decisions.set_option('soilCatTbl', 'ROSETTA')
s.decisions.set_option('vegeParTbl', 'MODIFIED_IGBP_MODIS_NOAH')
s.decisions.set_option('soilStress', 'NoahType')
s.decisions.set_option('stomResist', 'BallBerry')
s.decisions.set_option('fDerivMeth', 'analytic')
s.decisions.set_option('num_method', 'iterative')
s.decisions.set_option('LAI_method', 'monTable')
s.decisions.set_option('clIntercept', 'storageFunc')
s.decisions.set_option('f_Richards', 'mixdform')
s.decisions.set_option('groundwatr', 'bigBuckt')
s.decisions.set_option('hc_profile', 'pow_prof')
s.decisions.set_option('bcUpprTdyn', 'nrg_flux')
s.decisions.set_option('bcLowrTdyn', 'presTemp')
s.decisions.set_option('bcUpprSoiH', 'liq_flux')
s.decisions.set_option('bcLowrSoiH', 'drainage')
s.decisions.set_option('veg_traits', 'CM_QJRMS1988')
s.decisions.set_option('rootProfil', 'powerLaw')
s.decisions.set_option('canopyEmis', 'simplExp')
s.decisions.set_option('snowIncept', 'stickySnow') # lightSnow
s.decisions.set_option('windPrfile', 'logBelowCanopy')
s.decisions.set_option('astability', 'louisinv')

```

```
s.decisions.set_option('compaction', 'anderson')
s.decisions.set_option('snowLayers', 'CLM_2010')
s.decisions.set_option('thCondSnow', 'smnv2000')
s.decisions.set_option('thCondSoil', 'funcSoilWet')
s.decisions.set_option('canopySrad', 'noah_mp')
s.decisions.set_option('alb_method', 'varDecay')
s.decisions.set_option('spatial_gw', 'localColumn')
s.decisions.set_option('snowDenNew', 'hedAndPom')

# CANOPY
# Forest
s.global_hru_params['heightCanopyBottom'] = [ 2.0 , 1.0 , 3.0 ]
s.global_hru_params['heightCanopyTop'] = [ 40.0 , 40.0 , 50.0 ]
# Open
s.global_hru_params['heightCanopyBottom'] = [ 0.0 , 0.0 , 0.0 ]
s.global_hru_params['heightCanopyTop'] = [ 0.0 , 0.0 , 0.0 ]

s.run('local')
s.status
```